

Ras suppression potentiates rear actomyosin contractility-driven cell polarization and migration

Received: 7 September 2023

Accepted: 31 May 2024

Yiyan Lin  ^{1,2,7}, Dhiman Sankar Pal  ^{1,7,8} , Parijat Banerjee³, Tatsat Banerjee  ^{1,4}, Guanghui Qin  ⁵, Yu Deng  ^{1,4}, Jane Borleis¹, Pablo A. Iglesias  ^{1,6} & Peter N. Devreotes  ^{1,2,8} 

 Check for updates

Ras has been extensively studied as a promoter of cell proliferation, whereas few studies have explored its role in migration. To investigate the direct and immediate effects of Ras activity on cell motility or polarity, we focused on RasGAPs, C2GAPB in *Dictyostelium* amoebae and RASAL3 in HL-60 neutrophils and macrophages. In both cellular systems, optically recruiting the respective RasGAP to the cell front extinguished pre-existing protrusions and changed migration direction. However, when these respective RasGAPs were recruited uniformly to the membrane, cells polarized and moved more rapidly, whereas targeting to the back exaggerated these effects. These unexpected outcomes of attenuating Ras activity naturally had strong, context-dependent consequences for chemotaxis. The RasGAP-mediated polarization depended critically on myosin II activity and commenced with contraction at the cell rear, followed by sustained TORC2-dependent actin polymerization at the front. These experimental results were captured by computational simulations in which Ras levels control front- and back-promoting feedback loops. The discovery that inhibiting Ras activity can produce counterintuitive effects on cell migration has important implications for future drug-design strategies targeting oncogenic Ras.

Ras GTPases play a vital role in transmitting signals within cells, influencing growth and survival, and activating mutations in Ras genes are found in ~30% of all cancers^{1–3}. Therefore, targeting mutant Ras has become a major focus in cancer drug development. While extensive research has been dedicated to understanding the role of Ras mutations in promoting cancer growth, the impact of these mutations on metastasis has received less attention. Nevertheless, studies conducted in model systems, *Dictyostelium* amoebae and human neutrophils,

suggest that local Ras activity plays a direct and immediate role in tuning polarity and motility^{4–9}.

Ras is activated both by stimulation of G-protein-coupled receptors and spontaneously at cellular protrusions^{6,10–13}. Ras function is spatiotemporally controlled by its activators, RasGEFs and inhibitors, RasGAPs, which might be expected to create ‘front’ and ‘back’, respectively, during migration^{11,14–19}. However, Ras activity must be carefully balanced, as constitutively active Ras expression leads to

Q1 Q2
Q3 Q4
Q5 Q6
Q7 Q8
Q9 Q10

¹Department of Cell Biology and Center for Cell Dynamics, School of Medicine, Johns Hopkins University, Baltimore, MD, USA. ²Department of Biological Chemistry, School of Medicine, Johns Hopkins University, Baltimore, MD, USA. ³Department of Physics and Astronomy, Johns Hopkins University, Baltimore, MD, USA. ⁴Department of Chemical and Biomolecular Engineering, Whiting School of Engineering, Johns Hopkins University, Baltimore, MD, USA. ⁵Department of Computer Science, Whiting School of Engineering, Johns Hopkins University, Baltimore, MD, USA. ⁶Department of Electrical and Computer Engineering, Whiting School of Engineering, Johns Hopkins University, Baltimore, MD, USA. ⁷These authors contributed equally: Yiyan Lin, Dhiman Sankar Pal. ⁸These authors jointly supervised this work: Dhiman Sankar Pal, Peter N. Devreotes.  e-mail: dhimanpal8@gmail.com; pnd@jhmi.edu

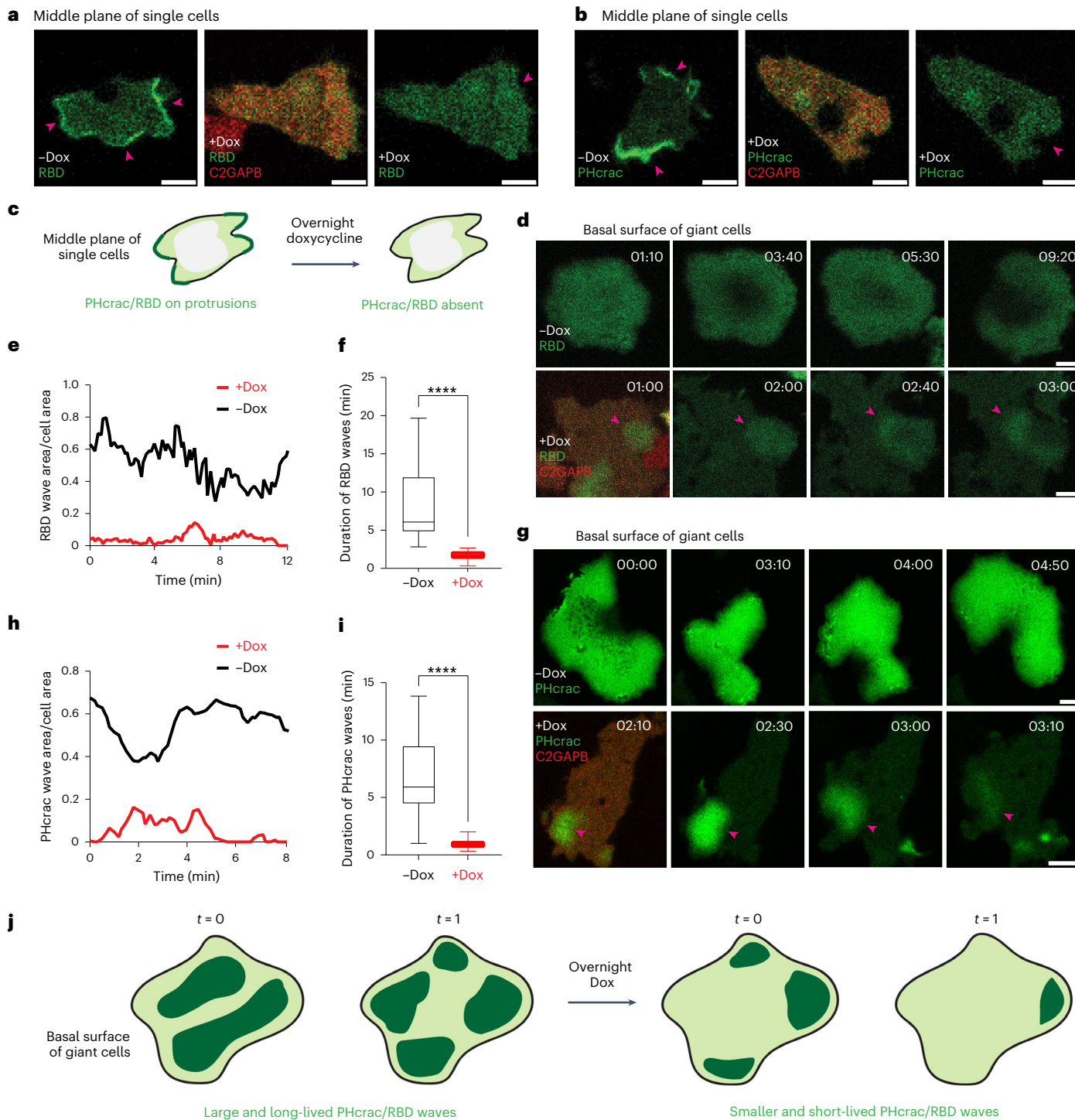


Fig. 1 | C2GAPB inhibits Ras and PI3K activities in single and electrofused *Dictyostelium*. **a,b**, Confocal images of vegetative *Dictyostelium* single cells expressing GFP-RBD (biosensor for activated Ras; green) (**a**) or PHcrac-YFP (biosensor for PIP3; green) (**b**) before and after doxycycline (Dox)-induced mRFPmars-C2GAPB (red) expression. Pink arrows highlight the front of these cells. Scale bars, 5 μ m. **c**, Cartoon summarizing our observations in **a** and **b** that both Ras activation and PIP3 level on the cell membrane significantly reduce with C2GAPB expression. **d,g**, Time-lapse confocal images of vegetative *Dictyostelium* electrofused or 'giant' cells expressing GFP-RBD (green) (**d**) or PHcrac-YFP (green) (**g**) before and after Dox-induced mRFPmars-C2GAPB (red) expression. Pink arrows point at reduced RBD or PHcrac waves in presence of C2GAPB. Time

is shown in min:s format. Scale bars, 5 μ m. **e,f,h,i**, RBD or PHcrac wave area (**e,h**) and duration (**f,i**) before ('-Dox'; black) and after ('+Dox'; red) Dox-induced mRFPmars-C2GAPB expression. $n = 10$ (-Dox, **f**), $n = 27$ (+Dox, **f**), $n = 10$ (-Dox, **i**) or $n = 31$ (+Dox, **i**) waves pooled from ten cells, examined over three independent experiments; asterisks indicate significant difference, **** $P \leq 0.0001$ (two-sided Mann–Whitney test; no adjustments were made for multiple comparisons). The boxes (**f,i**) extend from 25th to 75th percentiles, median is at the centre and whiskers and outliers are graphed according to Tukey's convention (GraphPad Prism 8). **j**, Cartoon depicting reduction in size and duration of RBD and PHcrac waves on the basal surface of giant *Dictyostelium* cells, after overnight Dox induction of C2GAPB. Source numerical data are provided.

hyper-activation of PI3K–TORC2–PKB pathways, causing significant cell spreading and defective migration^{5,20,21}. Additionally, knockout and knockdown of various RasGAPs have demonstrated their significant impact on Ras and protrusive activities^{8,11,17,18,22,23}. For example, genetic deletion of NF1 in *Dictyostelium* or humans causes increased macropinocytosis or severe neurofibromatosis type 1, respectively^{24–26}.

Understanding the physiological relevance of manipulating Ras activity is of paramount importance, but knockout studies have proven relatively ineffective, possibly due to redundancy. For example, *Dictyostelium* lacking Ras isoforms continue to grow and directed migration remains little affected^{27–29}. Furthermore, while new treatments with small molecule inhibitors targeting constitutively active KRasG12C show promise, they also pose significant challenges^{30–32}. A potentially powerful alternative route of suppressing Ras would be to activate RasGAPs. Indeed, in immune cells, locally activating a RasGAP could inhibit Ras and halt chemotaxis⁴.

We designed a series of studies to inhibit Ras activity using RasGAP proteins and see its immediate effects on cell behaviour and shape. Notably, different RasGAPs in amoebae and leucocytes can polarize cells and improve migration. Our evidence suggests that polarization was due to an increase in suppression of Ras activity leading to increased contraction at the back. We show that a direct linear relationship does not exist between Ras activation and motility, and an optimal level of activated Ras potentiates migration and polarity.

Results

Reduction of Ras and PI3K activities at cell fronts shuts off protrusions

We examined the effects of C2GAPB in modulating Ras and downstream PI3K activities in growing *Dictyostelium* cells. As we encountered challenges in expressing C2GAPB using standard methods, we developed a doxycycline-inducible system to improve expression. We first compared Ras/PI3K activities by expressing fluorescence-labelled biosensors, RBD or PHcrac, respectively, with or without C2GAPB expression. Confocal imaging of midline of cells revealed broad patches of RBD/PIP3 at the protrusions in absence of C2GAPB. However, upon overnight induction of C2GAPB expression, these patches reduced in size (Fig. 1a–c). Ras/PIP3 patches underlie protrusions which mediate cell movement and macropinocytosis^{11,33,34}. Uptake measurements showed that macropinocytosis was significantly reduced upon C2GAPB expression (Extended Data Fig. 1a,b). Alternatively, RBD patches at cell fronts were strongly diminished upon inducing expression of dominant negative RasG (RasG S17N) (Extended Data Fig. 1c).

Ras and PI3K activities form cortical waves on the basal surface of electrofused, giant *Dictyostelium* cells^{12,13,35–40}. We have used waves in electrofused cells or migration in single cells interchangeably throughout this study. Confocal images of migrating cells offer a cross-sectional

view, but in three dimensions, protrusions extend outwardly while expanding laterally, as a travelling wave. Wave characteristics strongly correlate with protrusion types and migration mode. Upon inducing C2GAPB expression, Ras/PIP3 waves became smaller and more transient (Fig. 1d,g,j and Supplementary Videos 1–4). In absence of C2GAPB, RBD/PHcrac wave area at steady-state varied between 35–80% of total cell area, but with C2GAPB, wave area decreased to less than 20% (Fig. 1e,h). Mean duration of a wave also decreased from 5 min to less than 1 min (Fig. 1f,i). Conversely, in C2GAPB-null cells, broad, propagating RBD waves were observed, validating that C2GAPB suppresses Ras activity (Extended Data Fig. 1d)¹¹.

Next, C2GAPB was optically recruited to cellular protrusions at the leading edge. Consequently, mature protrusions quickly vanished causing the cell to contract, whereas new protrusions emerged at the former back and the cell started to move in the opposite direction (Fig. 2a,c). Angular histogram analyses revealed that the probability of nascent protrusion formation was highest at -120–150 degrees away from C2GAPB recruitment area (Fig. 2d). To confirm that polarity reversal was due specifically to Ras suppression, we locally recruited CAAX-deleted RasG S17N to pre-existing cell fronts, which diminished them immediately (Extended Data Fig. 1e). In contrast, empty vector recruitment did not block production of new protrusions and the cell continued to move in its original direction (Fig. 2e,f).

As C2GAPB had a strong effect on cell behaviour, we checked whether it was having this effect by reducing Ras/PI3K activities. While unrecruited cells displayed multiple, small RBD/PHcrac patches ('00:00' in Fig. 2g,h), once C2GAPB was recruited it caused a simultaneous reduction in activated Ras/PIP3 levels at the protrusions ('00:15'–'2:30' in Fig. 2g,h). Similarly, activated Ras/PIP3 propagating waves substantially reduced upon C2GAPB recruitment (Fig. 2i,j and Supplementary Videos 5 and 6). Once we switched off the blue light, RBD waves recovered within 1 min (Supplementary Video 5). In latrunculin-treated cells, dynamic RBD membrane patches disappeared ~30 s of C2GAPB recruitment (Extended Data Fig. 1f).

We extended our investigation to differentiated neutrophils to assess the conservation of RasGAP function on cytoskeletal remodelling. We previously developed a membrane recruitable RASAL3 in neutrophils (Fig. 2b)⁴. Optically recruiting RASAL3 to F-actin-rich front, marked by LifeAct, caused mature protrusions to immediately disappear. Simultaneously, a new broad front emerged at the opposite end, causing the cell to migrate away (Fig. 2k and Supplementary Video 7). New protrusions appeared at -130–170 degrees from the recruitment site (Fig. 2l). Alternatively, recruiting KRas4B S17N ΔCAAX to mature fronts caused them to fold and form fresh ones instantaneously at the erstwhile back (Extended Data Fig. 1g,h and Supplementary Video 8). Altogether, these observations demonstrate that suppressing Ras activity at the cell front caused immediate shut down of local signalling, and consequently protrusions and migration.

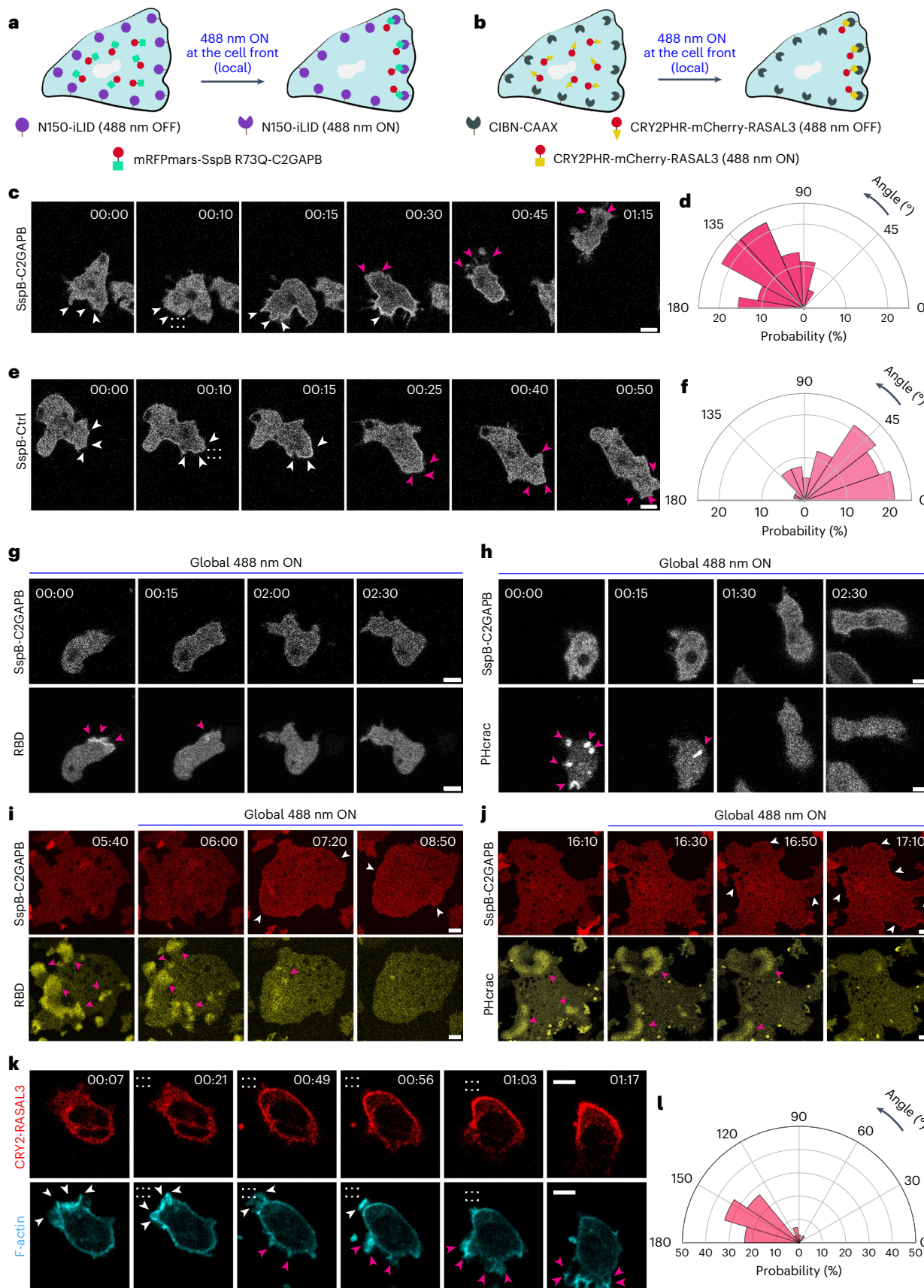
Fig. 2 | C2GAPB or RASAL3 recruitment shuts off protrusions by inhibiting Ras/PI3K activities in *Dictyostelium* or neutrophils. **a,b**, Cartoon illustrating opto-C2GAPB (**a**) or opto-RASAL3 recruitment (**b**) to the cell front after locally applying blue light. **c,e**, Time-lapse confocal images of vegetative *Dictyostelium* single cells expressing mRFPmars-SspB R73Q-C2GAPB (**c**) or tgRFPt-SspB R73Q-Ctrl (control without C2GAPB) (**e**). C2GAPB or Ctrl is recruited to migrating cell front by applying 488 nm laser near it, as shown by the dashed white box. White arrows denote existing older protrusions and pink arrows highlight emerging newer protrusions. Time is shown in min:s format. Scale bars, 5 μm. **d,f**, Polar histogram demonstrates higher probability of fresh protrusion formation away from C2GAPB recruitment area (**d**), whereas for Ctrl, new protrusions form near the recruitment area (**f**). *n* = 45 protrusions pooled from 11 cells (**d**) and *n* = 76 protrusions from 13 cells for **f**, examined over three independent experiments. **g,h**, Time-lapse confocal images of vegetative *Dictyostelium* single cells expressing mRFPmars-SspB R73Q-C2GAPB (top) and RBD-YFP (**g**) or PHcrac-YFP (both bottom) (**h**) after 488 nm laser was switched on globally. RBD

or PHcrac status at '00:00' is considered as control time point as C2GAPB was not recruited yet. Pink arrows denote RBD or PHcrac patches in cells. Time is shown in min:s format. Scale bars, 5 μm. **i,j**, Time-lapse confocal images of *Dictyostelium* electrofused cells expressing mRFPmars-SspB R73Q-C2GAPB (top; red) and RBD-YFP (**i**) or PHcrac-YFP (both bottom; yellow) (**j**) before and after 488 nm laser was switched on globally. White arrows highlight C2GAPB recruitment in red channel and pink arrows denote RBD or PHcrac waves near bottom cell surface. Time is shown in min:s format. Scale bars, 10 μm. **k,l**, Time-lapse confocal images of differentiated HL-60 neutrophil expressing CRY2PHR-mCherry-RASAL3 (red; top) and LifeAct-miRFP703 (cyan; bottom). RASAL3 was recruited to the cell front by applying a 488 nm laser near it, as shown by dashed white box. White arrows denote existing older protrusions and pink arrows highlight emerging newer protrusions. Time is shown in min:s format. Scale bars, 5 μm. **I**, Polar histogram demonstrates higher probability of fresh protrusion formation away from RASAL3 recruitment area; *n* = 30 protrusions pooled from 12 cells over three independent replicates. Source numerical data are provided.

Global Ras suppression induces polarity and enhances cell migration

Given the results from Figs. 1 and 2, we expected that ectopic RasGAP expression would strongly inhibit cellular activity and

migration. Notably, inducing C2GAPB expression resulted in a more polarized phenotype (Figs. 1a,b and 3a). Moreover, polarized C2GAPB-expressing cells exhibited accelerated movement compared with control cells expressing empty vector (Fig. 3b,c and



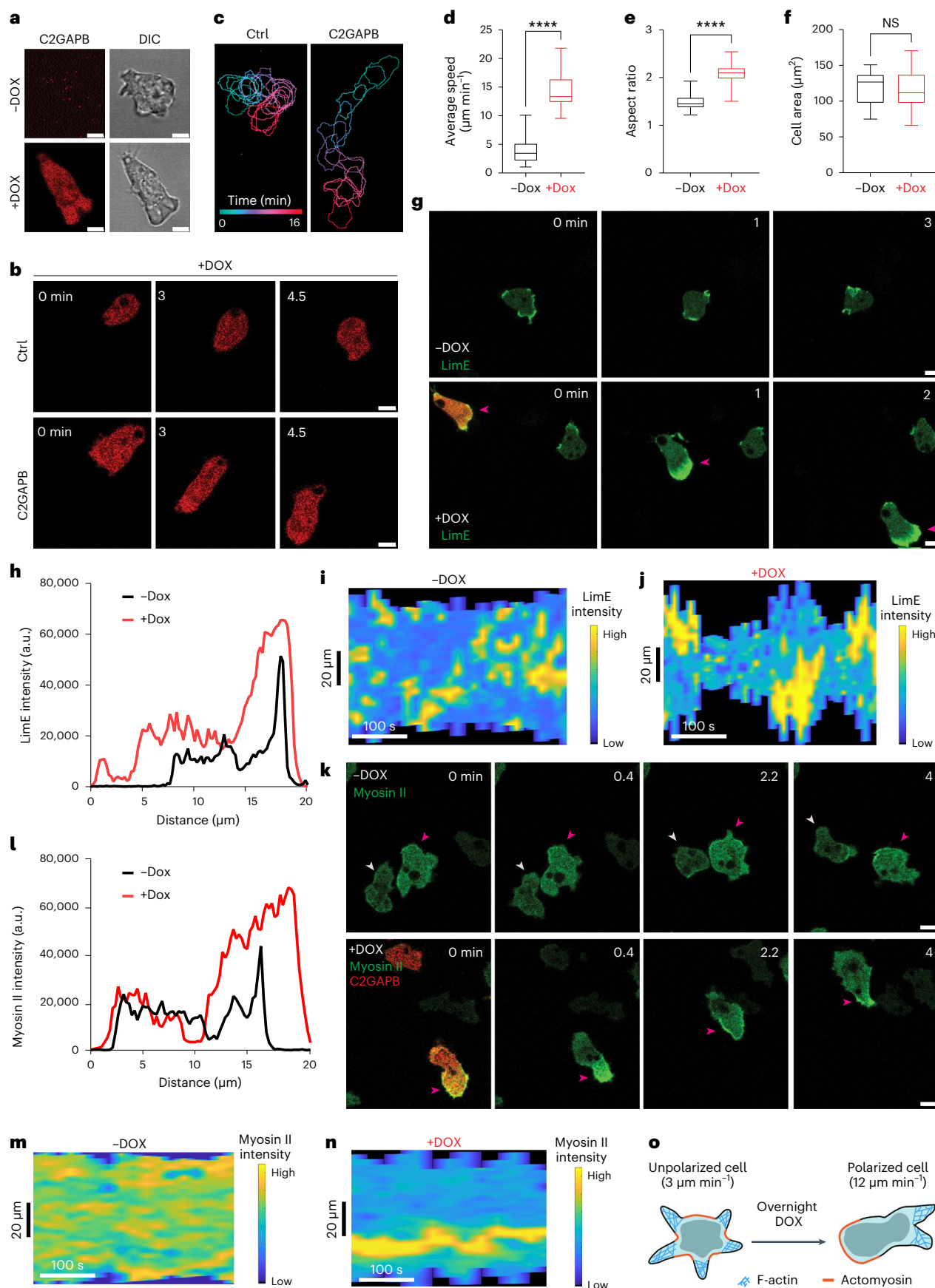


Fig. 3 | C2GAPB expression polarizes *Dictyostelium* and improves random cell migration. **a**, Confocal images demonstrating doxycycline-induced mRFPmars-C2GAPB expression (red) polarize vegetative *Dictyostelium* cell (shown in differential interference contrast; DIC). Scale bars, 5 μm. **b**, Time-lapse confocal images of vegetative *Dictyostelium* cells expressing tgRFp-Tctrl (empty vector control, red; top panel) or mRFPmars-C2GAPB (red; bottom) after overnight Dox treatment. Time is shown in minutes. Scale bars, 5 μm. **c**, Colour-coded (1-min interval) outlines of the Ctrl- or C2GAPB-expressing cell shown in **b**. **d–f**, Box-and-whisker plots of average cell speed (**d**), aspect ratio (**e**) and cell area (**f**) before (black; -DOX) or after (red; +DOX) overnight Dox induction of C2GAPB. $n = 35$ (-Dox) or $n = 34$ (+Dox) cells examined over three independent experiments; asterisks indicate significant difference, *** $P \leq 0.0001$ (**d,e**); NS, not significant, $P = 0.4167$ (**f**) (two-sided Mann-Whitney test). The boxes extend from 25th to 75th percentiles, median is at the centre and whiskers and outliers are graphed

Supplementary Video 9). Quantification revealed a twofold increase in average cell speed and aspect ratio, a proxy for cell polarity, but not basal cell area (Fig. 3d-f). This unexpected C2GAPB-induced polarity was a result of Ras suppression as inducible RasG S17N expression similarly improved polarity and migration (Extended Data Fig. 1c,i,j and Supplementary Video 10).

Wild-type (WT) *Dictyostelium* cells typically displayed multiple, transient, small F-actin fronts, whereas C2GAPB-null cells demonstrated an unpolarized morphology with wide fronts (Fig. 3g and Extended Data Fig. 2a). However, in C2GAPB-expressing cells, there was a single, broad, polarized LimE-rich protrusion persistently localized at the front (Fig. 3g,o). Similarly, C2GAPB expression caused myosin II to localize predominantly at the cell back, whereas a more diffused distribution was generally observed in uninduced cells (Fig. 3k,o). These observations were supported by linescan and kymograph analyses (Fig. 3h-j,l-n). This counterintuitive result could be recapitulated with RasG S17N expression (Extended Data Fig. 2b). Although polarity acquisition is a defining characteristic of *Dictyostelium* differentiation, C2GAPB-induced polarization neither required development nor GPCR signalling. Also, C2GAPB improved polarity and migration in Gβ-null cells, which are typically unpolarized with low motility (Extended Data Fig. 2c,d)^{41,42}.

We next checked whether recruiting C2GAPB to the cell membrane, in closer association with Ras, would exaggerate its polarization effects. We noticed that expressing the recruitable C2GAPB protein, fused to SspB, only moderately induced polarity (Fig. 4b), compared with the native C2GAPB (Figs. 1 and 3). The SspB tag may be responsible for a weaker C2GAPB function, but was not explored here. However, global recruitment of C2GAPB-SspB triggered a robust ‘instant polarization’ response within 1 min, resulting in a twofold increase in average migration speed and aspect ratio, but not basal cell area (Fig. 4a-e and Supplementary Videos 11 and 12). Once the blue laser was switched off, cells reverted to their original morphology within minutes (Fig. 4f-h)

Fig. 4 | Global C2GAPB recruitment polarizes *Dictyostelium* and enhances cell migration. **a**, Cartoon illustrating mechanism of opto-C2GAPB global recruitment on *Dictyostelium* cell membrane with SspB-iLID optogenetic system. **b**, Time-lapse confocal images of vegetative *Dictyostelium* cell expressing tgRFp-SspB R73Q-Ctrl (control without C2GAPB; left) or mRFPmars-SspB R73Q-C2GAPB (right), before or after the 488 nm laser was switched on globally. Colour-coded (1-min interval) outlines of the Ctrl- or C2GAPB-recruited cell (bottom). Time is shown in min:s format. **f**, Colour-coded (1-min interval) outlines of a representative cell in presence of intermittent 488 nm light. Scale bars, 10 μm. **c–e,g,h**, Box-and-whisker plots of average cell speed (**c,g**), aspect ratio (**d,h**) and cell area (**e**), before (black) or after (red) C2GAPB global recruitment. For plots in **g** and **h**, the laser was switched on or off multiple times. The boxes extend from 25th to 75th percentiles, median is at the centre, and whiskers and outliers are graphed according to Tukey’s convention. Connecting lines are provided between paired data points obtained from the same cell, before or after C2GAPB recruitment (GraphPad Prism 8). $n = 24$ opto-C2GAPB-expressing cells

according to Tukey’s convention (GraphPad Prism 8). Time is shown in min:s format. Scale bars, 5 μm. **g,k**, Time-lapse confocal images of vegetative *Dictyostelium* cells expressing GFP-LimE_{Δcoil} (LimE, F-actin biosensor; green) (**g**) or myosin II-GFP (green) (**k**), before (-DOX) and after (+DOX) overnight Dox induction of C2GAPB (red; not shown here). White or pink arrows denote cells of interest. Time is shown in minutes. Scale bars, 5 μm. **h,l**, Representative linescan of LimE (**h**) or myosin II (**l**) intensity of cells in **g** or **k**, respectively. **i,j,m,n**, Representative kymograph of cortical LimE (**i,j**) or myosin II (**m,n**) intensity in cells in **g** or **k**, respectively. A linear colour map shows that blue is the lowest LimE or myosin II intensity and yellow is the highest. **o**, Cartoon summarizing the polarizing effects of expressing C2GAPB in *Dictyostelium*. Unpolarized cells with small, transient protrusions become polarized with a distinct F-actin front and a myosin II-labelled back after C2GAPB is expressed. Source numerical data are provided.

and Supplementary Video 12). There were several F-actin-rich fronts in unrecruited cells (‘00:00’ in Fig. 4i). C2GAPB recruitment first reduced LimE signals everywhere on the membrane, then as the cell polarized, a single and persistent actin polymerization site grew at the leading front (Fig. 4i,j). We also successfully polarized Gβ-null cells with C2GAPB recruitment (Extended Data Fig. 2e and Supplementary Video 13).

Alternatively, globally recruiting RasG S17N ΔCAAX caused *Dictyostelium* to polarize and migrate rapidly whereas recruiting empty vector did not induce any change (Extended Data Fig. 3a-e, Fig. 4b and Supplementary Video 14). Although, these effects were relatively milder compared with C2GAPB recruitment, both showed a similar trend. In neutrophils, KRas4B S17N ΔCAAX recruitment formed a long uropod, localized protrusions at the front, and improved migration. Non-recruiting cells had multiple, transient smaller protrusions and did not move much (Extended Data Fig. 3f-m and Supplementary Video 15).

Next, we validated these C2GAPB-induced effects on LimE wave patterns on the basal surface of electrofused cells. Like single cells, expressing recruitable C2GAPB modestly affected wave patterns (Fig. 4k). However, upon recruitment, F-actin waves largely disappeared throughout the cell, except for one region on the basal membrane where the LimE signal remained strong and did not propagate (Fig. 4k,l and Supplementary Video 16). Thus, our data shows that both signalling and cytoskeletal waves are largely extinguished but cytoskeletal activity remains persistently confined to one location on the membrane, presumably indicating sustained polarity.

It is well established that response of growth-stage amoebae to folic acid is slow and less efficient, presumably due to their unpolarized morphology and transient protrusions^{43,44}. We therefore assessed whether C2GAPB-induced polarization could improve folic acid chemotaxis. Within 5 min of setting up a folic acid gradient, C2GAPB-expressing cells polarized and moved persistently towards the source, whereas non-expressing cells in the same population hardly moved (Extended Data Fig. 4 and Supplementary Video 17).

examined over three independent experiments; asterisks indicate significant difference, *** $P \leq 0.0001$ (**c,d,g,h**); NS, not significant, $P = 0.1011$ (**e**), $P = 0.7257$ (**g**), $P = 0.0557$ (**h**) (two-sided Wilcoxon signed-rank test). **i**, Time-lapse confocal images of vegetative *Dictyostelium* single cells co-expressing mRFPmars-SspB R73Q-C2GAPB (top) and LimE-YFP (middle) after the 488 nm laser was switched on globally. LimE patches are highlighted with pink arrows. ‘00:00’ is considered as the control time point as C2GAPB has not been recruited yet. DIC channel (bottom) shows change in cell polarity with C2GAPB recruitment. Time is shown in min:s format. Scale bars, 5 μm. **j**, Cartoon illustrates the phenomenon in cell in **i**. **k**, Time-lapse confocal images of electrofused *Dictyostelium* giant cells co-expressing mRFPmars-SspB R73Q-C2GAPB (top; red) and LimE-YFP (bottom; yellow) before or after the laser was switched on globally. White arrows highlight C2GAPB recruitment in the red channel and pink arrows denote LimE propagating waves near the bottom cell surface. Time is shown in min:s format. Scale bars, 10 μm. **l**, Cartoon illustrates phenomenon in giant cell in **k**. Source numerical data are provided.

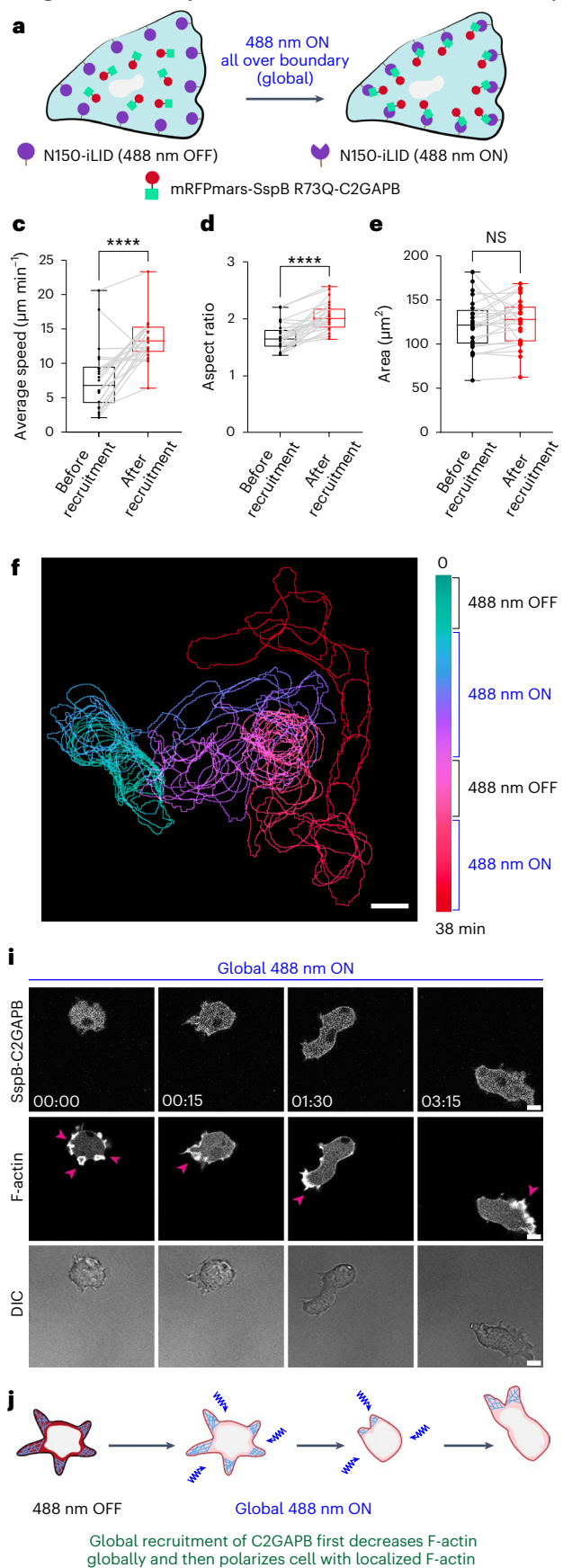
Q12

Q13

Ras attenuation at the cell rear leads to even stronger polarization

Previously, we showed that recruiting RASAL3 to the front in neutrophils extinguished mature protrusions and made the cells move away

(Fig. 2k,l). When we continued to extinguish any new protrusions, the cell rounded up completely and did not move (Fig. 5a). However, once we stopped, the cell continued to move away persistently from the last recruitment area (Fig. 5a,b and Supplementary Video 18). Notably,



Global recruitment of C2GAPB converts multiple F-actin waves into a stable non-propagating wave

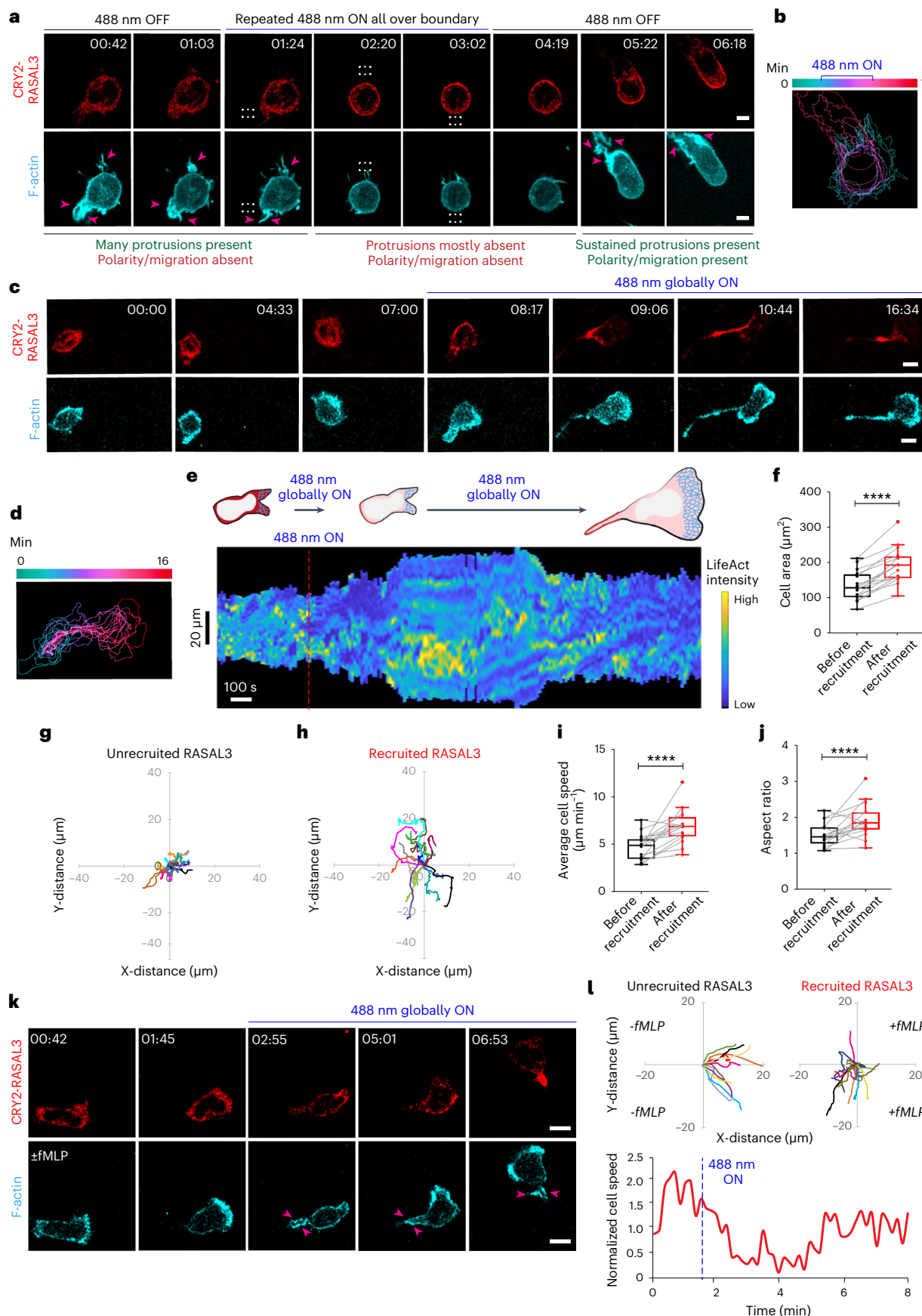


Fig. 5 | Localization of recruited RASAL3 to the back of the neutrophil led to even stronger polarization. **a**, Time-lapse confocal images of differentiated HL-60 neutrophil expressing CRY2PHR-mCherry-RASAL3 (red; top) and LifeAct-miRFP703 (cyan; bottom). Unpolarized, non-migratory neutrophil, post-RASAL3 recruitment over the entire periphery, caused the cell to shrink and protrusions disappeared. Once the laser was off, RASAL3 self-arranged to the back causing the cell to polarize and migrate. Pink arrows highlight protrusions. The region of illumination is shown by the dashed white box. Time is shown in min:s format. Scale bars, 5 μm. **b**, Colour-coded (1-min intervals) outlines of cell in **a**. **c**, Time-lapse confocal images of neutrophil expressing CRY2PHR-mCherry-RASAL3 (red; top) and LifeAct-miRFP703 (cyan; bottom), before or after the laser was switched on globally. Time is shown in min:s format. Scale bars, 5 μm. **d**, Colour-coded (1-min intervals) outlines of cell in **c**. **e**, Representative kymograph of cortical LifeAct intensity before or after RASAL3 recruitment. Linear colour map shows that blue is the lowest LifeAct intensity and yellow is the highest. Duration of kymograph is 24 min. Cartoon depicts recruitment, F-actin polymerization or cell shape corresponding to the kymograph. **f,j**, Box-and-whisker plots

of cell area (**f**), cell speed (**i**) and aspect ratio (**j**), before (black) or after (red) recruitment. $n = 16$ cells examined over three independent experiments; asterisks indicate significant difference, *** $P \leq 0.0001$ (two-sided Wilcoxon signed-rank test). Boxes extend from 25th to 75th percentiles, median is at the centre and whiskers and outliers are graphed according to Tukey's convention. Connecting lines are provided between paired data points obtained from the same cell, before or after RASAL3 recruitment (GraphPad Prism 8). **g,h**, Centroid tracks ($n = 15$ cells examined over three independent experiments) showing random motility before (**g**) or after (**h**) recruitment. Each track lasts 5 min and was reset to same origin. **k**, Time-lapse images of neutrophil expressing CRY2PHR-mCherry-RASAL3 (red; top) and LifeAct-miRFP703 (cyan; bottom) placed in a fMLP gradient before or after the laser was switched on. Pink arrows denote uropod in recruited cell. Time is shown in min:s format. Scale bars, 5 μm. **l**, Centroid tracks of chemotaxing neutrophils ($n = 11$ cells examined over three independent experiments) before or after RASAL3 recruitment. Each track lasts 2 min and was reset to same origin. Normalized speed of cell shown in **k**. Source numerical data are provided.

RASAL3 simultaneously rearranged itself to the back region, presumably dragging the CIBN-CAAX membrane anchor with it. The previously non-polarized, migration-incompetent cell now had a stable back and a sustained front, which allowed it to migrate (Fig. 5a,b).

This spontaneous 'back' rearrangement of RASAL3 made it necessary to repeatedly extinguish new fronts to prevent cell movement, as when RASAL3 was globally recruited over the entire cell periphery, it rapidly localized to the rear and polarized the cell. This self-arranged back localization was dependent on cytoskeletal dynamics (Extended Data Fig. 5a,b) and was mediated through C-terminal tail of RASAL3 (Extended Data Fig. 5c–e). Due to this strong back localization, neutrophils developed long adhesive uropods at RASAL3-enriched regions, became highly polarized and migrated (Fig. 5c,d and Supplementary Video 19). Although F-actin levels increased at the front with RASAL3 recruitment, they did not seem to be as high when activated Ras/RasGEF was recruited (Fig. 5c,e)⁴. Across the population, RASAL3-recruited cells moved more extensively with a 1.4-fold increase in average speed. Recruitment also induced a 1.44- and 1.26-fold improvement in cell area and polarity, respectively (Fig. 5f–j). The GAP domain fused to its C-terminal tail was responsible for these effects (Extended Data Fig. 5f–h). No such change was observed when only the CRY2PHR component was recruited (Extended Data Fig. 5i–k and Supplementary Video 20; also Fig. S3H–N in ref. 4). Similarly, when we recruited C2GAPB or RasG S17N ΔCAAX to the *Dictyostelium* rear, the cells moved away (Extended Data Fig. 6a–c). Adding to the generality of these findings, RASAL3 back recruitment polarized differentiated macrophages to migrate rapidly (Extended Data Fig. 6d and Supplementary Video 21).

Next, we explored the role of RASAL3-mediated polarization in neutrophil chemotaxis. Cells moving along a fMLP gradient, upon RASAL3 recruitment, contracted and shrank immediately. After a few seconds, cells formed distinct tails, repolarized and migrated in random directions, typically away from the attractant gradient (Fig. 5k,l and Supplementary Video 22). Eventually, these RASAL3-polarized cells turned and resumed migration towards the attractant source and moved similarly to unrecruited cells (Extended Data Fig. 6e,f and Fig. 5l). In summary, Ras suppression improves chemotaxis to folic acid in *Dictyostelium*, whereas in neutrophils, it initially blocks chemotaxis but then has little additional effect. These differential effects may be explained by the fact that amoebae are not strongly polarized by folic acid so an increase in polarity is beneficial, whereas as neutrophils are strongly polarized by fMLP, a further increase in polarity has minimal effect.

RasGAP-induced polarization is accompanied by rear actomyosin contractility

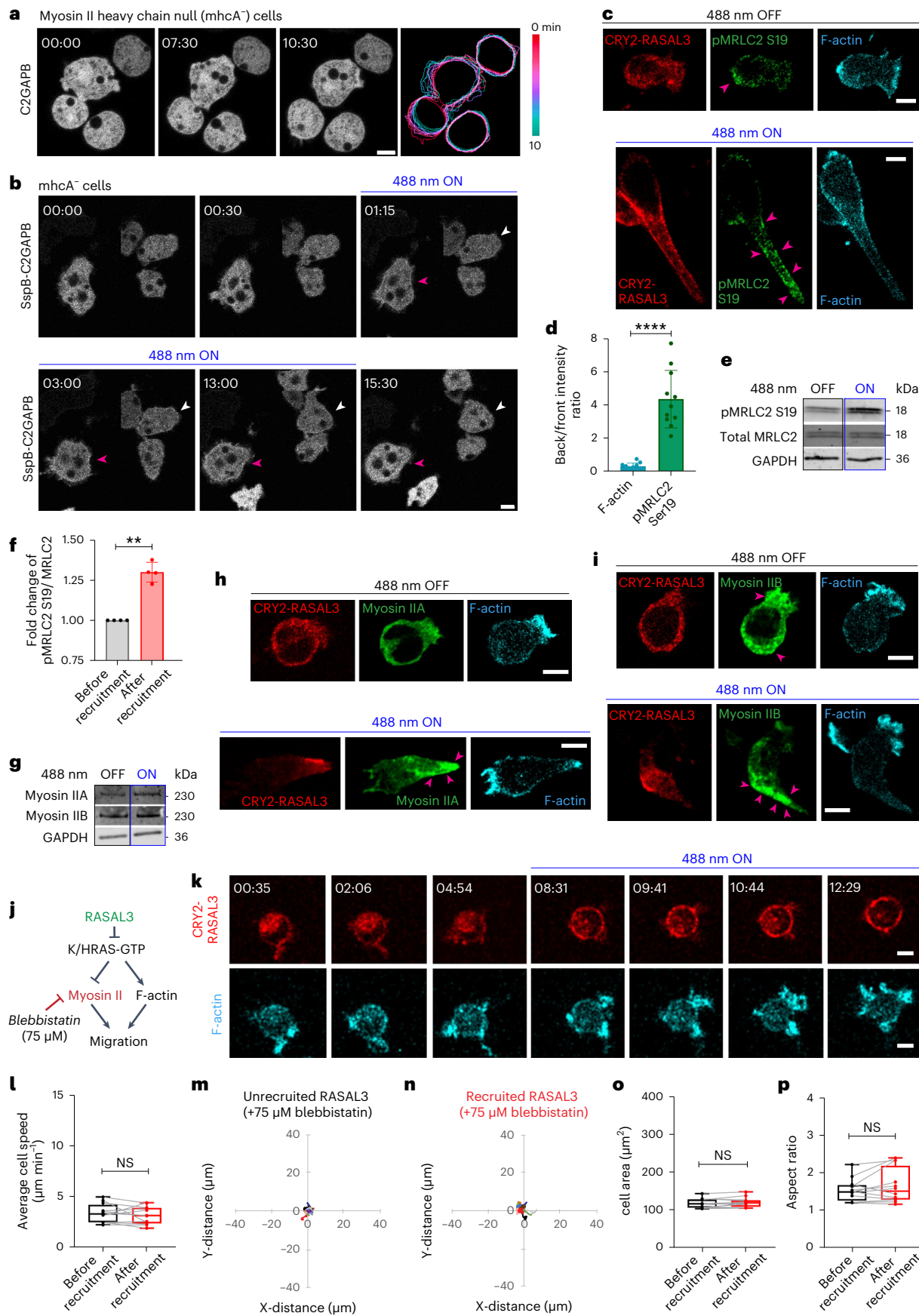
We next assessed whether the RasGAP-induced protrusions required Arp2/3-mediated actin. We used Arp2/3 inhibitor, CK666, which completely removed protrusions in neutrophils (Extended Data Fig. 6g)⁴. When recruited RASAL3 localized to the back, notably, the CK666-treated cells made long, thin protrusions that did not display LifeAct biosensor at the tips. Rather, the biosensor seemed to be along the lateral edges of these narrow protrusions (Extended Data Fig. 6g,h). Similarly, long blebs were induced upon C2GAPB expression in CK666-treated *Dictyostelium* cells, but not in control cells

Fig. 6 | RasGAP-mediated polarization is accompanied by actomyosin contractility at the back. **a**, Time-lapse images of vegetative mhCA⁺ *Dictyostelium* expressing mRFPmars-C2GAPB post-Dox treatment, with colour-coded (1-min interval) outlines. Time is shown in min:s format. Scale bars, 5 μm. **b**, Time-lapse images of mhCA⁺ *Dictyostelium* expressing opto-C2GAPB, before or after recruitment. White and pink arrows denote cells of interest. Time is shown in min:s format. Scale bars, 5 μm. **c,h,i**, Immunofluorescence images of neutrophil expressing CRY2PHR-mCherry-RASAL3 (red) and LifeAct-miRFP703 (cyan) and stained with anti-phospho-MRLC2 Ser19 (**c**) anti-myosin IIA heavy chain (**h**) or anti-myosin IIB heavy chain (**i**), before or after recruitment. Pink arrows denote MRLC2 phosphorylation or myosin IIA/B enrichment. Scale bars, 5 μm. **d**, Bar graph showing back-front intensity ratio of F-actin and myosin phosphorylation in **c**. Data are presented as mean ± s.d. $n = 11$ cells examined over three independent experiments; asterisks indicate significant difference, *** $P \leq 0.0001$ (two-sided Mann–Whitney test). **e,g**, Immunoblot comparing phospho-MRLC2 Ser19 (18 kDa; **e**) or myosin IIA/B (230 kDa, $n = 2$ independent experiments; **g**) in the opto-RASAL3-expressing population, before or after recruitment. GAPDH (36 kDa) was the loading control. **f**, Densitometric analysis of fold change of phospho-MRLC2 Ser19 level in population in **e**. $n = 4$

independent experiments; asterisks indicate significant difference, ** $P \leq 0.0024$ (two-sided unpaired *t*-test). Data are presented as mean values ± s.d. **j**, Strategy for testing effects of blebbistatin on RASAL3-mediated actomyosin contraction and migration. **k**, Time-lapse images of blebbistatin-treated neutrophil expressing CRY2PHR-mCherry-RASAL3 (red; top) and LifeAct-miRFP703 (cyan; bottom), before or after recruitment. Time is shown in min:s format. Scale bars, 5 μm. **l,o,p**, Box-and-whisker plots of cell speed (**l**), cell area (**o**) and aspect ratio (**p**), before (black) or after (red) recruitment. $n = 12$ cells examined over three independent experiments; NS, not significant, $P = 0.3013$ (**l**), $P = 0.1763$ (**o**), $P = 0.2334$ (**p**) (two-sided Wilcoxon signed-rank test). Boxes extend from 25th to 75th percentiles, median is at the centre and whiskers and outliers are graphed according to Tukey's convention. Connecting lines are provided between paired data points obtained from the same blebbistatin-treated cell, before or after RASAL3 recruitment (GraphPad Prism 8). **m,n**, Centroid tracks of blebbistatin-treated cells ($n = 11$ cells examined over three independent experiments) showing motility before (**m**) or after (**n**) recruitment. Each track lasts 5 min and was reset to the same origin. Source numerical data and unprocessed western blots are provided.

without C2GAPB (Extended Data Fig. 6i,j). These data suggest that RasGAP-induced protrusions at the front are mediated, at least in part, by increased contraction at the rear.

To test whether contraction was mediated by actomyosin, we induced C2GAPB expression in myosin II heavy chain-null (*mhcA*⁻) mutant of *Dictyostelium*. The *mhcA*⁻ cells are generally flattened,



Q14

unpolarized and multinucleated^{45,46}. C2GAPB expression had little effect on improving this existing phenotype (Fig. 6a). Furthermore, C2GAPB recruitment also failed to polarize *mhcA⁻* cells (Fig. 6b). Similarly, in C2GAPB-recruited polarized cells, blebbistatin (myosin II inhibitor) treatment diminished polarity although it was not as effective as complete loss of myosin in *mhcA⁻* cells (Extended Data Fig. 7a)⁴⁷.

Is Ras suppression-mediated actomyosin contractility necessary for neutrophil polarization? Upon RASAL3 recruitment, phosphorylated myosin regulatory light chain 2 (MRLC2) was highly enriched at the uropod, across the cell population (Fig. 6c–f). Although myosin II expression remained unaltered, RASAL3 recruitment strongly localized myosin IIA and IIB isoforms to the cell rear (Fig. 6g–i). Additionally, treatment with blebbistatin resulted in complete loss of cell movement and polarity which could not be recovered with RASAL3 recruitment (Fig. 6j–p, Extended Data Fig. 7b and Supplementary Video 23)⁴⁸. Notably, in the presence of a suboptimal dose of blebbistatin, once RASAL3 was recruited, it moved to a particular region, which became the new back. This local Ras suppression could overcome low blebbistatin inhibition, increased contraction and polarized cells to move (Extended Data Fig. 7c–k and Supplementary Video 24).

Treating neutrophils with low doses of ROCK inhibitor, Y-27632 (ref. 49), reduced myosin II phosphorylation but did not completely abolish it. Although basal motility was stalled, RASAL3 recruitment to the back mostly overcame the effects. RASAL3-recruited cells polarized and migrated due to increased myosin phosphorylation and rear contraction (Extended Data Fig. 8a–f and Supplementary Video 25). However, once treated with a higher Y-27632 dose⁵⁰, which abolished myosin phosphorylation completely, RASAL3 back recruitment was unable to polarize cells (Extended Data Fig. 8l–u and Supplementary Video 26). Altogether, ROCK-mediated myosin IIA and IIB activity generates contraction at the neutrophil rear in response to Ras attenuation. Additionally, the effects of Ras suppression on actomyosin in *Dictyostelium* and neutrophils are similar.

RASAL3 induces mTORC2-mediated actin polymerization at the front

Back localization of recruited RASAL3 induced F-actin to localize to a stable front, which caused neutrophils to polarize and migrate persistently (Fig. 5c–j). To confirm that RASAL3 at the back is directly affecting protrusive activity at the front, we pharmacologically targeted the front signalling pathways before recruiting RASAL3. First, we inhibited PI3K–PIP3 signalling using the pan-PI3K inhibitor, LY294002, which stalled neutrophil polarity and basal motility (Fig. 7a,b)⁴. Within 5 min of applying blue light, RASAL3 moved to the back of LY294002-treated cells and polarized them to move by generating broad F-actin-rich lamellipodium but without an appreciable uropod (Fig. 7b,c,f,g and Supplementary Video 27). A kymograph showed that LifeAct signal increased considerably, along with increase in cell area (Fig. 7d). RASAL3 recruitment caused 1.75-, 1.49- or 1.43-fold improvement in cell speed, basal area or aspect

ratio (Fig. 7e,h,i). Similarly, RASAL3 recruitment polarized PI3K^y inhibitor-treated cells for migration (Extended Data Fig. 9 and Supplementary Video 28)^{4,51}.

Next, we inhibited mTORC2 signalling with PP242 (Fig. 7j)⁵². Inhibitor treatment caused cells to round up (Fig. 7k)^{4,53}. Once RASAL3 was recruited to the back, PP242-treated cells displayed weak, intermittent polarity causing them to move slightly, but not persistently (Fig. 7k,l,o,p and Supplementary Video 29). Although we noticed a 1.3-fold improvement in average speed, we did not see significant change in cell area or polarity (Fig. 7m,n,q,r).

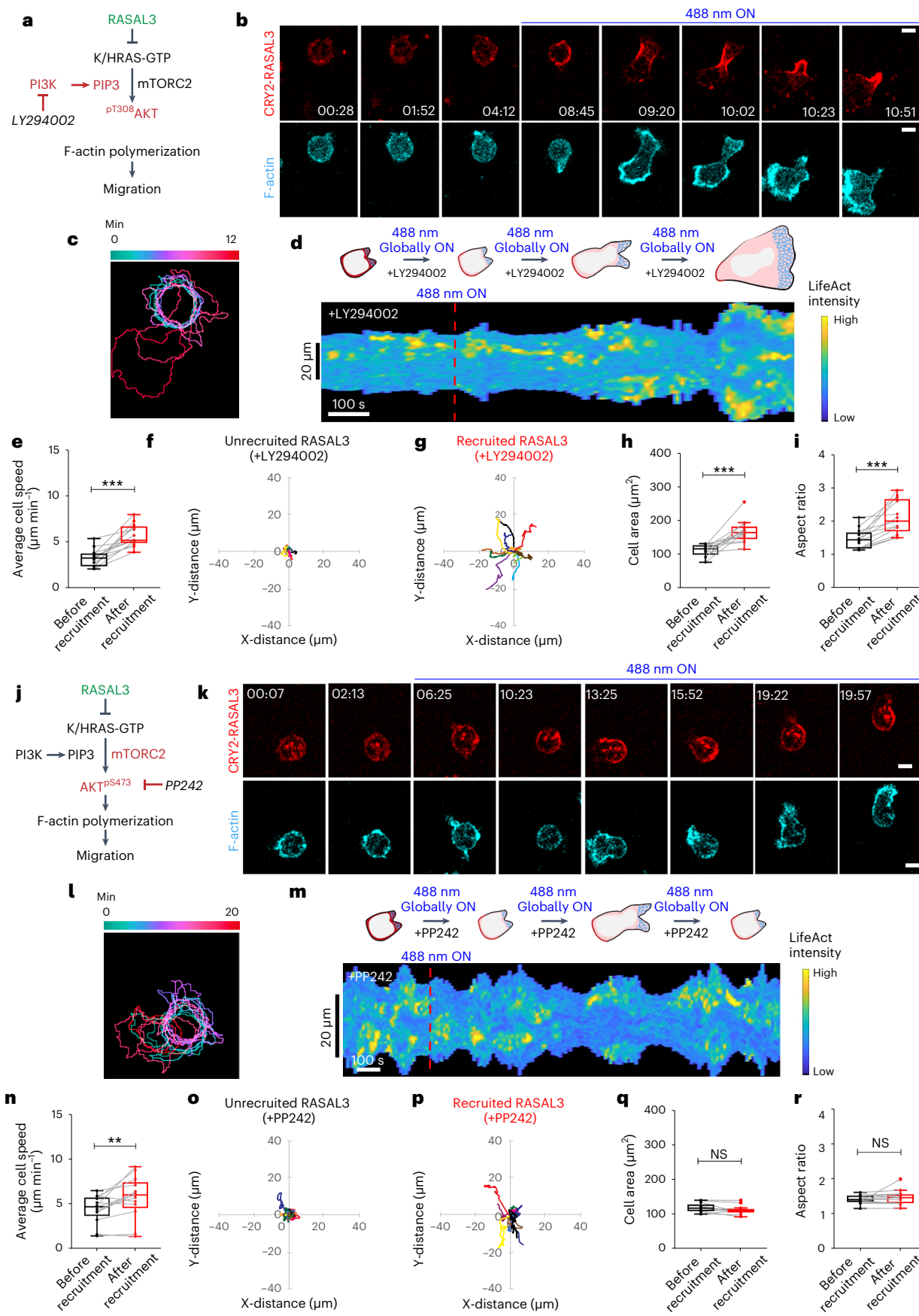
Model can explain counterintuitive effects of reducing Ras activity on cell polarization

To understand the role of counterintuitive effects of the RasGAPs, we turned to a legacy model of the excitable network that has successfully recreated cell migratory and ventral wave behaviour^{37,54–56} and incorporated the new information from this experimental study (Fig. 8a). In the model, complementary inhibition between Ras and PIP2 acts as a positive feedback loop^{11,57} and a competing negative feedback loop involves Ras and PKB^{37,57} (Fig. 8a). These three elements form the core of the signal transduction excitable network. We incorporated two further cytoskeleton-dependent feedbacks to capture the polarization that is observed over time^{54,58}. There is a front-promoting loop from PKB through branched actin to Ras. There is a back-promoting loop that involves PIP2 and myosin, which increases RasGAP activity and, in turn, inhibits Ras. Model simulations displayed characteristic excitable behaviour, including propagating waves that annihilate when they meet (Fig. 8b and Supplementary Video 30). We next modelled the effect of increasing/decreasing RasGAP activity as changes in inhibition rate of Ras activity, thus altering the activation threshold of the excitable system (Fig. 8c and Extended Data Fig. 10a–c). Whereas simulations in which RasGAP was reduced showed increased Ras activity and resulted in large, fast waves compared with WT levels of RasGAP, those with increased RasGAP showed small, slow waves (Fig. 8b, Extended Data Fig. 10d and Supplementary Video 30). The two-dimensional simulations described above model the basal surface of electrofused cells. Experimentally, we only increased RasGAP, which reduced Ras activity and wave size or speed, as did the model (Fig. 8b). These observations were quantitated by summing all Ras activity throughout the simulations (Fig. 8d). In simulations of a single cell, in which activity is measured along the perimeter (Fig. 8e), we saw high spontaneous activity all around the perimeter before changes in RasGAP level. Halfway through the simulation, RasGAP activity was increased leading to an overall decrease in Ras activity. Thereafter, single streaks representing one or two stationary waves appeared in the kymograph (Fig. 8e). A heatmap of Ras and PKB activity showed much lower activity after GAP addition (Fig. 8f and Extended Data Fig. 10e). Simulations also considered the effect of GAP addition on cell movement (Methods). Without RasGAP, cells showed high activity but moved minimally from their initial location. After GAP addition, the kymograph showed less

Fig. 7 | RASAL3 polarizes cells by localizing actin polymerization at the front through mTORC2. **a,j**, Strategy for testing effects of pan-PI3K inhibitor, LY294002 (a) or mTOR inhibitor, PP242 (j) on RASAL3-directed actin polymerization and motility. **b,k**, Time-lapse confocal images of LY294002-treated (b) or PP242-treated (k) HL-60 neutrophil expressing CRY2PHR-mCherry-RASAL3 (red; top) and LifeAct-miRFP703 (cyan; bottom), before or after 488 nm laser was turned on globally. Time is shown in min:s format. Scale bars, 5 μm. **c,l**, Colour-coded (1-min intervals) outlines of cells in b and k, respectively. **d,m**, Representative kymographs of cortical LifeAct intensity in LY294002- (d) or PP242-treated (m) RASAL3-expressing neutrophil before or after laser was turned on. A linear colour map shows that blue is the lowest LifeAct intensity whereas yellow is the highest. Duration of the kymographs are 12 and 20 min, respectively. Cartoons depict recruitment, actin polymerization or cell shape corresponding to the kymographs. **e,h,i,n,q,r**, Box-and-whisker plots of cell speed (e,n), cell area

(h,q) and aspect ratio (i,r), before (black) and after (red) RASAL3 recruitment in LY294002- or PP242-treated cells. **e,h,i,n,q,r** $n = 13$ LY294002- or PP242-treated cells examined over three independent experiments; asterisks indicate significant difference, *** $P = 0.0002$ (e,h,i), ** $P = 0.0081$ (n); NS, not significant, $P = 0.0574$ (q), $P = 0.5417$ (r) (two-sided Wilcoxon signed-rank test). The boxes extend from 25th to 75th percentiles, median is at the centre and whiskers and outliers are graphed according to Tukey's convention. Connecting lines are provided between paired data points obtained from the same LY294002- or PP242-treated cell, before or after RASAL3 recruitment (GraphPad Prism 8). **f,o,g,p**, Centroid tracks of LY294002- or PP242-treated neutrophils ($n = 12$ cells examined over three independent experiments) showing random motility before (f,o) or after (g,p) recruitment. Each track lasts 5 min and was reset to same origin. Source numerical data are provided.

activity, but greater polarization and the trajectories displayed greater dispersion (Fig. 8g and Extended Data Fig. 10f,g). In the kymograph of actomyosin response, we saw multiple streaks of myosin activity along the perimeter before GAP addition. However, after GAP addition, myosin was uniform except for the single cell front (Fig. 8h and Extended Data Fig. 8h).



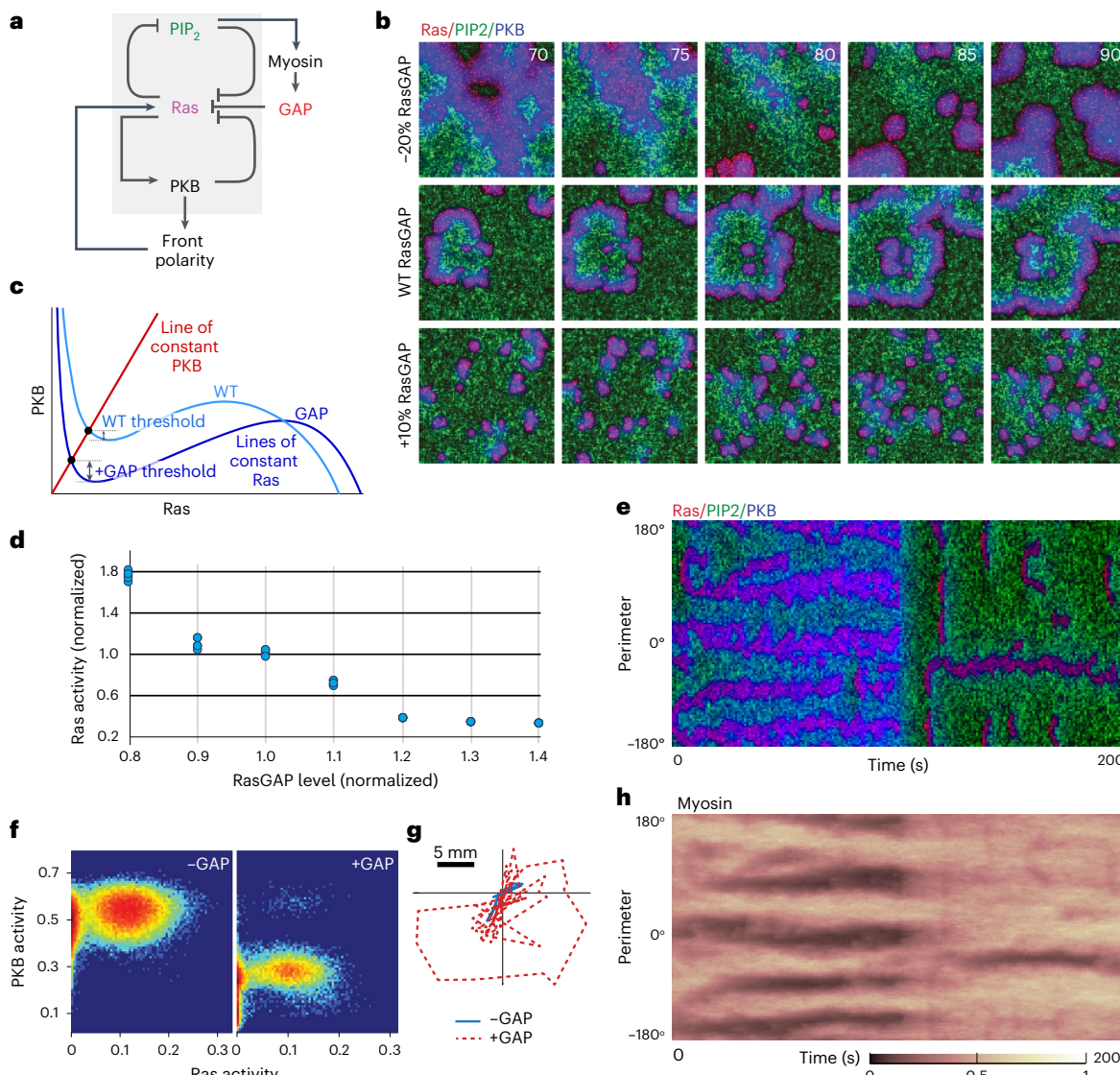


Fig. 8 | STEN simulations show that increasing RasGAP reduces Ras activity, but cells still polarize. **a**, Schematic of the signal transduction excitable network and feedback loops regulating cell polarity. GAP hydrolyses active RasGTP to inactive RasGDP. GAP is part of the back-mediated loop because this inhibition increases Ras inactivation rate. Based on many experimental observations, the interactions shown summarize the invariable direction of movement of the activities and concentrations of components and are not meant to convey direct interactions and are representative of a series of back effectors that behave similarly. **b**, With WT RasGAP levels, EN firings were seen and generated waves of high Ras activity (red) moving at $\sim 10 \mu\text{m min}^{-1}$ and absence of PiP2 (green). The wave trailing edge was marked by high PKB (blue). While lowering RasGAP by 20% increased wave size (~50%) and speed (~100%), a 10% increase had the opposite effect: firings were still seen, but waves broke up frequently and were smaller (~75%) and slower (~40%). The simulation denotes a square where each side is $40 \mu\text{m}$; time is in seconds. **c**, Cartoon of the phase-plane diagram of the Ras-PKB EN showing curves on which Ras and PKB stay constant, the equilibrium (black circle) and activation threshold of two EN systems, representing WT and lowered GAP conditions. The latter has a larger threshold. **d**, Total Ras level over the simulations ($n = 5$ for each condition) for varying RasGAP from 80–140% of WT levels. After ~30% increase in RasGAP, no firings were observed and hence the Ras level plateaus. **e**, Kymograph of one-dimensional simulations representing perimeter of smaller cells represented by an environment in which RasGAP strength was increased 50% halfway during the simulation. **f**, Two-dimensional histograms showing total activity across cell perimeter in the Ras-PKB phase plane for 70 s each for WT conditions and after increasing GAP by 50% ($n = 10$). **g**, Trajectory of the centre-of-mass of a single cell across a 100-s time interval before and after GAP recruitment. **h**, Kymographs of normalized myosin species corresponding to the cell in **e**. Myosin appears in high PiP2 regions showing a positive correlation between the two species.

Ras-PKB EN showing curves on which Ras and PKB stay constant, the equilibrium (black circle) and activation threshold of two EN systems, representing WT and lowered GAP conditions. The latter has a larger threshold. **d**, Total Ras level over the simulations ($n = 5$ for each condition) for varying RasGAP from 80–140% of WT levels. After ~30% increase in RasGAP, no firings were observed and hence the Ras level plateaus. **e**, Kymograph of one-dimensional simulations representing perimeter of smaller cells represented by an environment in which RasGAP strength was increased 50% halfway during the simulation. **f**, Two-dimensional histograms showing total activity across cell perimeter in the Ras-PKB phase plane for 70 s each for WT conditions and after increasing GAP by 50% ($n = 10$). **g**, Trajectory of the centre-of-mass of a single cell across a 100-s time interval before and after GAP recruitment. **h**, Kymographs of normalized myosin species corresponding to the cell in **e**. Myosin appears in high PiP2 regions showing a positive correlation between the two species.

Discussion

Our optogenetic study on RasGAPs, C2GAPB and RASAL3, expressed in *Dictyostelium* and leucocytes, respectively, yielded significant insights. Notably, locally dampening Ras activity could extinguish cellular protrusions, reverse pre-existing polarity and impede migration. However, contrary to expectations, a global reduction in Ras activity heightened both polarity and motility. Furthermore, in *Dictyostelium*, targeting C2GAPB to the cell back amplified migration and polarity, whereas in neutrophils and macrophages, spontaneous movement of RASAL3 to

the back-generated uropods and localized F-actin protrusions at the front. Thus, polarity could be regulated by manipulating Ras activity along the membrane and, therefore, a cell must maintain an optimum Ras level to achieve directed migration. Although Ras and its downstream pathways are typically associated with longer-term growth control, our studies establish an immediate and evolutionarily conserved role in cell polarity and motility.

The counterintuitive effect of Ras suppression in promoting polarity can be understood by including a ‘back-promoting’ loop

to our pre-existing model. Ras plays a central role in regulating two strong opposing feedback loops consisting of molecules, such as myosin and PI(4,5)P₂ that typically form the back, and PIP3 and F-actin that generate the front (Fig. 8)^{8,11,18,22,23}. Our observation on the effects on RBD/PHcrac wave activity with RasGAP strongly suggests that reducing Ras activity raises the activation threshold of the system. The increased threshold causes the broad, propagating cortical waves to break up into smaller, short-lived waves in electro-fused cells. Analogously, in single cells, RasGAPs suppress multiple, co-existing protrusions all around the periphery and confine them to a single protrusion. Obviously, if all protrusions were shut down that would block migration, which we were able to achieve in the model. However, this was not accomplished experimentally, presumably because our RasGAPs were not strong enough to raise the activation threshold enough.

Previous studies have suggested that increases in actomyosin contraction at the back, occurring spontaneously or locally triggered by optogenetic RhoA or RGS4, can initiate polarity and cause cells to move away^{50,59–62}. Contraction-driven migration also occurs through Ras/ERK-mediated myosin light chain kinase activation and subsequent MRLC phosphorylation⁶³. We demonstrate that spatiotemporal regulation of Ras signalling pathways not only controls F-actin protrusive activity at the front, but also directly coordinates non-muscle myosin II-dependent contraction at the back. In neutrophils, contraction possibly works through ROCK-mediated MRLC2 phosphorylation. Even when Arp2/3 was inhibited, the ability of back suppression to polarize a cell was indicated. Without F-actin, instead of making normal protrusions, suppressing Ras activity at the back caused formation of long bleb-like structures.

In addition to increasing contractility at the back, Ras inhibition at the back triggered increased F-actin polymerization at the front. We noted that while inhibitors of signalling downstream of Ras suppressed protrusions and stopped cells from moving, this could be partially overcome by recruiting RasGAP to the rear. These RasGAP-mediated long-range effects on the cell front were mediated primarily through mTORC2, rather than PI3K/PIP3. Traditionally, these possibilities have been difficult to distinguish as conventional chemotactic gradient studies lack sufficient spatiotemporal resolution to determine the chronology of front and back formation during symmetry breaking^{60,62,64}. However, we showed that back suppression triggers polarization, which simultaneously activates the front.

Our findings have important implications for cancer treatment, where targeting Ras may not always be beneficial. Caution must be exercised to avoid, while attempting to abrogate cell proliferation, forcing cells into a more polarized migratory state. The increased migration could induce cells to exit the epithelium and metastasize. Consistently, it is well known that metastasizing cells do not readily divide^{65–67}. A deeper understanding of the different roles that Ras plays in cell migration versus growth is essential for developing therapeutic strategies.

Online content

Any methods, additional references, Nature Portfolio reporting summaries, source data, extended data, supplementary information, acknowledgements, peer review information; details of author contributions and competing interests; and statements of data and code availability are available at <https://doi.org/10.1038/s41556-024-01453-4>.

References

- Kolch, W., Berta, D. & Rosta, E. Dynamic regulation of RAS and RAS signaling. *Biochem. J.* **480**, 1–23 (2023).
- Prior, I. A., Lewis, P. D. & Mattos, C. A comprehensive survey of Ras mutations in cancer. *Cancer Res.* **72**, 2457–2467 (2012).
- Simanshu, D. K., Nissley, D. V. & McCormick, F. RAS proteins and their regulators in human disease. *Cell* **170**, 17–33 (2017).
- Pal, D. S. et al. Actuation of single downstream nodes in growth factor network steers immune cell migration. *Dev. Cell* **58**, 1170–1188 (2023).
- Sasaki, A. T., Chun, C., Takeda, K. & Firtel, R. A. Localized Ras signaling at the leading edge regulates PI3K, cell polarity, and directional cell movement. *J. Cell Biol.* **167**, 505–518 (2004).
- Kae, H., Lim, C. J., Spiegelman, G. B. & Weeks, G. Chemoattractant-induced Ras activation during Dictyostelium aggregation. *EMBO Rep.* **5**, 602–606 (2004).
- Kortholt, A., Keizer-Gunnink, I., Kataria, R. & Van Haastert, P. J. Ras activation and symmetry breaking during *Dictyostelium* chemotaxis. *J. Cell Sci.* **126**, 4502–4513 (2013).
- Zhang, S., Charest, P. G. & Firtel, R. A. Spatiotemporal regulation of Ras activity provides directional sensing. *Curr. Biol.* **18**, 1587–1593 (2008).
- Devreotes, P. N. et al. Excitable signal transduction networks in directed cell migration. *Annu. Rev. Cell Dev. Biol.* **33**, 103–125 (2017).
- Fukushima, S., Matsuoka, S. & Ueda, M. Excitable dynamics of Ras triggers spontaneous symmetry breaking of PIP3 signaling in motile cells. *J. Cell Sci.* **132**, jcs224121 (2019).
- Li, X. et al. Mutually inhibitory Ras-PI(3,4)P₂ feedback loops mediate cell migration. *Proc. Natl Acad. Sci. USA* **115**, E9125–E9134 (2018).
- Li, X., Miao, Y., Pal, D. S. & Devreotes, P. N. Excitable networks controlling cell migration during development and disease. *Semin. Cell Dev. Biol.* **100**, 133–142 (2020).
- Pal, D. S., Li, X., Banerjee, T., Miao, Y. & Devreotes, P. N. The excitable signal transduction networks: movers and shapers of eukaryotic cell migration. *Int. J. Dev. Biol.* **63**, 407–416 (2019).
- Hennig, A., Markwart, R., Esparza-Franco, M. A., Ladds, G. & Rubio, I. Ras activation revisited: role of GEF and GAP systems. *Biol. Chem.* **396**, 831–848 (2015).
- Insall, R. H., Borleis, J. & Devreotes, P. N. The aimless RasGEF is required for processing of chemotactic signals through G-protein-coupled receptors in *Dictyostelium*. *Curr. Biol.* **6**, 719–729 (1996).
- Suire, S. et al. GPCR activation of Ras and PI3Kc in neutrophils depends on PLC_b2/b3 and the RasGEF RasGRP4. *EMBO J.* **31**, 3118–3129 (2012).
- Xu, X., Wen, X., Moosa, A., Bhimani, S. & Jin, T. Ras inhibitor CAPRI enables neutrophil-like cells to chemotax through a higher-concentration range of gradients. *Proc. Natl Acad. Sci. USA* **118**, e2002162118 (2021).
- Xu, X. et al. GPCR-controlled membrane recruitment of negative regulator C2GAP1 locally inhibits Ras signaling for adaptation and long-range chemotaxis. *Proc. Natl Acad. Sci. USA* **114**, E10092–E10101 (2017).
- Charest, P. G. et al. A Ras signaling complex controls the RasC-TORC2 pathway and directed cell migration. *Dev. Cell* **18**, 737–749 (2010).
- Cai, H. et al. Ras-mediated activation of the TORC2-PKB pathway is critical for chemotaxis. *J. Cell Biol.* **190**, 233–245 (2010).
- Edwards, M. et al. Insight from the maximal activation of the signal transduction excitable network in *Dictyostelium discoideum*. *Proc. Natl Acad. Sci. USA* **115**, E3722–E3730 (2018).
- Xu, X. et al. Membrane targeting of C2GAP1 enables *Dictyostelium discoideum* to sense chemoattractant gradient at a higher concentration range. *Front. Cell Dev. Biol.* **9**, 725073 (2021).
- Xu, X. et al. C2GAP2 is a common regulator of Ras signaling for chemotaxis, phagocytosis, and macropinocytosis. *Front. Immunol.* **13**, 1075386 (2022).
- Bloomfield, G. et al. Neurofibromin controls macropinocytosis and phagocytosis in *Dictyostelium*. *eLife* **4**, e04940 (2015).

- Q26
- 25. Sawada, S. et al. Identification of NF1 mutations in both alleles of a dermal neurofibroma. *Nat. Genet.* **14**, 110–112 (1996).
 - 26. Serra, E. et al. Confirmation of a double-hit model for the NF1 gene in benign neurofibromas. *Am. J. Hum. Genet.* **61**, 512–519 (1997).
 - 27. Khosla, M., Spiegelman, G. B., Insall, R. & Weeks, G. Functional overlap of the *dictyostelium* RasG, RasD and RasB proteins. *J. Cell Sci.* **113**, 1427–1434 (2000).
 - 28. Srinivasan, K. et al. Delineating the core regulatory elements crucial for directed cell migration by examining folic-acid-mediated responses. *J. Cell Sci.* **126**, 221–233 (2013).
 - 29. Wilkins, A. et al. *Dictyostelium* RasD is required for normal phototaxis, but not differentiation. *Genes Dev.* **14**, 1407–1413 (2000).
 - 30. Cox, A. D., Fesik, S. W., Kimmelman, A. C., Luo, J. & Der, C. J. Drugging the undruggable RAS: mission possible? *Nat. Rev. Drug Discov.* **13**, 828–851 (2014).
 - 31. Spencer-Smith, R. & O'Bryan, J. P. Direct inhibition of RAS: quest for the Holy Grail? *Semin. Cancer Biol.* **54**, 138–148 (2019).
 - 32. Spiegel, J., Cromm, P. M., Zimmermann, G., Grossmann, T. N. & Waldmann, H. Small-molecule modulation of Ras signaling. *Nat. Chem. Biol.* **10**, 613–622 (2014).
 - 33. Buckley, C. M. et al. Coordinated Ras and Rac activity shapes macropinocytic cups and enables phagocytosis of geometrically diverse bacteria. *Curr. Biol.* **30**, 2912–2926 (2020).
 - 34. Veltman, D. M. et al. A plasma membrane template for macropinocytic cups. *eLife* **5**, e20085 (2016).
 - 35. Banerjee, T. et al. Spatiotemporal dynamics of membrane surface charge regulates cell polarity and migration. *Nat. Cell Biol.* **24**, 1499–1515 (2022).
 - 36. Banerjee, T. et al. A dynamic partitioning mechanism polarizes membrane protein distribution. Preprint at bioRxiv <https://doi.org/10.1101/2023.01.03.522496> (2023).
 - 37. Miao, Y. et al. Wave patterns organize cellular protrusions and control cortical dynamics. *Mol. Syst. Biol.* **15**, e8585 (2019).
 - 38. Bhattacharya, S. et al. Traveling and standing waves mediate pattern formation in cellular protrusions. *Sci. Adv.* **6**, eaay7682 (2020).
 - 39. Ecke, M. & Gerisch, G. Co-existence of Ras activation in a chemotactic signal transduction pathway and in an autonomous wave-forming system. *Small GTPases* **10**, 72–80 (2019).
 - 40. Gerhardt, M. et al. Actin and PIP3 waves in giant cells reveal the inherent length scale of an excited state. *J. Cell Sci.* **127**, 4507–4517 (2014).
 - 41. Lilly, P., Wu, L., Welker, D. L. & Devreotes, P. N. A G-protein β-subunit is essential for *Dictyostelium* development. *Genes Dev.* **7**, 986–995 (1993).
 - 42. Wu, L., Valkema, R., Van Haastert, P. J. & Devreotes, P. N. The G protein β subunit is essential for multiple responses to chemoattractants in *Dictyostelium*. *J. Cell Biol.* **129**, 1667–1675 (1995).
 - 43. Pan, M., Xu, X., Chen, Y. & Jin, T. Identification of a chemoattractant G-protein-coupled receptor for folic acid that controls both chemotaxis and phagocytosis. *Dev. Cell* **36**, 428–439 (2016).
 - 44. Aufderheide, K. J. & Janetopoulos, C. Migration of *Dictyostelium discoideum* to the chemoattractant folic acid. *Methods Mol. Biol.* **1407**, 25–39 (2016).
 - 45. De Lozanne, A. & Spudich, J. A. Disruption of the *Dictyostelium* myosin heavy chain gene by homologous recombination. *Science* **236**, 1086–1091 (1987).
 - 46. Knecht, D. A. & Loomis, W. F. Developmental consequences of the lack of myosin heavy chain in *Dictyostelium discoideum*. *Dev. Biol.* **128**, 178–184 (1988).
 - 47. Kovacs, M., Toth, J., Hetenyi, C., Malnasi-Csizmadia, A. & Sellers, J. R. Mechanism of blebbistatin inhibition of myosin II. *J. Biol. Chem.* **279**, 35557–35563 (2004).
 - 48. Houk, A. R. et al. Membrane tension maintains cell polarity by confining signals to the leading edge during neutrophil migration. *Cell* **148**, 175–188 (2012).
 - 49. Narumiya, S., Ishizaki, T. & Uehata, M. Use and properties of ROCK-specific inhibitor Y-27632. *Methods Enzymol.* **325**, 273–284 (2000).
 - 50. O'Neill, P. R. et al. Membrane flow drives an adhesion-independent amoeboid cell migration mode. *Dev. Cell* **46**, 9–22 e24 (2018).
 - 51. Azzi, J. et al. The novel therapeutic effect of phosphoinositide 3-kinase-γ inhibitor AS605240 in autoimmune diabetes. *Diabetes* **61**, 1509–1518 (2012).
 - 52. Hoang, B. et al. Targeting TORC2 in multiple myeloma with a new mTOR kinase inhibitor. *Blood* **116**, 4560–4568 (2010).
 - 53. Zhan, H. et al. An excitable Ras/PI3K/ERK signaling network controls migration and oncogenic transformation in epithelial cells. *Dev. Cell* **54**, 608–623 (2020).
 - 54. Shi, C., Huang, C. H., Devreotes, P. N. & Iglesias, P. A. Interaction of motility, directional sensing, and polarity modules recreates the behaviors of chemotaxing cells. *PLoS Comput. Biol.* **9**, e1003122 (2013).
 - 55. Shi, C. & Iglesias, P. A. Excitable behavior in amoeboid chemotaxis. *Wiley Interdiscip. Rev. Syst. Biol. Med.* **5**, 631–642 (2013).
 - 56. Cheng, Y. & Othmer, H. A model for direction sensing in *Dictyostelium discoideum*: Ras activity and symmetry breaking driven by a Gβγ-mediated, Ga2-Ric8-dependent signal transduction network. *PLoS Comput. Biol.* **12**, e1004900 (2016).
 - 57. Miao, Y. et al. Altering the threshold of an excitable signal transduction network changes cell migratory modes. *Nat. Cell Biol.* **19**, 329–340 (2017).
 - 58. Huang, C. H., Tang, M., Shi, C., Iglesias, P. A. & Devreotes, P. N. An excitable signal integrator couples to an idling cytoskeletal oscillator to drive cell migration. *Nat. Cell Biol.* **15**, 1307–1316 (2013).
 - 59. O'Neill, P. R. & Gautam, N. Subcellular optogenetic inhibition of G proteins generates signaling gradients and cell migration. *Mol. Biol. Cell* **25**, 2305–2314 (2014).
 - 60. Mseka, T., Bamburg, J. R. & Cramer, L. P. ADF/cofilin family proteins control formation of oriented actin-filament bundles in the cell body to trigger fibroblast polarization. *J. Cell Sci.* **120**, 4332–4344 (2007).
 - 61. Verkhovsky, A. B., Svitkina, T. M. & Borisy, G. G. Self-polarization and directional motility of cytoplasm. *Curr. Biol.* **9**, 11–20 (1999).
 - 62. Yam, P. T. et al. Actin-myosin network reorganization breaks symmetry at the cell rear to spontaneously initiate polarized cell motility. *J. Cell Biol.* **178**, 1207–1221 (2007).
 - 63. Nguyen, D. H. et al. Myosin light chain kinase functions downstream of Ras/ERK to promote migration of urokinase-type plasminogen activator-stimulated cells in an integrin-selective manner. *J. Cell Biol.* **146**, 149–164 (1999).
 - 64. Mitchison, T. J. & Cramer, L. P. Actin-based cell motility and cell locomotion. *Cell* **84**, 371–379 (1996).
 - 65. Cheung, K. J., Gabrielson, E., Werb, Z. & Ewald, A. J. Collective invasion in breast cancer requires a conserved basal epithelial program. *Cell* **155**, 1639–1651 (2013).
 - 66. Hatzikirou, H., Basanta, D., Simon, M., Schaller, K. & Deutsch, A. Go or grow: the key to the emergence of invasion in tumour progression? *Math. Med. Biol.* **29**, 49–65 (2012).
 - 67. Matus, D. Q. et al. Invasive cell fate requires G1 cell-cycle arrest and histone deacetylase-mediated changes in gene expression. *Dev. Cell* **35**, 162–174 (2015).

Publisher's note Springer Nature remains neutral with regard to jurisdictional claims in published maps and institutional affiliations.

Springer Nature or its licensor (e.g. a society or other partner) holds exclusive rights to this article under a publishing agreement with

the author(s) or other rightsholder(s); author self-archiving of the accepted manuscript version of this article is solely governed by the terms of such publishing agreement and applicable law.

© The Author(s), under exclusive licence to Springer Nature Limited 2024

Methods

Reagents and inhibitors

A 200 µg ml⁻¹ fibronectin stock (Sigma-Aldrich, F4759-2MG) was prepared in sterile water, followed by dilution in PBS. Folic acid (Sigma-Aldrich, 329823065) was dissolved in sterile water, with the addition of 2 M NaOH, to prepare a 1.25 mM stock solution. N-Formyl-Met-Leu-Phe (fMLP; Sigma-Aldrich, 47729) was dissolved in dimethylsulfoxide (DMSO) (Sigma-Aldrich, D2650) to make a stock solution of 10 mM. Phorbol 12-myristate 13-acetate (PMA; Sigma-Aldrich, P8139) was dissolved in DMSO to make a 1 mM stock solution. Then, 20 mM AS605240 (Sigma-Aldrich, A0233), 20 mM PP242 (EMD Millipore, 475988), 50 mM LY294002 (Thermo Fisher, PHZ1144), 50 mM CK666 (EMD Millipore, 182515), 50 mM blebbistatin (Peptech, 8567182), 5 mM latrunculin A (Enzo Life Sciences, BML-T119-0100), 10 mM latrunculin B (Sigma-Aldrich, 428020) or 5 mM Y-27632 (Sigma-Aldrich, 688001) stock solution was made in DMSO. Jasplakinolide (Sigma-Aldrich, 420127) was available as a ready-made 1 mM stock. Hygromycin B (Thermo Fisher Scientific, 10687010) or G418 sulfate (Thermo Fisher Scientific, 10131035) was purchased as 50 mg ml⁻¹ stock solution and blasticidin S (Sigma-Aldrich, 15205) or puromycin (Sigma-Aldrich, P8833) was dissolved in sterile water to make stock solutions of 10 mg ml⁻¹ or 2.5 mg ml⁻¹, respectively. Doxycycline hyyclate (Sigma, D9891-1G) was dissolved in sterile water to make a stock of 5 mg ml⁻¹. Then, 50 mg ml⁻¹ TRITC-dextran (Sigma-Aldrich, T1162) was made in sterile water. All stock solutions were aliquoted and stored at -20 °C. According to experimental requirements, further dilutions were made in development buffer (DB), PBS or growth medium before adding to the cells.

Plasmid construction

All DNA oligonucleotides were purchased from Sigma-Aldrich and are listed in Supplementary Table 1. *Dictyostelium C2GAPB* (RasGAP2) gene was cloned in KF2 expression plasmid¹¹. RasG S17N-expressing plasmid was obtained from dictyBase (cat. no. 254). Using these constructs, we subcloned *C2GAPB* or *RasGS17N* into doxycycline-inducible pDM335 plasmid (dictyBase, cat. no. 523) using BglII/SpeI restriction digestion to generate mRFPmars-C2GAPB/pDM335, GFP-C2GAPB/pDM335 and mRFPmars-RasG S17N/pDM335 constructs. *SspBR73Q* ORF was amplified from tgRFPt-SspB R73Q plasmid (Addgene #60416, RRID: Addgene_60416) and then subcloned into C2GAPB/pDM335 at the BglII site to generate the opto-C2GAPB construct, mRFPmars-SspB R73Q-C2GAPB⁸. tgRFPt-SspB R73Q ORF was introduced into pCV5 vector to generate the tgRFPt-SspB R73Q-Ctrl/pCV5 construct (Addgene #201761)⁴. CAAX-deleted *RasGS17N* ORF was introduced to opto-Ctrl construct by restriction digestion to generate opto-RasG S17N ΔCAAX. Similarly, tgRFPt-SspB R73Q ORF was introduced into pDM335 to generate tgRFPt-SspB R73Q-Ctrl construct. N150-Venus-iLID/pDM358 construct was made previously⁴. This was used to subclone *PHcrac-YFP*, *LimE_{Δcoil}-YFP* or *RBD-YFP* ORF to generate dual expressing N150-Venus-iLID/PHcrac-YFP, N150-Venus-iLID/LimE-YFP or N150-Venus-iLID/RBD-YFP construct, respectively. The shuttle vector, pDM344 (dictyBase, cat. no. 551), was used for this purpose. Constructs for *GFP-RBD* and *GFP-LimE_{Δcoil}* were procured from the Firtel laboratory (UCSD) and Marriott laboratory (University of Wisconsin-Madison), respectively, whereas myosin-GFP/pDRH was obtained from the Robinson laboratory (School of Medicine, JHU)^{5,69,70}.

CRY2PHR-mCherry-RASAL3/pPB (Addgene #201755), CIBN-CAAX/pLJM1 (Addgene #201749) or LifeAct-miRFP703/pLJM1 (Addgene #201750) construct was made previously⁴. DNA sequences (2,064–3,036 or 1,276–3,036 bases) encoding the last 322 or 585 amino acids of RASAL3, and CAAX-deleted KRas4B S17N (*KRas4BS17NΔCAAX*) were PCR-amplified (from Addgene #201755 or #83156, RRID: Addgene_83156) and cloned into the BspEI/NotI sites of the PiggyBac transposon plasmid to generate CRY2PHR-mCherry-RASAL3_{689-1,011}/pPB, CRY2PHR-mCherry-RASAL3_{426-1,011}/pPB or CRY2PHR-mCherry-KRas4B

S17N ΔCAAX/pPB construct, respectively (the PiggyBac transposon system was gifted by the Collins laboratory at UC Davis)^{71,72}. Constructs were verified by diagnostic restriction digestion and sequenced at the JHMI Synthesis and Sequencing Facility.

Cell culture

WT *Dictyostelium discoideum* cells of the AX2 strain (dictyBase, cat. no. DBS0235521) was obtained from the Kay laboratory (MRC Laboratory of Molecular Biology). Gβ-null (Gβ⁻) cells were created in our laboratory previously⁴¹. The myosin heavy chain-null strain (mhcA⁻) was obtained from the Robinson laboratory (School of Medicine, JHU)⁷³. The C2GAPB-null strain (C2GAPB⁻) was generated in our laboratory¹¹. All lines were cultured axenically in HL5 medium (laboratory stock) at 22 °C. Growth-stage cells were used for imaging⁷⁴.

The human HL-60 cell line (ATCC CCL-240; RRID: CVCL_0002) was obtained from the Weiner laboratory (UCSF) and cultured in RPMI 1640 medium (Gibco, 22400-089) supplemented with 15% heat-inactivated fetal bovine serum (Thermo Fisher, 16140071)^{4,75}. To obtain migration-competent neutrophils, WT or stable lines were differentiated in presence of 1.3% DMSO over 5–7 days^{4,75}. Differentiated cells are an effective model to study human neutrophils⁷⁶. To differentiate HL-60 cells into macrophages, cells were incubated with 32 nM PMA for 48–72 h^{77,78}. Cells were grown in humidified conditions at 5% CO₂ and 37 °C.

Electroporation

Dictyostelium stable lines were generated by electroporating 2 µg DNA in 10⁷ cells using a chilled 0.1-cm cuvette (Bio-Rad, cat. no. 1652089) at 0.85 kV/25 µF twice with a 5-s interval, followed by antibiotic selection over 3–4 weeks^{4,79}. The HL-60 cell line stably co-expressing CIBN-CAAX, opto-RASAL3 and LifeAct-miRFP703 was generated previously^{4,79}. Here, we introduced 5 µg opto-RASAL3_{689-1,011}, opto-RASAL3_{426-1,011} or opto-KRas4B S17N ΔCAAX constructs with 5 µg PiggyBac transposase plasmid in 2 × 10⁶ CIBN-CAAX- and LifeAct-miRFP703-expressing HL-60 stable cells using the Neon transfection system 100 µl kit (Thermo Fisher, MPK10025). *Dictyostelium* cells, at a density of 1.5 × 10⁷ cells per ml, were rolled for 30 min and electroporated in a 4-mm cuvette (Bio-Rad, 1652088) at 1,000 V/3 µF once followed by 1,000 V/1 µF three times with a 2-s interval to generate electrofused cells^{35,36}.

Confocal microscopy

Vegetative *Dictyostelium* or differentiated macrophages were adhered on an eight-well coverslip chamber for 40 min. Differentiated neutrophils, pre-treated with heat-killed *Klebsiella aerogenes*, were adhered to fibronectin-coated chambers for 40 min^{4,79}. Next, fresh DB or RPMI 1640 medium was added to attached cells and used for imaging. To induce C2GAPB expression in *Dictyostelium*, doxycycline (50 µg ml⁻¹) was added 8 h before imaging. For macropinocytosis assay, cells were incubated with TRITC-dextran for 4 min, washed and imaged subsequently^{33,80}. All live- or fixed-cell imaging was acquired with 0.3–0.5% (*Dictyostelium*) or 0.2–10% (HL-60) laser intensity using the following microscopes: (1) a Zeiss LSM780-FCS single-point, laser scanning confocal microscope with 780-Quasar; 34-channel spectral, high-sensitivity gallium arsenide phosphide detectors supported with ZEN Black software, and (2) a Zeiss LSM800 GaAsP single-point laser scanning confocal microscope with wide-field camera supported with ZEN Blue software. All images were acquired with either ×63/1.40 PlanApo oil or ×40/1.30 PlanNeofluar oil DIC objective, along with a digital zoom. In single cells, confocal imaging was performed at a middle plane of the cells, whereas in electrofused cells, the laser was focused near the bottom surface to visualize the cortical waves^{4,35,79,81}. For the inhibitor experiments, neutrophils were treated with 20 µM AS605240, 20 µM PP242, 50 µM LY294002, 50 µM CK666, 20 or 75 µM blebbistatin and 10 or 50 µM Y-27632 for at least 10 min before imaging. For pre-treatment with the JLY cocktail, neutrophils were incubated with 10 µM Y-27632

Q15

Q16

Q17

for 10 min. Cells were then treated with 8 μ M jasplakinolide and 5 μ M latrunculin B without changing the final concentration of Y-27632 (refs. 82,83). In *Dictyostelium*, 50 μ M blebbistatin or CK666 was added during imaging.

Optogenetics

Optogenetic experiments with vegetative *Dictyostelium* or differentiated HL-60 cells were conducted in the absence of a chemoattractant, except for chemotaxis assays. Throughout image acquisition, a solid-state laser (561 nm excitation and 579–632 nm emission) was used for visualizing proteins or recruitable effectors fused to an mCherry, mRFPmars or tgRFPt tag, whereas a diode laser (633 nm excitation and 659–709 nm emission) was used to capture miRFP703 expression. Images were acquired for 5–10 min, after which a 450/488 nm excitation laser was switched on globally to activate recruitment. Image acquisition and photoactivation was performed at ~7-s intervals. Using the T-PMT associated with the red channel, we acquired DIC images. The interactive photobleaching module on a Zeiss LSM800 was used to perform local recruitment experiments. A small region of interest (ROI) was placed in front or back of migrating cells, and bleached with a 488 nm laser (laser power of ~0.5% or 7% for *Dictyostelium* or HL-60 cells, respectively) in multiple iteration. The time interval of photoactivation and image acquisition was ~10 s (refs. 4,35,79,81,84).

Indirect immunofluorescence

Differentiated opto-RASAL3-expressing HL-60 neutrophils were attached on an eight-well coverslip chamber and illuminated with 6 \times 10-s pulses of 420–480 nm LED using a hand-held lamp (LY-A180). Immediately, non-illuminated and illuminated samples were incubated with a fixative (3.7% buffered paraformaldehyde (Fisher Scientific, T353-500), 0.25% glutaraldehyde (Sigma-Aldrich, 340855) and 0.1% Triton X-100 (Sigma-Aldrich, T8787) in serum-supplemented RPMI 1640) for 10 min at room temperature (RT). Following quenching with sodium borohydride (Fisher Scientific, S678-10), samples were blocked with 3% BSA (Sigma-Aldrich, A-9647) for 1 h at RT. Endogenous phospho-myosin regulatory light chain 2 (pMRLC2 Ser19), myosin heavy chain IIA (myosin IIA) or myosin heavy chain IIB (myosin IIB) localization was detected by incubating them for 1 h at RT with respective antibodies: mouse anti-pMRLC2 Ser19 (1:200 dilution, Cell Signalling, 3675, RRID: AB_2250969), rabbit anti-myosin IIA (1:100 dilution, Sigma-Aldrich, M8064, RRID: AB_260673) or rabbit anti-myosin IIB antibody (1:50 dilution, Sigma-Aldrich, M7939, RRID: AB_260669). Finally, samples were incubated with Alexa Fluor 488 goat anti-mouse (Thermo Fisher, A11001, RRID: AB_2534069) or anti-rabbit (Thermo Fisher, A11008, RRID: AB_143165) antibody (1:1,000 dilution) for 40 min at RT, before imaging.

Two-dimensional chemotaxis assay

Chemotaxis assays with doxycycline pre-treated, vegetative mRFPmars-C2GAPB-expressing *Dictyostelium* or differentiated opto-RASAL3-expressing neutrophils were performed on a μ -Slide Chemotaxis Collagen IV chamber (Ibidi, 80322) using freshly-prepared 10 nM fMLP or 100 nM folic acid as a chemoattractant⁴.

SDS-PAGE and western blotting

WT or mRFPmars-C2GAPB-expressing *Dictyostelium* was developed and 6 \times 10⁶ cells were collected every hour, up to 8 h, for western blot analysis^{79,85}. Samples were resuspended and lysed in pre-chilled RIPA buffer (supplemented with protease inhibitor cocktail; Thermo Scientific, 89900) for 20 min, and then incubated with 3× Laemmli sample buffer (laboratory stock) at RT for 5 min. For neutrophils, 10⁷ differentiated opto-RASAL3-expressing cells were resuspended in 1 ml growth medium. For inhibitor experiments, cell suspension was incubated with 10 or 50 μ M Y-27632 for 10 min. Next, samples were illuminated with a 420–480 nm LED lamp. Non-illuminated and untreated

or Y-27632-treated samples were maintained throughout as control. Samples were lysed by boiling in the sample buffer.

Samples equivalent to 1.5 \times 10⁶ cells were loaded into pre-cast 4–15% polyacrylamide gel and immunoblotting was performed as per laboratory protocols^{4,79}. Endogenous cAR1 (~44 kDa), phospho-MRLC2 Ser19 (18 kDa), MRLC2 (18 kDa), myosin IIA (230 kDa), myosin IIB (230 kDa) or GAPDH (36 kDa) expression was detected by incubating a PVDF membrane (Bio-Rad, 162-0262) with rabbit anti-cAR1 (1:1,000 dilution; generated in our laboratory⁸⁶), mouse anti-pMRLC2 Ser19 (1:1,000 dilution), rabbit anti-MRLC2 (1:1,000 dilution; Cell Signalling, 3672, RRID: AB_10692513), rabbit anti-myosin IIA (1:1,000 dilution), rabbit anti-myosin IIB (1:200 dilution) or rabbit anti-GAPDH antibody (1:3,000 dilution; Thermo Fisher, PA1-987, RRID: AB_2107311) overnight at 4 °C, followed by goat anti-rabbit IRDye 680RD-conjugated (1:10,000 dilution; Li-Cor, 925-68071, RRID: AB_2721181) or goat anti-mouse IRDye 800CW-conjugated (1:10,000 dilution; Li-Cor, 925-32210, RRID: AB_2687825) secondary antibody for 1 h in dark. The Odyssey CLx imaging system (Li-Cor) detected near-infra-red signals from the blots.

Image analysis

All images were analysed with Fiji/ImageJ 1.52i (NIH), Python v.3.10, and MATLAB 2019b (MathWorks) software⁸⁷. We utilized GraphPad Prism 8 (GraphPad), OriginPro v.9.0 (Originlab Corporation) and Microsoft Excel (Microsoft) for plotting our results^{4,35,79}.

To get the ratio of wave area to cell area in Fig. 1e,h, images were first binarized using ImageJ, by adjusting threshold to cover all pixels of the wave or cell. The range was not reset and the ‘Calculate threshold for each image’ option was unchecked. Subsequently, using the ‘Analyze Particle’ function, a size-based thresholding was applied (to exclude non-cell particles) and cell masks were generated. Next, ‘Fill holes’, ‘Erode’ and ‘Dilate’ options were applied, sequentially and judiciously, to obtain the proper binarized mask for waves or cells^{4,35}. The ratio of wave area to cell area for each frame was obtained and plotted with time. The duration of waves for Fig. 1f,i was obtained by counting the number of frames from when a wave starts to when it ends, and then multiplying it by the time interval.

Cell outline overlays (Figs. 3c, 4b,f, 5b,d, 6a and 7c,i and Extended Data Figs. 1i,j, 2d,e, 3g, 5j, 7e, 8d,n and 9c) were obtained from segmented cells^{4,35}. For membrane kymographs (Figs. 3i,j,m,n, 5e and 7d,m and Extended Data Figs. 3h, 5k, 7f, 8e,o and 9d), cells were segmented against the background following standard image-processing steps with custom code written in MATLAB^{4,35,79}. Next, kymographs were created from segmented cells using a custom-written MATLAB function⁵⁸. For linescan analysis (Fig. 3h,l), a straight-line segment (5-pixel width) was drawn using ‘Straight’ tool in ImageJ^{35,79}.

Local protrusion (Fig. 2d, f, l and Extended Data Fig. 1h) and cell migration (Figs. 5f–j, 6l–p and 7e–i,n–r and Extended Data Figs. 3i–m, 4b,c, 6f, 7g–k, 8g–k,q–u and 9e–i) analyses were performed as detailed previously^{4,35,79}. For cell speed, area and aspect ratio quantifications (Figs. 3d–f, 4c,e,g,h and 3b–e), cells were segmented against the background following standard image-processing steps with custom code written in Python based on package scikit-image, Trackpy v.0.6.2 and Pylimage v.1.4.1. Human supervision was involved during the process with an integration to Fiji, and we obtained the X position, Y position, cell area and aspect ratio for each frame of each cell. The distance between adjacent frames was calculated from the X position and Y position, and was divided by the time interval to obtain an instantaneous velocity. The average cell speeds were calculated by taking an average of all instantaneous velocities. For Extended Data Fig. 1b, macropinocytosis uptake was analysed by outlining each cell and quantifying the total TRITC fluorescence signal within each outline divided by the cell area⁸⁰. For Extended Data Fig. 6h, numbers of blebs for each cell, before or after recruitment, were quantified by summing them over 1 min (ref. 88).

Back/front intensity ratios for F-actin and pMRLC2 Ser19 in fixed samples (Fig. 6d) were quantified in ImageJ. Using the ‘freehand’ tool,

an ROI was outlined at the cell back (488 nm channel) and signal intensity for Alexa Fluor 488 (pMRLC2) was measured. Next, this ROI was added to 'ROI Manager' and the same region in the 633 nm channel was outlined to measure the corresponding LifeAct-miRFP703 (F-actin) signal. Similarly, ROIs were drawn at the front of a cell in both channels and signal intensities for F-actin and pMRLC2 were quantified. Using 'back' and 'front' intensity values, graphs were generated. Protein bands between different immunoblot samples were quantified by densitometric analysis using ImageJ (Fig. 6e,f).

Simulations

The simulations are based on a model, previously described, in which three interacting species, RasGTP, PIP2 and PKB, form an excitable network³⁷. In this model, Ras and PIP2 are complementary (wherever Ras activity is high, PIP2 is low and vice versa). This is achieved through mutually inhibitory connections that give rise to the traditional positive feedback loop seen in the canonical excitable networks. In our model, PKB acts as the traditional refractory species; it is activated by Ras but provides slow, negative feedback to the latter. The network connections are shown in Extended Data Fig. 10a. The concentrations of each of these molecules are described by stochastic, reaction-diffusion partial differential equations:

$$\frac{\partial[\text{Ras}]}{\partial t} = -(a_1 + a_2[\text{PKB}])[\text{Ras}] + \frac{a_3}{1 + a_4^2[\text{PIP2}]^2} + a_5 + w_{\text{Ras}} + D_{\text{Ras}} \nabla^2[\text{Ras}]$$

$$\frac{\partial[\text{PIP2}]}{\partial t} = -(b_1 + b_2[\text{Ras}])[\text{PIP2}] + b_3 + w_{\text{PIP2}} + D_{\text{PIP2}} \nabla^2[\text{PIP2}]$$

$$\frac{\partial[\text{PKB}]}{\partial t} = -c_1[\text{PKB}] + c_2[\text{Ras}] + w_{\text{PKB}} + D_{\text{PKB}} \nabla^2[\text{PKB}]$$

In each of these equations, the final term represents the diffusion of the species, where D_* is the respective diffusion coefficient and ∇^2 is the spatial Laplacian (in one or two dimensions). The second-to-last terms represent molecular noise. Our model assumes a Langevin approximation in which the size of the noise is based on the reaction terms⁸⁹. For example, in the case of PKB, the noise is given by

$$w_{\text{PKB}}(t) = \alpha \sqrt{c_1[\text{PKB}] + c_2[\text{Ras}]} w(t)$$

where $w(t)$ is a zero-mean, unit-variance Gaussian, Brown noise process. In the simulations, the size of this noise was adjusted with the empirical parameter α .

In addition to the EN dynamics described above, we incorporated two other terms related to cell polarization^{37,54}. These feedback loops come from PIP2 and PKB and denote actions at the front (P_F) and rear (P_R), respectively¹⁹:

$$\frac{\partial[P_F]}{\partial t} = -p_1[P_F] + p_2[\text{PKB}] + w_{P_F} + D_{P_F} \nabla^2[P_F]$$

$$\frac{\partial[P_R]}{\partial t} = -p_3[P_R] + p_4[\text{PIP2}] + w_{P_R} + D_{P_R} \nabla^2[P_R]$$

Both these terms modify the terms in the RasGTP equation related to hydrolysis:

$$(a_1 + a_2[\text{PKB}])[\text{Ras}] \mapsto \frac{(a_1 + a_2[\text{PKB}] + a_{P_B}[P_B])[\text{Ras}]}{1 + a_{P_F}[P_F]}$$

having the effect of increasing front and back contributions. Last, we note that changes in RasGAP contributions are modelled as changes in the parameters a_1 and a_2 .

Parameter values, listed in Supplementary Table 2, were obtained to recreate experimental observations on the level of excitable activities (number of firings per unit time, wave propagation etc.).

The system is largely robust to parameter changes, in that variations from the nominal values below continue to give rise to excitable behaviour. To test this, we note that excitable behaviour arises from the stochastic crossing of a threshold that is determined by the nullclines of the differential equations (Extended Data Fig. 10b). To measure the level of robustness, we varied each of the parameters $a_1, \dots, a_5, b_1, \dots, b_3, c_1$ and c_2 from their nominal values and computed the size of the threshold (Extended Data Fig. 10c). Some, such as a_2, b_2 and c_1 are quite robust, allowing large changes in either direction. Others allow large changes only in one direction.

To simulate the movement of cells, we followed the procedure outlined previously⁹⁰. In brief, Ras activity along the perimeter of the cell (in a one-dimensional simulation) was thresholded to generate a force normal to the cell surface. The vector sum of these forces around the perimeter were used to generate a net force scaled so that it was in the range of experimentally observed protrusive stresses $0.5\text{--}5 \text{ nN } \mu\text{m}^{-1}$, and then fed into a viscoelastic model⁹¹ of *Dictyostelium* mechanics:^{Q20}

$$\ddot{x} + \left(\frac{k_c}{\gamma_c}\right)\dot{x} = \left(\frac{1}{\gamma_c} + \frac{1}{\gamma_a}\right)\dot{\sigma}_x + \left(\frac{k_c}{\gamma_c}\right)\sigma_x$$

Here, σ_x is the x component of the stress and the viscoelastic parameters are $\gamma_a = 6.09 \text{ nNs } \mu\text{m}^3$, $\gamma_c = 0.064 \text{ nNs } \mu\text{m}^3$ and $k_c = 0.098 \text{ nN } \mu\text{m}^{-3}$. A similar formula is used to denote the displacement in the y direction.^{Q21}

Simulations were run on MATLAB 2023a (MathWorks) on custom code based on the Itô solution in the Stochastic Differential Equation toolbox (<http://sdetoolbox.sourceforge.net>). Two-dimensional simulations were used to recreate the observed wave patterns of larger electrofused cells, and so assume a grid $40 \times 4 \mu\text{m}$ with a spacing of $0.4 \times 0.4 \mu\text{m}$ per grid point (100×100 points) and zero flux boundary conditions. The one-dimensional simulations aim to recreate the membrane fluorescence observed in single-cell confocal images. The dimension is therefore smaller, assuming a cell radius of $5 \mu\text{m}$ and a spacing of $0.25 \mu\text{m}$, resulting in $2\pi \times 5 / 0.25 \approx 126$ points along the perimeter and periodic boundary conditions.

Statistics and reproducibility

Statistical analyses were executed using unpaired or paired two-tailed nonparametric tests on GraphPad Prism 8. Results are expressed as mean \pm s.d. from at least three independent experiments. NS, $P > 0.05$, $*P \leq 0.05$, $**P \leq 0.01$, $***P \leq 0.001$, $****P \leq 0.0001$. Tukey's convention was used to plot box-and-whisker plots. Statistical test details are indicated in the figure legends. No statistical methods were used to predetermine sample sizes, but our sample sizes are similar to those reported in previous publications^{4,35,79}. Each micrograph, including images presented in Figs. 1a,b, 3a, 4f, 6c,h,i and 7c,l and Extended Data Fig. 1a, shows a representative image or image series from $n > 3$ independent experiments. The experiments were not randomized; randomization is not relevant to our study as all experiments were conducted on cultured cells. Any variations observed between treatment groups are not attributed to sampling bias. Individual data points in each plot are available in the source datasheet and data distribution was assumed to be normal but this was not formally tested. No data were excluded from the analyses. Data collection and analysis were not performed blind to the conditions of the experiments.

Manuscript writing

ChatGPT v.3.5 software (<https://chat.openai.com/chat>) was employed in the writing of the Results section. Each figure was manually examined and a series of bullet points explaining each panel of the figure was written by the authors. Then ChatGPT was asked to convert the bullet points to better sentences with correct grammar. Next, the

text was carefully reviewed by each author where incorrect sentences were removed. Finally, the manuscript was run on several plagiarism software platforms which returned no instances.

Reporting summary

Further information on research design is available in the Nature Portfolio Reporting Summary linked to this article.

Data availability

All data needed to evaluate the conclusions are provided in the main text and figures, extended data figures or supplementary tables and videos. All unprocessed immunoblots or raw data and associated statistical calculations are provided with this study. Data in Fig. 2k,l were re-analysed here from our previous study⁴. All other data supporting the findings of this study are available from the corresponding authors on reasonable request. Source data are provided with this paper.

Q23

Code availability

Custom computational simulation codes are available on GitHub at <https://github.com/piglesi1/GAP-role-in-polarization>. They are available under the GNU General Public License v.3.0. These codes are also available on Zenodo at <https://zenodo.org/records/11121861> (ref. 92) licensed under Creative Commons Attribution 4.0 International. Any additional information will be available from the corresponding authors upon reasonable request.

References

68. Guntas, G. et al. Engineering an improved light-induced dimer (iLID) for controlling the localization and activity of signaling proteins. *Proc. Natl Acad. Sci. USA* **112**, 112–117 (2015).
69. Dickinson, D. J., Robinson, D. N., Nelson, W. J. & Weis, W. I. α-Catenin and IQGAP regulate myosin localization to control epithelial tube morphogenesis in *Dictyostelium*. *Dev. Cell* **23**, 533–546 (2012).
70. Schneider, N. et al. A Lim protein involved in the progression of cytokinesis and regulation of the mitotic spindle. *Cell Motil. Cytoskeleton* **56**, 130–139 (2003).
71. Yang, H. W., Collins, S. R. & Meyer, T. Locally excitable Cdc42 signals steer cells during chemotaxis. *Nat. Cell Biol.* **18**, 191–201 (2016).
72. Yusa, K., Rad, R., Takeda, J. & Bradley, A. Generation of transgene-free induced pluripotent mouse stem cells by the piggyBac transposon. *Nat. Methods* **6**, 363–369 (2009).
73. Manstein, D. J., Titus, M. A., De Lozanne, A. & Spudich, J. A. Gene replacement in *Dictyostelium*: generation of myosin null mutants. *EMBO J.* **8**, 923–932 (1989).
74. Li, X., Pal, D. S., Biswas, D., Iglesias, P. A. & Devreotes, P. N. Reverse fountain flow of phosphatidylinositol-3,4-bisphosphate polarizes migrating cells. *EMBO J.* **40**, e105094 (2021).
75. Millius, A. & Weiner, O. D. Manipulation of neutrophil-like HL-60 cells for the study of directed cell migration. *Methods Mol. Biol.* **591**, 147–158 (2010).
76. Rincon, E., Rocha-Gregg, B. L. & Collins, S. R. A map of gene expression in neutrophil-like cell lines. *BMC Genomics* **19**, 573 (2018).
77. Mishra, A. K. et al. Hyperactive Rac stimulates cannibalism of living target cells and enhances CAR-M-mediated cancer cell killing. *Proc. Natl Acad. Sci. USA* **120**, e2310221120 (2023).
78. Rovera, G., Santoli, D. & Damsky, C. Human promyelocytic leukemia cells in culture differentiate into macrophage-like cells when treated with a phorbol ester. *Proc. Natl Acad. Sci. USA* **76**, 2779–2783 (1979).
79. Pal, D. S. et al. Optogenetic modulation of guanine nucleotide exchange factors of Ras superfamily proteins directly controls cell shape and movement. *Front. Cell Dev. Biol.* **11**, 1195806 (2023).
80. Jiao, Z. et al. Statin-induced GGPP depletion blocks macropinocytosis and starves cells with oncogenic defects. *Proc. Natl Acad. Sci. USA* **117**, 4158–4168 (2020).
81. Kuhn, J., Lin, Y. & Devreotes, P. N. Using live-cell imaging and synthetic biology to probe directed migration in *Dictyostelium*. *Front. Cell Dev. Biol.* **9**, 740205 (2021).
82. Peng, G. E., Wilson, S. R. & Weiner, O. D. A pharmacological cocktail for arresting actin dynamics in living cells. *Mol. Biol. Cell* **22**, 3986–3994 (2011).
83. Wang, M. J., Artemenko, Y., Cai, W. J., Iglesias, P. A. & Devreotes, P. N. The directional response of chemotactic cells depends on a balance between cytoskeletal architecture and the external gradient. *Cell Rep.* **9**, 1110–1121 (2014).
84. Zhan, H. et al. Self-organizing glycolytic waves fuel cell migration and cancer progression. Preprint at *bioRxiv* <https://doi.org/10.1101/2024.01.28.577603> (2024). Q27
85. Kamimura, Y., Tang, M. & Devreotes, P. Assays for chemotaxis and chemoattractant-stimulated TorC2 activation and PKB substrate phosphorylation in *Dictyostelium*. *Methods Mol. Biol.* **571**, 255–270 (2009).
86. Klein, P., Theibert, A., Fontana, D. & Devreotes, P. N. Identification and cyclic AMP-induced modification of the cyclic AMP receptor in *Dictyostelium discoideum*. *J. Biol. Chem.* **260**, 1757–1764 (1985).
87. Schneider, C. A., Rasband, W. S. & Eliceiri, K. W. NIH Image to ImageJ: 25 years of image analysis. *Nat. Methods* **9**, 671–675 (2012).
88. Zatulovskiy, E., Tyson, R., Bretschneider, T. & Kay, R. R. Bleb-driven chemotaxis of *Dictyostelium* cells. *J. Cell Biol.* **204**, 1027–1044 (2014).
89. Gillespie, D. T. The chemical Langevin equation. *J. Chem. Phys.* **113**, 297–306 (2000).
90. Biswas, D., Bhattacharya, S. & Iglesias, P. A. Enhanced chemotaxis through spatially regulated absolute concentration robustness. *Int. J. Robust. Nonlin.* **33**, 4923–4944 (2023).
91. Yang, L. et al. Modeling cellular deformations using the level set formalism. *BMC Syst. Biol.* **2**, 68 (2008).
92. piglesi1. piglesi1/GAP-role-in-polarization: v1.00. Zenodo <https://doi.org/10.5281/zenodo.11121861> (2024).

Acknowledgements

We thank all members of the P. Devreotes, P. Iglesias and D. Robinson laboratories (Schools of Medicine and Engineering, JHU) for helpful discussions and providing resources. We acknowledge O. Weiner (UCSF) for providing HL-60 cell line. We thank S. Collins (UC Davis), M. Edwards (Amherst College) and Y. Miao (Harvard Medical School) for providing plasmids. We thank S. Gould (School of Medicine, JHU) for help with instrumentation. We appreciate X. Zhang (Ross Research Flow Cytometry Core, JHU) for helping with cell sorting. We acknowledge dictyBase and Addgene for plasmids. This work was supported by National Institutes of Health (NIH) grant R35 GM118177 (to P.N.D.), DARPA HRO0116-C-0139 (to P.A.I. and P.N.D.), AFOSR MURI FA95501610052 (to P.N.D.), as well as NIH grant S10OD016374 (to S. Kuo of the JHU Microscope Facility). Q22

Author contributions

D.S.P., P.N.D. and Y.L. conceived and developed the study with input from T.B., P.B. and P.A.I. Y.L. and D.S.P. engineered constructs/stable lines, designed and executed experiments, and performed the majority of data analyses. P.B. and P.A.I. devised and conducted computational simulations, and deposited codes. T.B. and G.Q. assisted with image analyses. Y.D. performed uptake assays. J.B. made some constructs. First authors are listed alphabetically. D.S.P., P.N.D. and Y.L. prepared initial drafts, and wrote and revised the final version of manuscript with help from P.A.I. and P.B. D.S.P. and P.N.D. supervised the study.

Competing interests

Q24 The authors declare no competing interests.

Correspondence and requests for materials should be addressed to Dhiman Sankar Pal or Peter N. Devreotes.

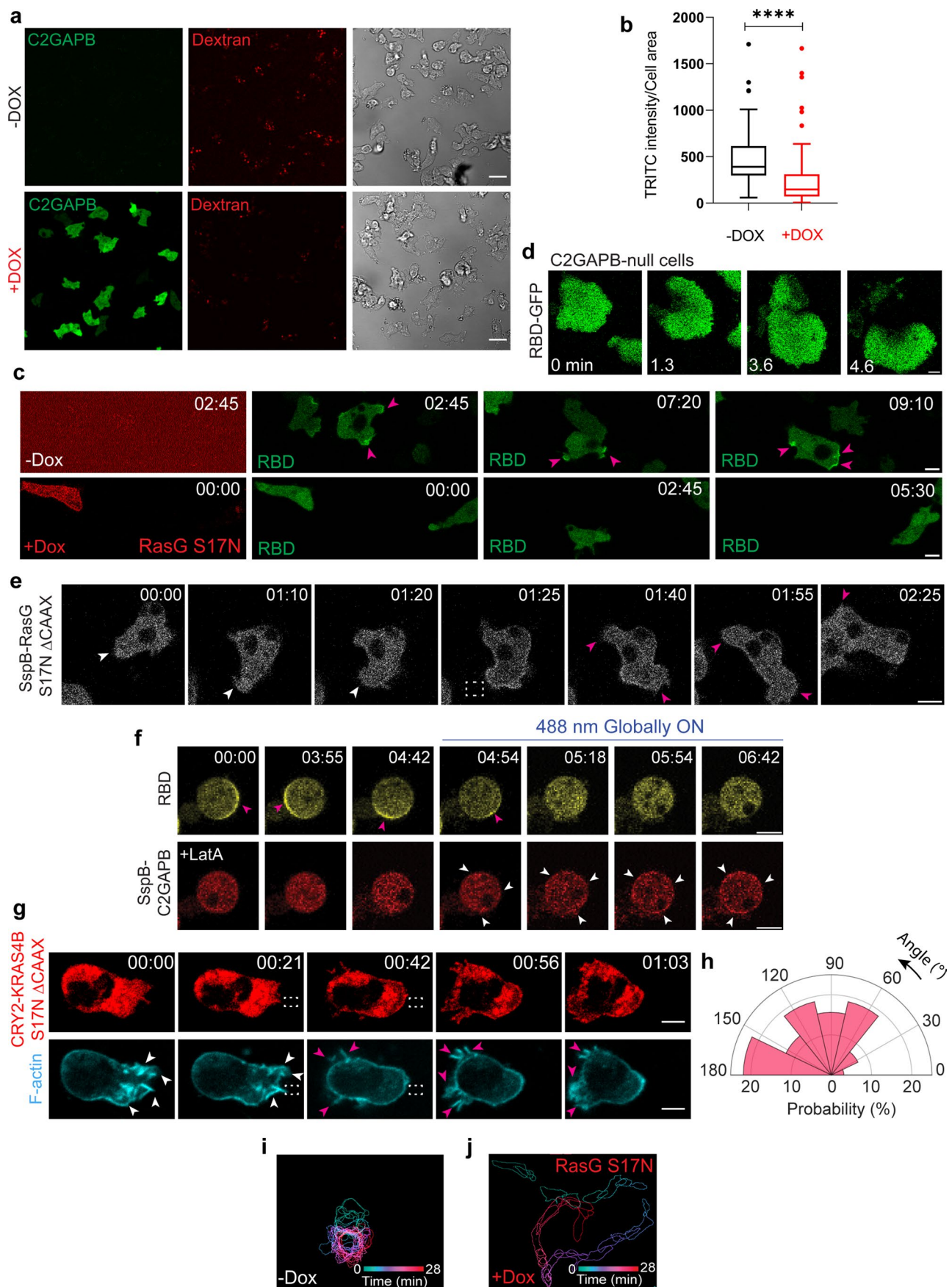
Additional information

Extended data is available for this paper at <https://doi.org/10.1038/s41556-024-01453-4>.

Peer review information *Nature Cell Biology* thanks Cornelis Weijer and the other, anonymous, reviewer(s) for their contribution to the peer review of this work. Peer reviewer reports are available.

Supplementary information The online version contains supplementary material available at <https://doi.org/10.1038/s41556-024-01453-4>.

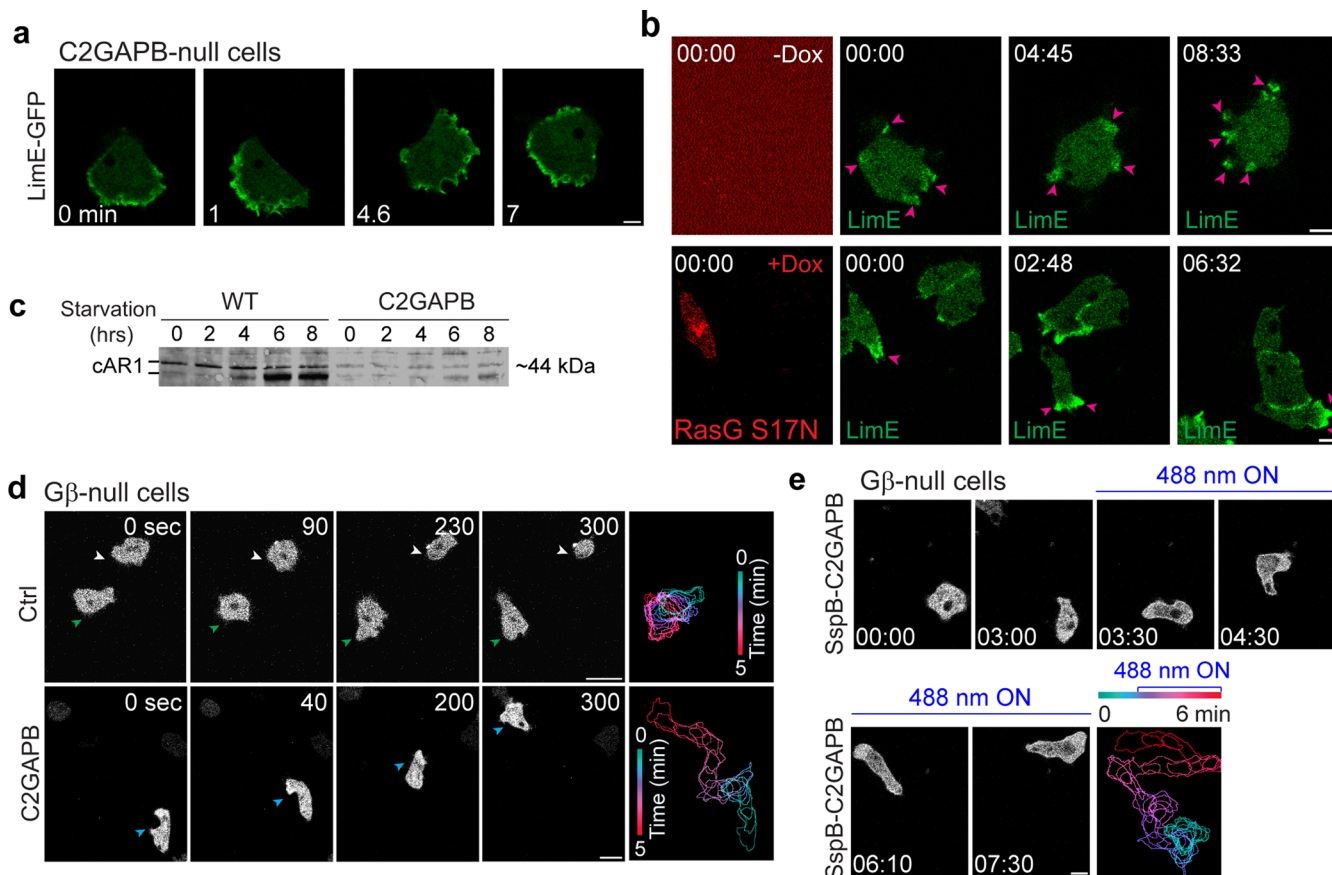
Reprints and permissions information is available at www.nature.com/reprints.



Extended Data Fig. 1 | See next page for caption.

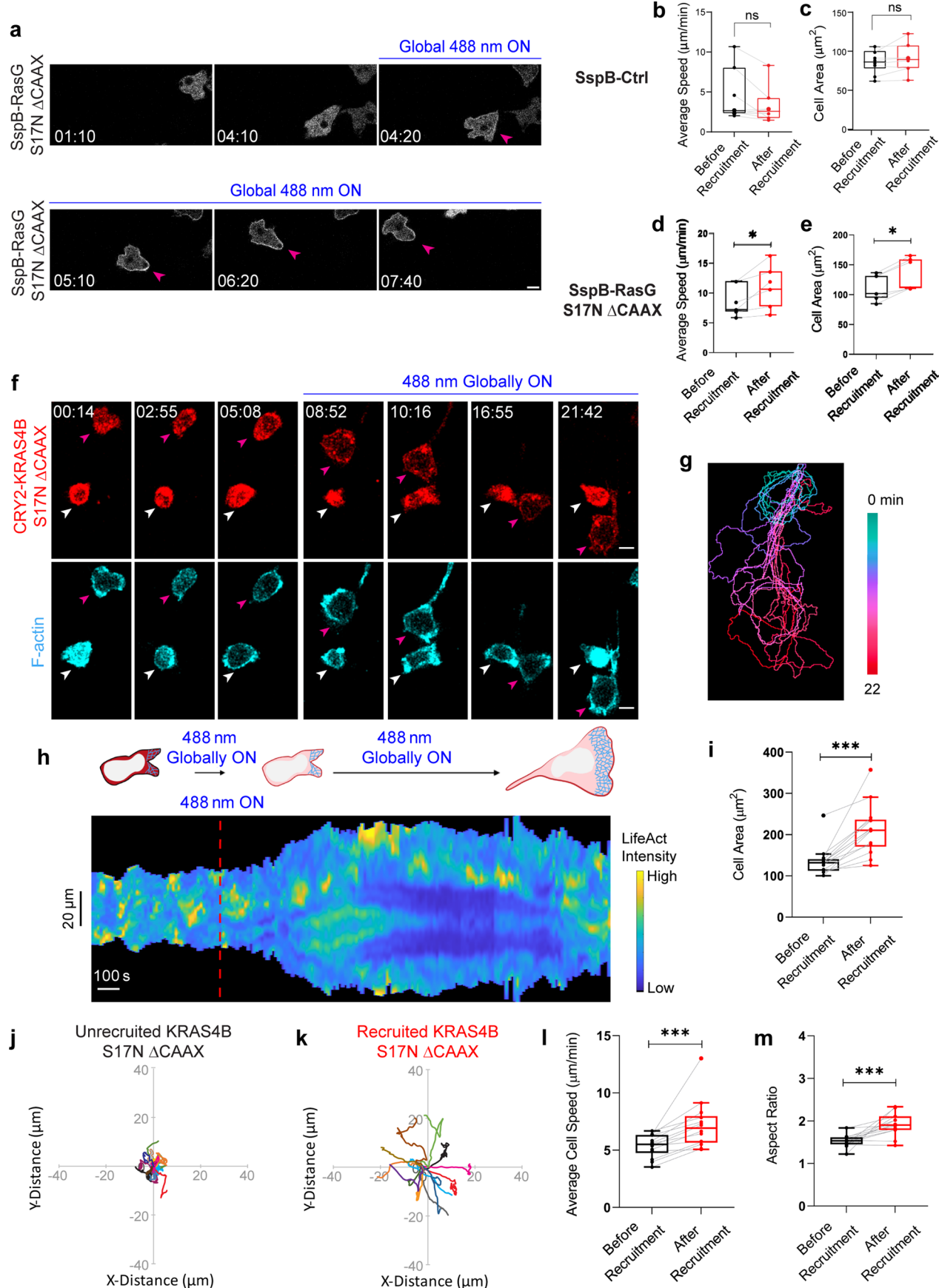
Extended Data Fig. 1 | C2GAPB or RasG S17N regulates Ras and protrusive activities. (a) Representative images of vegetative *Dictyostelium* before (top panel, ‘-DOX’) and after (bottom panel, ‘+DOX’) doxycycline-induced GFP-C2GAPB (green) expression. Cells (DIC) were treated with TRITC-dextran (red) before imaging. Scale bars: 10 μ m. (b) Macropinocytosis uptake measurements, before (black) and after (red) C2GAPB expression. n = 103 cells for ‘-DOX’ and n = 103 cells for ‘+DOX’, over 3 independent experiments; asterisks indicate significant difference, ***P \leq 0.0001 (Two-sided Mann-Whitney test). Boxes extend from 25th to 75th percentiles, median is at the centre, and whiskers and outliers are graphed according to Tukey’s convention (GraphPad Prism 8). (c) Time-lapse images of vegetative *Dictyostelium* expressing mRFPmars-RasG S17N (red, bottom panel, ‘+DOX’) and RBD-GFP (green) after doxycycline treatment. Pink arrows denote RBD patches without RasG S17N. Time in ‘min’ format. Scale bars represent 5 μ m. (d) Time-lapse images of C2GAPB-null *Dictyostelium* expressing RBD-GFP. Time in ‘min’ format. Scale bars: 5 μ m.

Time-lapse images of *Dictyostelium* or neutrophil expressing mRFPmars-SspB R73Q-RasG S17N Δ CAAX (e) or CRY2PHR-mCherry-KRAS4B S17N Δ CAAX (red; upper panel) and LifeAct-miRFP703 (cyan; lower panel) (g). RasG or KRAS4B S17N Δ CAAX was recruited to cell front by applying laser near it, as shown by dashed white box. White arrows denote existing protrusions whereas pink arrows highlight newer protrusions. Time in min:s format. Scale bars: 5 μ m. (h) Polar histogram demonstrates higher probability of fresh protrusion formation away from recruitment area; n = 32 protrusions pooled from 14 cells, examined over 3 independent experiments. (f) Time-lapse images of latrunculin A-treated *Dictyostelium* expressing mRFPmars-SspB R73Q-C2GAPB (red; bottom panel) and RBD-YFP (yellow; top panel) before or after global recruitment. Pink arrows indicate RBD patches whereas white arrows denote recruitment. Time in min:s format. Scale bars: 5 μ m. (i,j) Colour-coded (2-mins intervals) outlines of cells in (c). Source numerical data are provided.



Extended Data Fig. 2 | C2GAPB or RasG S17N-induced polarization localizes actin polymerization to a single front, and does not require development or GPCR signalling. (a) Time-lapse confocal images of vegetative C2GAPB-null *Dictyostelium* cells expressing LimE-GFP. Time in 'min' format. Scale bars represent 5 μm. (b) Time-lapse confocal images of vegetative *Dictyostelium* cells expressing mRFPmars-RasG S17N (red) and LimE-GFP (green) after overnight doxycycline treatment. Pink arrows denote LimE-rich F-actin patches at the cellular protrusions. Time in 'min' format. Scale bars represent 5 μm. (c) Representative western blot ($n = 2$ independent experiments) showing endogenous expression of cAR1 (~44 kDa) in developing wild-type (WT) or

C2GAPB-expressing *Dictyostelium* cells during starvation (0–8 hrs). cAR1 appears as a doublet denoting its two forms, unmodified (lower band) and phosphorylated (upper band). (d) Time-lapse confocal images of vegetative Gβ-null *Dictyostelium* cells expressing mRFPmars-C2GAPB (bottom panel) or tgRFPt-Ctrl (control without C2GAPB; top panel) after overnight doxycycline treatment. Time in 'sec' format. Scale bars represent 5 μm. Colour-coded (at 1-min interval) outlines of the C2GAPB- or Ctrl-expressing cell. (e) Time-lapse confocal images of Gβ-null *Dictyostelium* cell expressing mRFPmars-SspB R73Q-C2GAPB, before or after 488 nm laser was switched on globally. Time in min:sec format. Scale bars represent 5 μm. Colour-coded (at 1-min interval) outlines of this cell are provided.



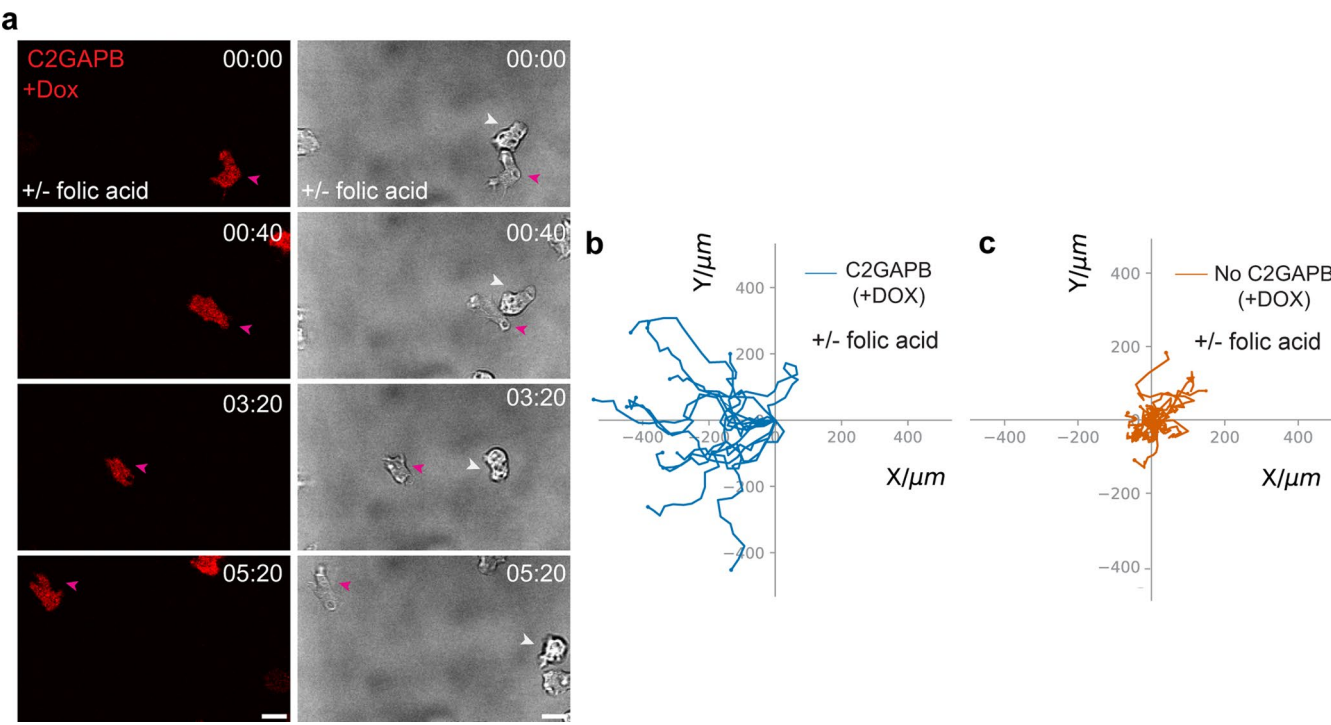
Extended Data Fig. 3 | See next page for caption.

Extended Data Fig. 3 | Global recruitment of dominant negative Ras isoforms improves polarity and migration in *Dictyostelium* and neutrophils.

(a) Time-lapse confocal images of vegetative *Dictyostelium* expressing mRFPmars-SspB R73Q-RasG S17N ΔCAAX before or after laser was switched on globally. Pink arrows denote recruitment causing increased movement. Time in min:sec format. Scale bars: 5 μm. Box-and-whisker plots of (b, d) average cell speed, and (c, e) cell area, before (black) or after (red) opto-Ctrl (control) or opto-RasG S17N ΔCAAX recruitment. n = 10 (Ctrl) or n = 7 cells (RasGS17N ΔCAAX) examined over 3 independent experiments; asterisks indicate significant difference, *P = 0.0313 (d), *P = 0.0156 (e); ns denotes non-significant difference, P = 0.2730 (b), P = 0.7394 (c) (Two-sided Wilcoxon signed-rank test). (f) Time-lapse images of neutrophil expressing CRY2PHR-mCherry-KRAS4B S17N ΔCAAX (red; upper panel) and LifeAct-miRFP703 (cyan; lower panel), before or after recruitment. Pink arrows denote recruited cell; white arrows indicate control cell where there was no recruitment. Time in min:sec format. Scale bars: 5 μm.

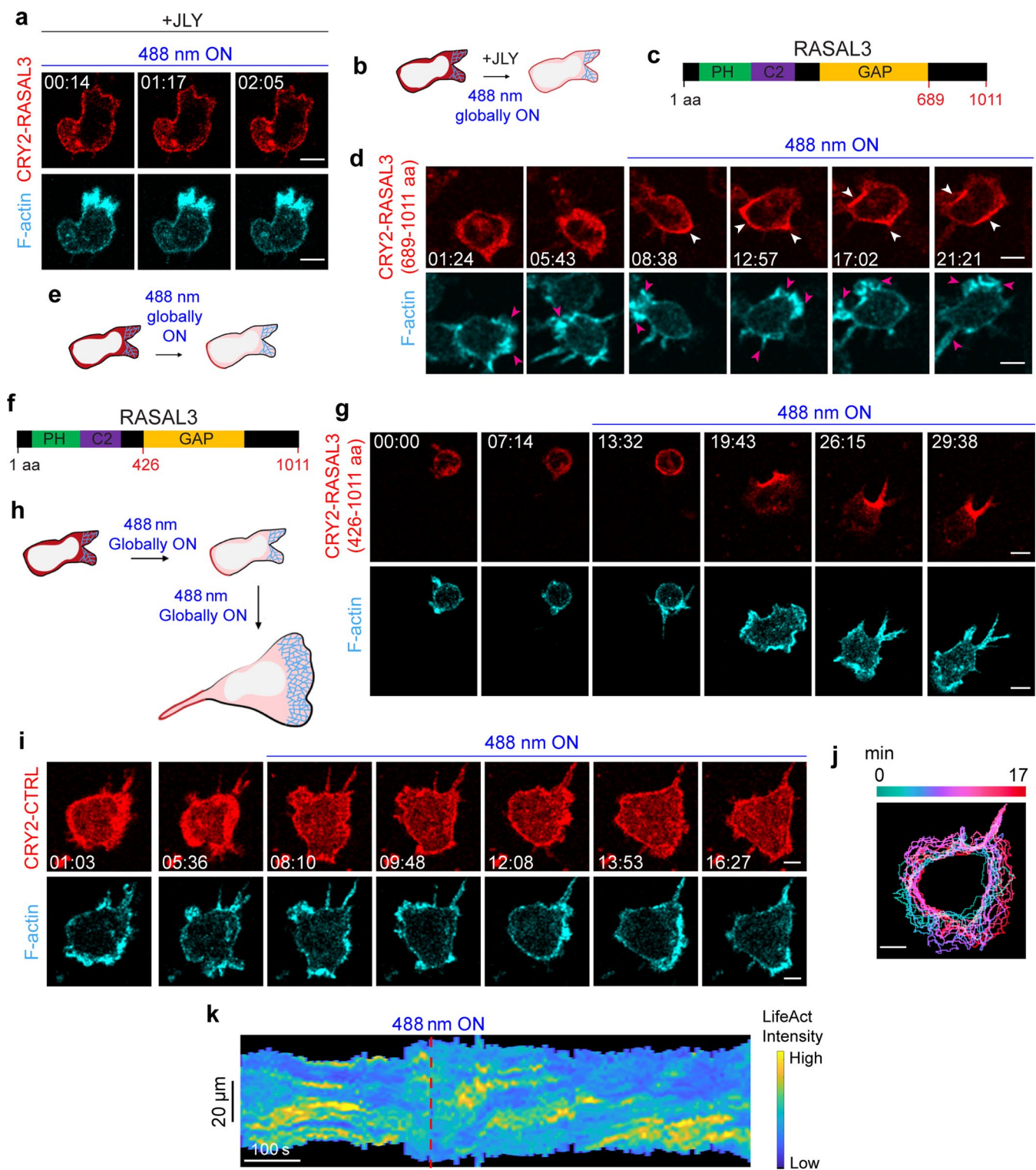
(g) Colour-coded (1-min intervals) outlines of recruited cell in (f).

(h) Representative kymograph of cortical LifeAct intensity before or after recruitment. Linear colour map shows that blue is the lowest LifeAct intensity whereas yellow is the highest. Duration of kymograph is 22 mins. Cartoon depicts recruitment, F-actin polymerization or cell shape corresponding to kymograph. Box-and-whisker plots of (i) cell area, (l) average speed, and (m) aspect ratio, before (black) or after (red) recruitment. n = 14 cells examined over 3 independent experiments; asterisks indicate significant difference, ***P ≤ 0.001 (Two-sided Wilcoxon signed-rank test). Centroid tracks (n = 13 cells from 3 independent experiments) showing motility before (j) or after (k) recruitment. Each track lasts 5 mins and was reset to same origin. (b-e,i,l,m) Boxes extend from 25th to 75th percentiles, median is at the centre, and whiskers and outliers are graphed according to Tukey's convention. Connecting lines are provided between paired data points obtained from the same cell, before or after KRAS4B S17N ΔCAAX recruitment (GraphPad Prism 8). Source numerical data are provided.



Extended Data Fig. 4 | C2GAPB-induced polarity promotes vegetative *Dictyostelium* migration in folic acid gradients. (a) Time-lapse confocal images of vegetative *Dictyostelium* cells, with (red arrow) or without (white arrow; right panel) mRFPmars-SspB R73Q-C2GAPB inducible expression, chemotaxing to 100 nM folic acid. '+/- folic acid' denotes that chemoattractant source was on the left-hand side of this field. Time in min:sec format. Scale bars represent 10 μ m.

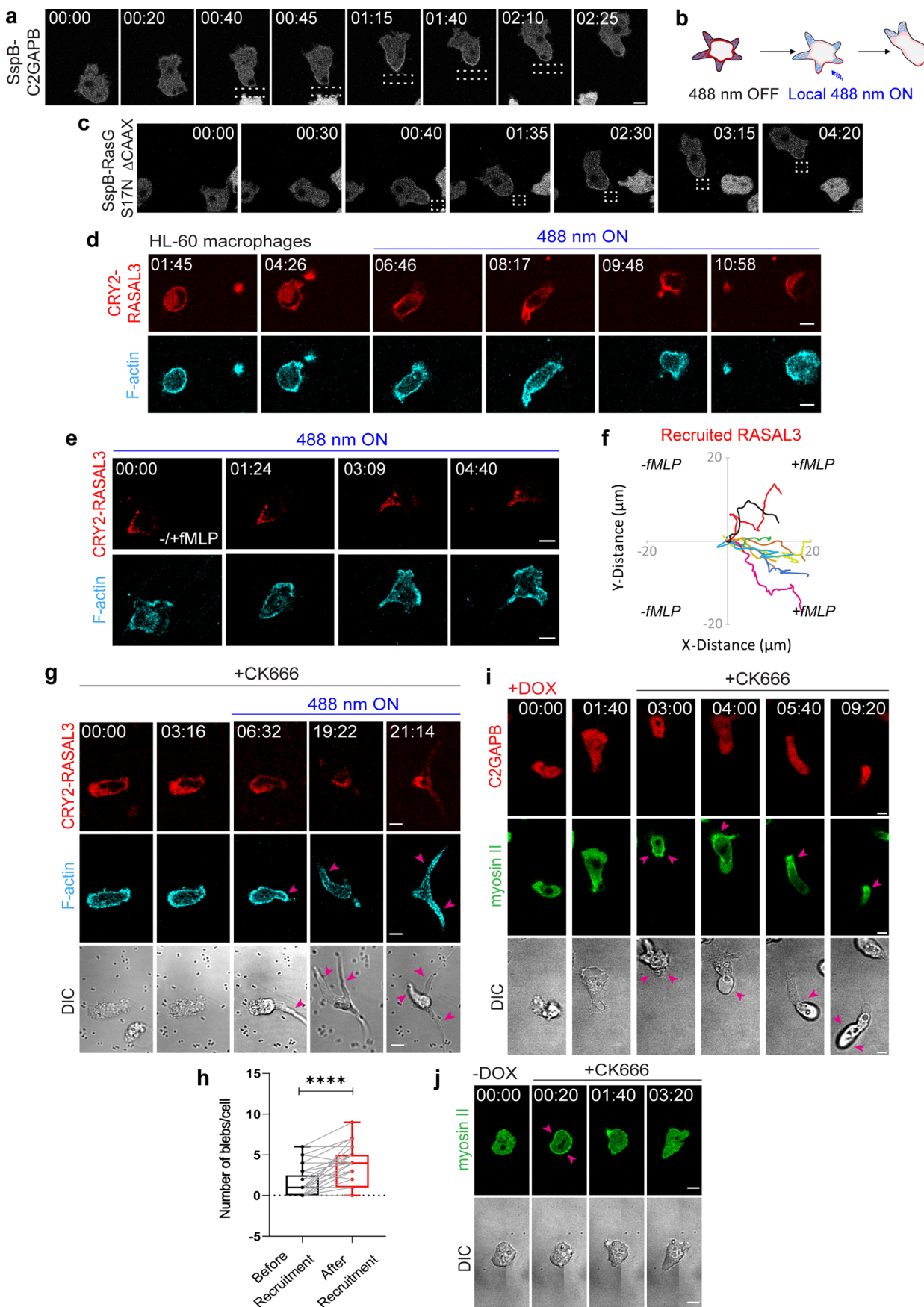
(b) Centroid tracks of cells with (blue) or without (orange) C2GAPB expression. $n = 20$ cells (C2GAPB, b) or $n = 20$ cells (No C2GAPB, c) were pooled from the same doxycycline-treated population migrating to a folic acid gradient, examined over 3 independent experiments. Each track lasts at least 20 mins and was reset to same origin. Source numerical data are provided.



Extended Data Fig. 5 | See next page for caption.

Extended Data Fig. 5 | RASAL3 back localization is dependent on cytoskeletal dynamics and its C-terminal tail whereas it induces polarity through its GAP domain. (a) Time-lapse confocal images of JLY cocktail-treated HL-60 neutrophil expressing CRY2PHR-mCherry-RASAL3 (red; upper panel) and LifeAct-miRFP703 (cyan; lower panel), after 488 nm laser was turned on globally. Time in min:sec format. Scale bars represent 5 μ m. (b) Cartoon shows that JLY treatment caused RASAL3 to recruit uniformly instead of localizing to the back. (c, f) Schematics showing RASAL3 protein sequence (1–1011 amino acid long). Two truncation mutants were generated in this study: (c) RASAL3₆₈₉₋₁₀₁₁ which consists of only the C-terminal tail (689–1011 amino acids) and (f) RASAL3₄₂₆₋₁₀₁₁ consisting of the GAP domain along with the C-terminal tail (426–1011 amino acids). (d, g) Time-lapse confocal images of differentiated HL-60 neutrophil expressing (d) CRY2PHR-mCherry-RASAL3 (689-1011aa) or (g) CRY2PHR-mCherry-RASAL3 (426-1011 aa)

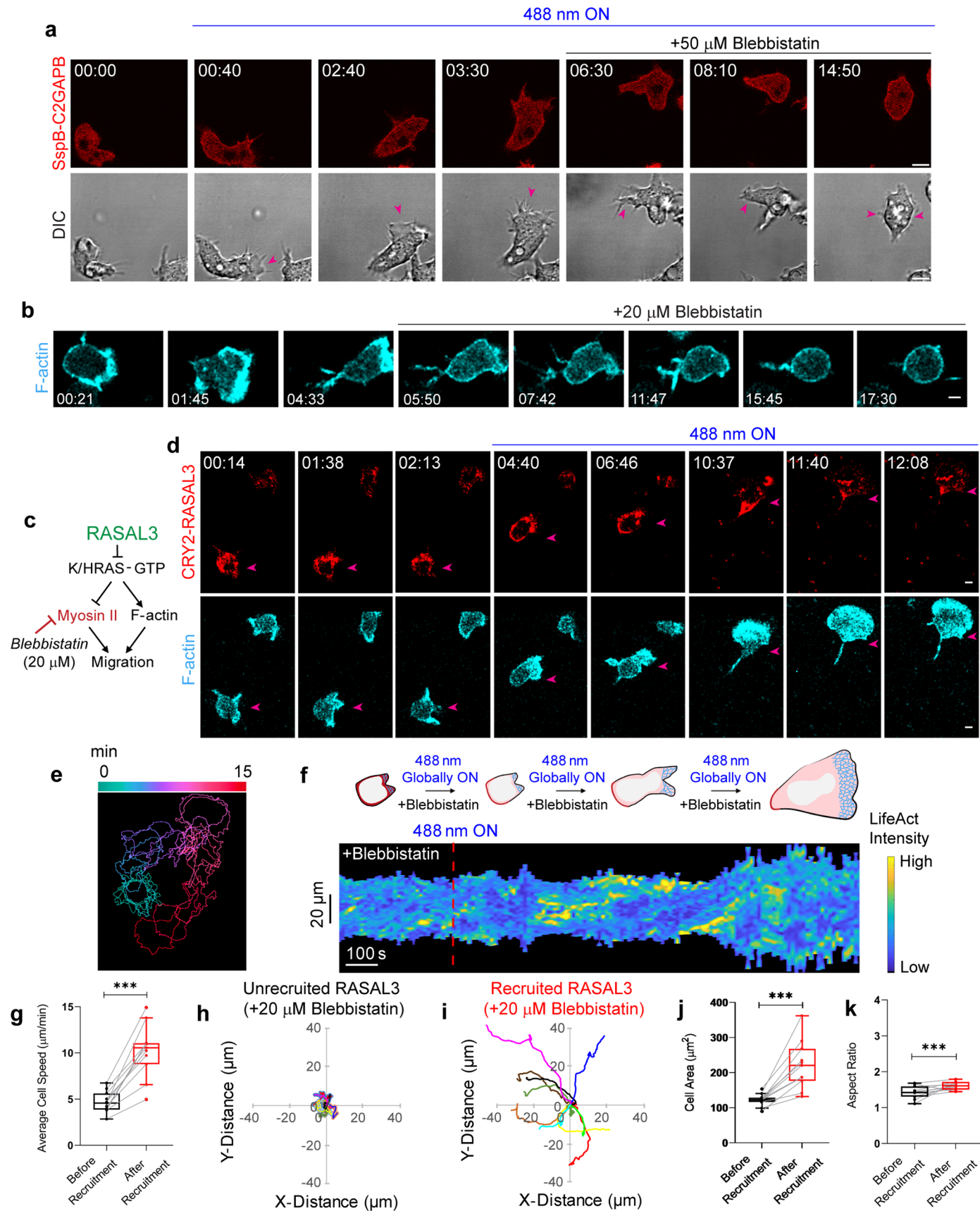
(red; upper panel) and LifeAct-miRFP703 (cyan; lower panel), before or after 488 nm laser was turned on globally. Time in min:sec format. Scale bars represent 5 μ m. (e, h) Cartoons demonstrate phenomenon observed with recruiting CRY2PHR-mCherry-RASAL3 (689-1011aa) or CRY2PHR-mCherry-RASAL3 (426-1011 aa) in differentiated neutrophils. (i) Time-lapse confocal images of differentiated HL-60 neutrophil expressing CRY2PHR-mCherry-CTRL (control without RASAL3, red; upper panel) and LifeAct-miRFP703 (cyan; lower panel), before or after 488 nm laser was globally applied. Time in min:sec format. Scale bars represent 5 μ m. (j) Colour-coded (at 1-min intervals) outlines of the cell shown in (i). (k) Representative kymograph of cortical LifeAct intensity in CTRL-expressing neutrophil before or after 488 nm laser was switched on. A linear colour map shows that blue is the lowest LifeAct intensity whereas yellow is the highest. Duration of the kymograph is 17 mins.



Extended Data Fig. 6 | See next page for caption.

Extended Data Fig. 6 | Ras suppression at the back improves polarity and contraction-driven migration. Representative images of *Dictyostelium* expressing (a) mRFPmars-SspB R73Q-C2GAPB or (c) mRFPmars-SspB R73Q-RasG S17N ΔCAAX recruited to the back by applying laser near it (dashed white box). Time in min:sec format. Scale bars: 5 μm. (b) Cartoon demonstrates phenomenon in (a) and (c). (d) Time-lapse images of macrophage expressing CRY2PHR-mCherry-RASAL3 (red; upper panel) and LifeAct-miRFP703 (cyan; lower panel), before or after global recruitment. Time in min:sec format. Scale bars represent 5 μm. (e) Time-lapse images of neutrophil expressing CRY2PHR-mCherry-RASAL3 (red; upper panel) and LifeAct-miRFP703 (cyan; lower panel), placed in fMLP gradient, post-global recruitment. Chemoattractant was located on right-hand side of the field. Time in min:sec format. Scale bars: 5 μm. (f) Centroid tracks of chemotaxing opto-RASAL3-recruited neutrophils (n = 10 cells pooled from 3 independent experiments). Tracks last 2 mins and was reset to same origin. (g) Time-lapse images of CK666-treated neutrophil expressing CRY2PHR-mCherry-RASAL3 (red; upper panel) and LifeAct-miRFP703 (cyan;

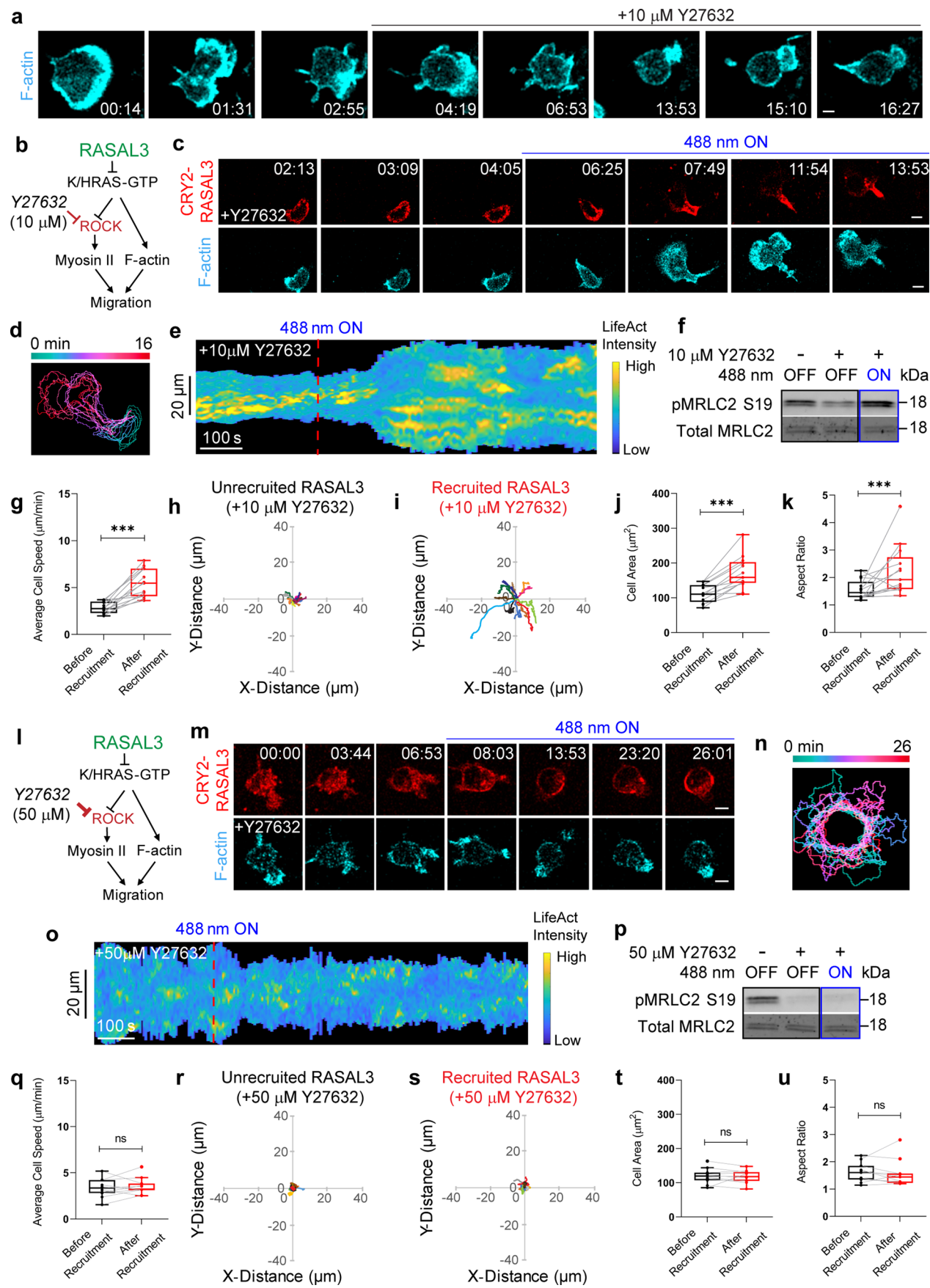
lower panel), before or after recruitment. Pink arrows denote long blebs which appear after recruited RASAL3 localized to back. Time in min:sec format. Scale bars: 5 μm. (h) Quantification of number of blebs per cell within a minute, before (black) or after (red) recruitment. n = 37 CK666-treated cells examined over 3 independent experiments; asterisks indicate significant difference, ****P ≤ 0.0001 (Two-sided Wilcoxon signed-rank test). Boxes extend from 25th to 75th percentiles, median is at the centre, and whiskers and outliers are graphed according to Tukey's convention. Connecting lines are provided between paired data points obtained from the same CK666-treated cell, before or after RASAL3 recruitment (GraphPad Prism 8). Time-lapse images of *Dictyostelium* expressing mRFPmars-C2GAPB (red; top panel) and myosin II-GFP (green; middle panel) before (j) or after (i) doxycycline treatment. CK666 was added during imaging. Since there is no C2GAPB expression without doxycycline, red panel is not shown in (j). Pink arrows denote long blebs (DIC) in C2GAPB-expressing cells after CK666 was added. Time in min:sec format. Scale bars: 5 μm. Source numerical data are provided.



Extended Data Fig. 7 | See next page for caption.

Extended Data Fig. 7 | RasGAP recruitment cannot overcome blebbistatin inhibition but partially overcomes a sub-optimal dose. **(a)** Time-lapse images of *Dictyostelium* expressing mRFPmars-SspB R73Q-C2GAPB (red; top panel), before or after global recruitment. 50 μM blebbistatin was added during imaging. Pink arrows denote cell of interest (DIC). Time in min:sec format. Scale bars: 5 μm. **(b)** Time-lapse images of neutrophil expressing LifeAct-miRFP703 (cyan; lower panel), before or after low-dose blebbistatin (20 μM) treatment. Time in min:sec format. Scale bars: 5 μm. **(c)** Strategy for testing low-dose blebbistatin on RASAL3-directed myosin II contraction and migration. **(d)** Time-lapse images of 20 μM blebbistatin-treated neutrophil expressing CRY2PHR-mCherry-RASAL3 (red; upper panel) and LifeAct-miRFP703 (cyan; lower panel), before or after recruitment. Time in min:sec format. Scale bars: 5 μm. **(e)** Colour-coded (1-min intervals) outlines of cell in **(d)**. **(f)** Representative kymograph of cortical LifeAct intensity before or after recruitment. Linear colour map shows that blue is the

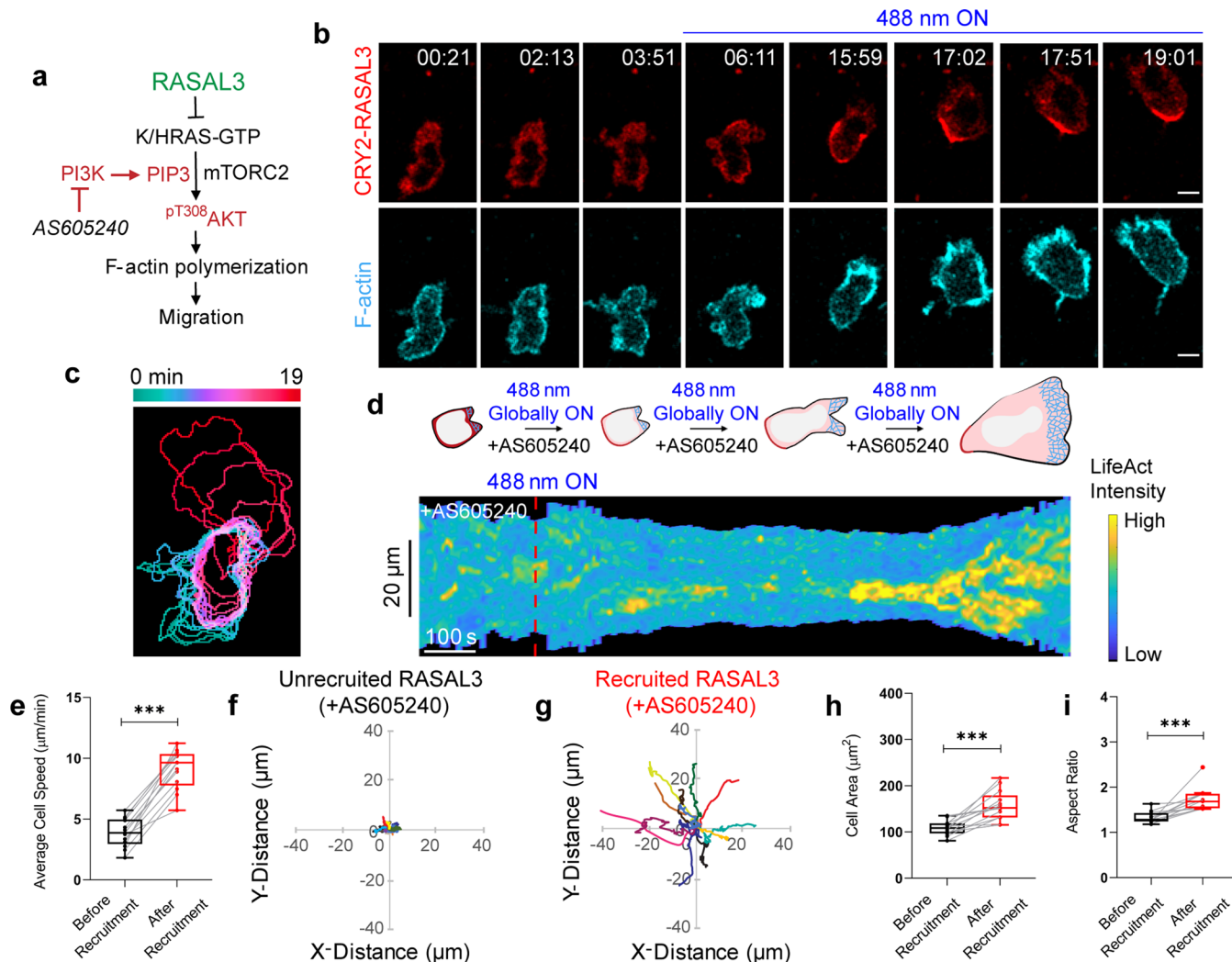
lowest LifeAct intensity whereas yellow is the highest. Duration of kymograph is 16 mins. Cartoon summarizes recruitment, actin polymerization or cell shape corresponding to kymograph. Box-and-whisker plots of **(g)** average speed, **(j)** basal area, and **(k)** aspect ratio, before (black) and after (red) recruitment in blebbistatin-treated cells. n = 11 cells examined over 3 independent experiments; asterisks indicate significant difference, ***P = 0.001 (Two-sided Wilcoxon signed-rank test). Boxes extend from 25th to 75th percentiles, median is at the centre, and whiskers and outliers are graphed according to Tukey's convention. Connecting lines are provided between paired data points obtained from the same blebbistatin-treated cell, before or after RASAL3 recruitment (GraphPad Prism 8). Centroid tracks of 20 μM blebbistatin-treated neutrophils (n = 10 cells from 3 independent experiments) showing motility before **(h)** or after **(i)** RASAL3 recruitment. Each track lasts 5 mins and was reset to same origin. Source numerical data are provided.



Extended Data Fig. 8 | See next page for caption.

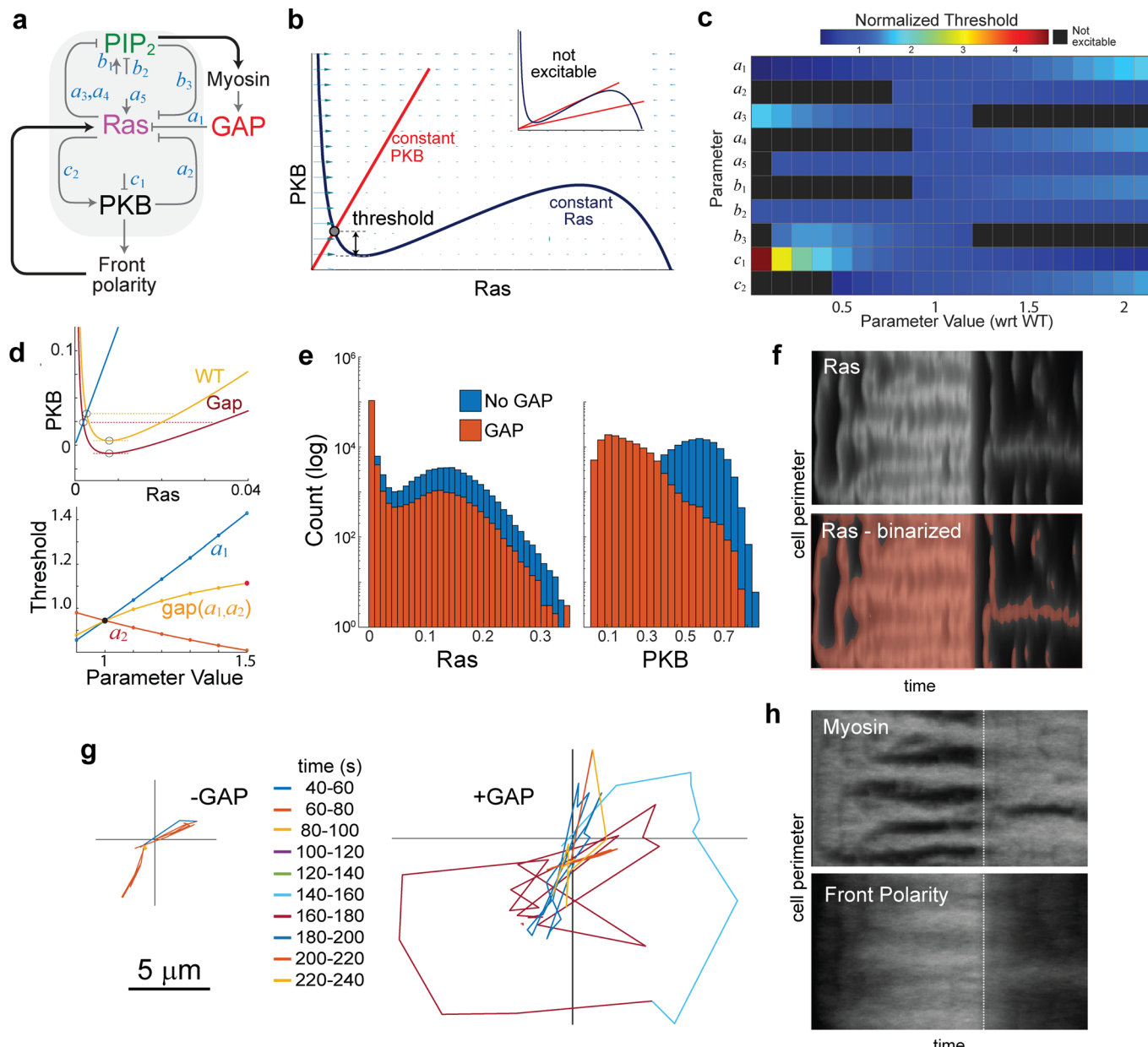
Extended Data Fig. 8 | RasGAP-induced polarization works through ROCK-mediated myosin II phosphorylation. (a) Time-lapse images of neutrophil expressing LifeAct-miRFP703 (cyan; lower panel), before or after low-dose Y27632 (10 μM) treatment. Time in min:sec format. Scale bars: 5 μm. Strategy for testing (b) low (10 μM) or (l) high (50 μM) Y27632 dose on RASAL3-directed myosin II contraction and migration. Time-lapse images of (c) 10 μM or (m) 50 μM Y27632-treated neutrophil expressing CRY2PHR-mCherry-RASAL3 (red; upper panel) and LifeAct-miRFP703 (cyan; lower panel), before or after global recruitment. Time in min:sec format. Scale bars: 5 μm. (d, n) Colour-coded (1-min intervals) outlines of cells in (c) or (m). (e, o) Representative kymograph of cortical LifeAct intensity in (c) or (m). Linear colour map shows that blue is the lowest LifeAct intensity whereas yellow is the highest. Duration of kymograph is 16 (e) or 26 (o) mins. Immunoblot comparing phospho-MRLC2 Ser19 (18 kDa) in cell lysates of 10 μM (f) or 50 μM (p) Y27632-treated, opto-RASAL3-expressing population, before or after recruitment (n = 3 independent experiments).

Quantifications of (g, q) cell speed, (j, t) area, and (k, u) aspect ratio, before (black) and after (red) recruitment in 10 or 50 μM Y27632-treated cells. n = 13 (g,j,k) or n = 11 cells (q,t,u) examined over 3 independent experiments; asterisks indicate significant difference, ***P = 0.0002 (g,j,k); ns denotes non-significant difference P = 0.4648 (q), P = 0.2402 (t), P = 0.3652 (u) (Two-sided Wilcoxon signed-rank test). Boxes extend from 25th to 75th percentiles, median is at the centre, and whiskers and outliers are graphed according to Tukey's convention. Connecting lines are provided between paired data points obtained from the same Y27632-treated cell, before or after RASAL3 recruitment (GraphPad Prism 8). Centroid tracks of 10 μM (n = 12 cells from 3 independent experiments) or 50 μM (n = 10 cells from 3 independent experiments) Y27632-treated neutrophils showing random motility before (h, r) or after (i, s) RASAL3 recruitment. Each track lasts 5 mins and was reset to same origin. Source numerical data and unprocessed blots are provided.



Extended Data Fig. 9 | Global RASAL3 recruitment overcomes PI3K γ inhibition. (a) Strategy for testing effect of PI3K γ inhibitor, AS605240, on RASAL3-directed actin polymerization and motility. (b) Time-lapse confocal images of AS605240-treated HL-60 neutrophil expressing CRY2PHR-mCherry-RASAL3 (red; upper panel) and LifeAct-mRFP703 (cyan; lower panel), before or after 488 nm laser was turned on globally. Time in min:sec format. Scale bars represent 5 μ m. (c) Colour-coded (1-min intervals) outlines of the cells shown in (b). (d) Representative kymograph of cortical LifeAct intensity in AS605240-treated RASAL3-expressing neutrophils before or after 488 nm laser was turned on. A linear colour map shows that blue is the lowest LifeAct intensity whereas yellow is the highest. Duration of the kymograph is 19 mins. Cartoon summarizes membrane recruitment, actin polymerization or cell shape status

corresponding to the kymograph. Box-and-whisker plots of (e) cell speed, (h) cell area, and (i) aspect ratio, before (black) and after (red) RASAL3 recruitment in AS605240-treated cells. n = 13 cells examined over 3 independent experiments; asterisks indicate significant difference, ***P = 0.0002 (Two-sided Wilcoxon signed-rank test). The boxes extend from 25th to 75th percentiles, median is at the centre, and whiskers and outliers are graphed according to Tukey's convention. Connecting lines are provided between paired data points obtained from the same AS605240-treated cell, before or after RASAL3 recruitment (GraphPad Prism 8). Centroid tracks of AS605240-treated neutrophils (n = 12 cells from 3 independent experiments) showing random motility before (f) or after (g) RASAL3 recruitment. Each track lasts 5 mins and was reset to same origin. Source numerical data are provided.



Extended Data Fig. 10 | Effect of GAP on EN system threshold and feedback loops that affect cell polarization. (a) Model schematic of signal transduction pathway showing relevant parameters of Ras-PIP₂-PKB excitable network. (b) Phase-plane diagram of Ras-PKB excitable network showing curves on which Ras and PKB stay constant, the equilibrium and the threshold of the EN system. The inset depicts two sets of parameter values in which the system is no longer excitable. (c) Sensitivity analysis of the system. The heatmap shows the change in threshold values normalized with respect to WT threshold for each of the ten parameters (a) of the EN. (d) Top: Thresholds in presence and absence (WT) of GAP on the Ras-PKB phase-plane. Bottom: Variation of value of the threshold between 0–1.5 times the WT value for two parameters a_1 and a_2 and their combined effect to captures the GAP effect. In our simulations the GAP value of the parameters is 1.5 times the WT value. (e) Histogram of cumulative Ras (left)

and PKB (right) across 10 simulations before and after GAP recruitment. (f) Kymograph showing Ras activity around cell perimeter as a function of time (x-axis; 0–240 seconds). The bottom superimposes binarized locations where Ras > 0.25. Points before 140 seconds correspond to WT, and after 140 seconds correspond to global GAP recruitment. (g) The trajectory of CM of a single cell before and after GAP recruitment. The two plots show the path taken across different time segments of the simulation (denoted by the colour) before and after recruitment of GAP. Absent colours from the graph shown in the legend, denote no movement in that interval. The thresholded Ras kymographs of panel f were used to generate trajectories in g. (h) Kymographs of the myosin and front polarity terms. The dotted line shows the time at which the GAP value was increased.

QUERY FORM

Manuscript ID	[Art. Id: 1453]
Author	Yiyan Lin

AUTHOR:

The following queries have arisen during the editing of your manuscript. Please answer by making the requisite corrections directly in the e.proofing tool rather than marking them up on the PDF. This will ensure that your corrections are incorporated accurately and that your paper is published as quickly as possible.

Query No.	Nature of Query
Q1:	Please check your article carefully, coordinate with any co-authors and enter all final edits clearly in the eproof, remembering to save frequently. Once corrections are submitted, we cannot routinely make further changes to the article.
Q2:	Note that the eproof should be amended in only one browser window at any one time; otherwise changes will be overwritten.
Q3:	Author surnames have been highlighted. Please check these carefully and adjust if the first name or surname is marked up incorrectly, as this will affect indexing of your article in public repositories such as PubMed. Also, carefully check the spelling and numbering of all author names and affiliations, and the corresponding author(s) email address(es). Please note that email addresses should only be included for designated corresponding authors, and you cannot change corresponding authors at this stage except to correct errors made during typesetting.
Q4:	You cannot alter accepted Supplementary Information files except for critical changes to scientific content. If you do resupply any files, please also provide a brief (but complete) list of changes. If these are not considered scientific changes, any altered Supplementary files will not be used, only the originally accepted version will be published.
Q5:	Please check Figures for accuracy as they have been relabelled. Please markup minor changes in the eProof. For major changes, please provide revised figures. (Please note that in the eProof the figure resolution will appear at lower resolution than in the pdf and html versions of your paper.)
Q6:	If applicable, please ensure that any accession codes and datasets whose DOIs or other identifiers are mentioned in the paper are scheduled for public release as soon as possible, we recommend within a few days of submitting your proof, and update the database record with publication details from this article once available.
Q7:	Please ensure that genes are correctly distinguished from gene products: for genes, official gene symbols (e.g., NCBI Gene) for the relevant species should be used and italicized; gene products such as proteins and noncoding RNAs should not be italicized.

QUERY FORM

Manuscript ID	[Art. Id: 1453]
Author	Yiyan Lin

AUTHOR:

The following queries have arisen during the editing of your manuscript. Please answer by making the requisite corrections directly in the e.proofing tool rather than marking them up on the PDF. This will ensure that your corrections are incorporated accurately and that your paper is published as quickly as possible.

Query No.	Nature of Query
Q8:	Your paper has been copy edited. Please review every sentence to ensure that it conveys your intended meaning; if changes are required, please provide further clarification rather than reverting to the original text. Please note that formatting (including hyphenation, Latin words, and any reference citations that might be mistaken for exponents) has been made consistent with our house style.
Q9:	Please note that <i>Nature Cell Biology</i> is a UK English journal and so the language has been edited accordingly.
Q10:	Please note, we reserve 'significant' and its derivatives for statistical significance. Please reword where this is not the intended meaning (for example to important, notable, substantial); there are 16 instances throughout your text
Q11:	In the sentence 'In latrunculin-treated cells, dynamic RBD membrane patches disappeared ~30 s of C2GAPB...' please check whether this should be 'within ~30 s of C2GAPB' or '~30 s after C2GAPB'
Q12:	In Fig. 3a caption, please confirm that definition of DIC is correct.
Q13:	Figure panels should be introduced sequentially (alphabetically) in the captions. Please check this in all figure captions. In particular panel f is described out of order in Figure 4.
Q14:	Please check the consistency of the italics for mhcA ⁻ cells throughout. For example, in the sentence beginning 'The mhcA ⁻ cells...'
Q15:	Please check that constructs/compounds are written with an en dash – and not a hyphen throughout.
Q16:	Please check that all RRID url links have been provided throughout.
Q17:	Please check that edits to the sentence beginning 'Here, we introduced...' retain the intended meaning.

QUERY FORM

Manuscript ID	[Art. Id: 1453]
Author	Yiyan Lin

AUTHOR:

The following queries have arisen during the editing of your manuscript. Please answer by making the requisite corrections directly in the e.proofing tool rather than marking them up on the PDF. This will ensure that your corrections are incorporated accurately and that your paper is published as quickly as possible.

Query No.	Nature of Query
Q18:	Please check the figure callouts in the sentence beginning 'For cell speed, area and aspect ratio ...'. Should this be 'Figs. 3d–f and 4c,e,g,h and Extended Data Fig. 3b–e)'?
Q19:	Please check the equations and the term P_B - please define this in the text (and check that this should not be the already defined P_R .)
Q20:	Please check that edit to '...0.5–5 nN/ μm ...' retains the intended meaning in the sentence beginning 'The vector sum of these forces...'.
Q21:	Please confirm that edit to ' μm^{-3} ' is correct in the sentence beginning 'Here...'
Q22:	Please check that all funders have been appropriately acknowledged and that all grant numbers are correct.
Q23:	If applicable, please ensure accession codes are scheduled for release on or before this article's scheduled publication date, and update the database record with publication details from this article once available.
Q24:	Please check that the Competing Interests declaration is correct as stated. If you declare competing interests, please check the full text of the declaration for accuracy and completeness.
Q25:	Panel 'c' is present in the artwork of Extended Data Fig. 4, but it is not mentioned in the figure legend. Please provide a corresponding text of the panel.
Q26:	If ref. 36 (preprint) has now been published in final peer-reviewed form, please update the reference details if appropriate.
Q27:	If ref. 84 (preprint) has now been published in final peer-reviewed form, please update the reference details if appropriate.

Reporting Summary

Nature Portfolio wishes to improve the reproducibility of the work that we publish. This form provides structure for consistency and transparency in reporting. For further information on Nature Portfolio policies, see our [Editorial Policies](#) and the [Editorial Policy Checklist](#).

Statistics

For all statistical analyses, confirm that the following items are present in the figure legend, table legend, main text, or Methods section.

n/a Confirmed

- The exact sample size (n) for each experimental group/condition, given as a discrete number and unit of measurement
- A statement on whether measurements were taken from distinct samples or whether the same sample was measured repeatedly
- The statistical test(s) used AND whether they are one- or two-sided
Only common tests should be described solely by name; describe more complex techniques in the Methods section.
- A description of all covariates tested
- A description of any assumptions or corrections, such as tests of normality and adjustment for multiple comparisons
- A full description of the statistical parameters including central tendency (e.g. means) or other basic estimates (e.g. regression coefficient) AND variation (e.g. standard deviation) or associated estimates of uncertainty (e.g. confidence intervals)
- For null hypothesis testing, the test statistic (e.g. F , t , r) with confidence intervals, effect sizes, degrees of freedom and P value noted
Give P values as exact values whenever suitable.
- For Bayesian analysis, information on the choice of priors and Markov chain Monte Carlo settings
- For hierarchical and complex designs, identification of the appropriate level for tests and full reporting of outcomes
- Estimates of effect sizes (e.g. Cohen's d , Pearson's r), indicating how they were calculated

Our web collection on [statistics for biologists](#) contains articles on many of the points above.

Software and code

Policy information about [availability of computer code](#)

Data collection	Videos of confocal imaging were collected using ZEN Black (2.3 SP1 FP2); Zen Blue (2.3); NIS Elements (Ar 4.40.00 Build 1084) on Zeiss LSM800 and Zeiss LSM780 microscopes. Western blot images were captured with Odyssey CLx imaging system.
Data analysis	Custom-written MATLAB and Python codes, Fiji/ImageJ macros, TrackPY v0.6.2, Pyimagej 1.4.1, along with Microsoft Excel were used for image quantification and analysis. Custom-written MATLAB codes were used for computational simulations. SDE Toolbox of MATLAB was used in simulations. MATLAB and GraphPad Prism were used for statistical analysis. Versions: MATLAB 2019a, Python 3.10, SDE toolbox 1.4.1, Microsoft Excel 2019, Fiji/ImageJ 1.52i, OriginPro 9.0, Graphpad Prism 8. Custom computational simulation codes are available on GitHub: https://github.com/piglesi1/GAP-role-in-polarization . They are available under the GNU General Public License v3.0. These codes are also available on Zenodo: https://zenodo.org/records/11121861 licensed under Creative Commons Attribution 4.0 International. Any additional information will be available from the corresponding authors upon reasonable request.

For manuscripts utilizing custom algorithms or software that are central to the research but not yet described in published literature, software must be made available to editors and reviewers. We strongly encourage code deposition in a community repository (e.g. GitHub). See the Nature Portfolio [guidelines for submitting code & software](#) for further information.

Data

Policy information about [availability of data](#)

All manuscripts must include a [data availability statement](#). This statement should provide the following information, where applicable:

- Accession codes, unique identifiers, or web links for publicly available datasets
- A description of any restrictions on data availability
- For clinical datasets or third party data, please ensure that the statement adheres to our [policy](#)

All data needed to evaluate the conclusions are provided in the main text and figures, extended data figures, or supplementary tables and videos. All unprocessed immunoblots or raw data and associated statistical calculations are provided along with this study. Data in Fig. 2k and l were reanalyzed here from our previous study (PMID:37220748). Source data are provided with this study. All other data supporting the findings of this study are available from the corresponding authors on reasonable request.

Research involving human participants, their data, or biological material

Policy information about studies with [human participants or human data](#). See also policy information about [sex, gender \(identity/presentation\), and sexual orientation](#) and [race, ethnicity and racism](#).

Reporting on sex and gender	Not Applicable.
Reporting on race, ethnicity, or other socially relevant groupings	Not Applicable.
Population characteristics	Not Applicable.
Recruitment	Not Applicable.
Ethics oversight	Not Applicable.

Note that full information on the approval of the study protocol must also be provided in the manuscript.

Field-specific reporting

Please select the one below that is the best fit for your research. If you are not sure, read the appropriate sections before making your selection.

Life sciences Behavioural & social sciences Ecological, evolutionary & environmental sciences

For a reference copy of the document with all sections, see nature.com/documents/nr-reporting-summary-flat.pdf

Life sciences study design

All studies must disclose on these points even when the disclosure is negative.

Sample size	Sample sizes were chosen large enough to account for the heterogeneity among cells. No statistical methods were used to pre-determine sample sizes, but our sample sizes are similar to those reported in previous publications with similar experiments in our laboratory (Miao Y et al. 2017, Lampert T J et al., 2017, Li X et al. 2018, Miao Y et al. 2019, Zhan H et al. 2020, etc). Chosen sample sizes are consistent with those that were reported by other researchers in the field as well (Yang Y et al. 2017, Shellard A. et al. 2018, O'Neill P R et al. 2018, Matsuoka S et al. 2018, Graziano B R et al. 2019, Bisaria A et al. 2020, etc). Similar sample sizes were used for experiment and control group. To generate any data point, usually at least 200 images were analyzed.
Data exclusions	No data were excluded from the analyses.
Replication	All reported findings were reliably reproduced using atleast three independent biological replicates.
Randomization	The experiments were not randomized. Randomization is not relevant to our study since all experiments were conducted on cultured cells. Any variations observed between treatment groups are not attributed to sampling bias.
Blinding	Data collection and analysis were not performed blind to the conditions of the experiments.

Behavioural & social sciences study design

All studies must disclose on these points even when the disclosure is negative.

Study description	<i>Briefly describe the study type including whether data are quantitative, qualitative, or mixed-methods (e.g. qualitative cross-sectional, quantitative experimental, mixed-methods case study).</i>
Research sample	<i>State the research sample (e.g. Harvard university undergraduates, villagers in rural India) and provide relevant demographic information (e.g. age, sex) and indicate whether the sample is representative. Provide a rationale for the study sample chosen. For studies involving existing datasets, please describe the dataset and source.</i>
Sampling strategy	<i>Describe the sampling procedure (e.g. random, snowball, stratified, convenience). Describe the statistical methods that were used to predetermine sample size OR if no sample-size calculation was performed, describe how sample sizes were chosen and provide a rationale for why these sample sizes are sufficient. For qualitative data, please indicate whether data saturation was considered, and what criteria were used to decide that no further sampling was needed.</i>
Data collection	<i>Provide details about the data collection procedure, including the instruments or devices used to record the data (e.g. pen and paper, computer, eye tracker, video or audio equipment) whether anyone was present besides the participant(s) and the researcher, and whether the researcher was blind to experimental condition and/or the study hypothesis during data collection.</i>
Timing	<i>Indicate the start and stop dates of data collection. If there is a gap between collection periods, state the dates for each sample cohort.</i>
Data exclusions	<i>If no data were excluded from the analyses, state so OR if data were excluded, provide the exact number of exclusions and the rationale behind them, indicating whether exclusion criteria were pre-established.</i>
Non-participation	<i>State how many participants dropped out/declined participation and the reason(s) given OR provide response rate OR state that no participants dropped out/declined participation.</i>
Randomization	<i>If participants were not allocated into experimental groups, state so OR describe how participants were allocated to groups, and if allocation was not random, describe how covariates were controlled.</i>

Ecological, evolutionary & environmental sciences study design

All studies must disclose on these points even when the disclosure is negative.

Study description	<i>Briefly describe the study. For quantitative data include treatment factors and interactions, design structure (e.g. factorial, nested, hierarchical), nature and number of experimental units and replicates.</i>
Research sample	<i>Describe the research sample (e.g. a group of tagged Passer domesticus, all Stenocereus thurberi within Organ Pipe Cactus National Monument), and provide a rationale for the sample choice. When relevant, describe the organism taxa, source, sex, age range and any manipulations. State what population the sample is meant to represent when applicable. For studies involving existing datasets, describe the data and its source.</i>
Sampling strategy	<i>Note the sampling procedure. Describe the statistical methods that were used to predetermine sample size OR if no sample-size calculation was performed, describe how sample sizes were chosen and provide a rationale for why these sample sizes are sufficient.</i>
Data collection	<i>Describe the data collection procedure, including who recorded the data and how.</i>
Timing and spatial scale	<i>Indicate the start and stop dates of data collection, noting the frequency and periodicity of sampling and providing a rationale for these choices. If there is a gap between collection periods, state the dates for each sample cohort. Specify the spatial scale from which the data are taken.</i>
Data exclusions	<i>If no data were excluded from the analyses, state so OR if data were excluded, describe the exclusions and the rationale behind them, indicating whether exclusion criteria were pre-established.</i>
Reproducibility	<i>Describe the measures taken to verify the reproducibility of experimental findings. For each experiment, note whether any attempts to repeat the experiment failed OR state that all attempts to repeat the experiment were successful.</i>
Randomization	<i>Describe how samples/organisms/participants were allocated into groups. If allocation was not random, describe how covariates were controlled. If this is not relevant to your study, explain why.</i>
Blinding	<i>Describe the extent of blinding used during data acquisition and analysis. If blinding was not possible, describe why OR explain why blinding was not relevant to your study.</i>

Did the study involve field work? Yes No

Field work, collection and transport

Field conditions	Describe the study conditions for field work, providing relevant parameters (e.g. temperature, rainfall).
Location	State the location of the sampling or experiment, providing relevant parameters (e.g. latitude and longitude, elevation, water depth).
Access & import/export	Describe the efforts you have made to access habitats and to collect and import/export your samples in a responsible manner and in compliance with local, national and international laws, noting any permits that were obtained (give the name of the issuing authority, the date of issue, and any identifying information).
Disturbance	Describe any disturbance caused by the study and how it was minimized.

Reporting for specific materials, systems and methods

We require information from authors about some types of materials, experimental systems and methods used in many studies. Here, indicate whether each material, system or method listed is relevant to your study. If you are not sure if a list item applies to your research, read the appropriate section before selecting a response.

Materials & experimental systems		Methods	
n/a	Involved in the study	n/a	Involved in the study
<input type="checkbox"/>	<input checked="" type="checkbox"/> Antibodies	<input checked="" type="checkbox"/>	<input type="checkbox"/> ChIP-seq
<input type="checkbox"/>	<input checked="" type="checkbox"/> Eukaryotic cell lines	<input checked="" type="checkbox"/>	<input type="checkbox"/> Flow cytometry
<input checked="" type="checkbox"/>	<input type="checkbox"/> Palaeontology and archaeology	<input checked="" type="checkbox"/>	<input type="checkbox"/> MRI-based neuroimaging
<input checked="" type="checkbox"/>	<input type="checkbox"/> Animals and other organisms		
<input checked="" type="checkbox"/>	<input type="checkbox"/> Clinical data		
<input checked="" type="checkbox"/>	<input type="checkbox"/> Dual use research of concern		
<input checked="" type="checkbox"/>	<input type="checkbox"/> Plants		

Antibodies

Antibodies used	anti-cAR1 antibody, rabbit (generated in our lab) phospho-MRLC2 Ser19 antibody, mouse (Cell Signaling; #3675) anti-MRLC2 antibody, rabbit (Cell Signaling; #3672) anti-myosin IIA antibody, rabbit (Sigma-Aldrich; #M8064) anti-myosin IIB antibody, rabbit (Sigma-Aldrich; #M7939) anti-GAPDH antibody, rabbit (Invitrogen; #PA1-987) anti-rabbit IRDye 680RD-conjugated, secondary antibody, goat (Li-Cor; #925-68071) anti-mouse IRDye 800CW-conjugated, goat (Li-Cor; #925-32210) secondary antibody Alexa Fluor 488 goat anti-mouse (Thermo Fisher; #A11001) secondary antibody Alexa Fluor 488 goat anti-rabbit (Thermo Fisher; #A11008) secondary antibody
-----------------	--

Validation	cAR1 antibody was generated and validated in our lab previously, and has been used in previous publications (Klein et al JBC 1985, PMID: 2981872; Klein et al Science 1988, PMID: 3047871). phospho-MRLC2 Ser19 antibody, mouse (Cell Signaling; #3675): The antibody guarantee covers the use of the antibody for WB and IF applications. Species reactivity: Human, Mouse, Rat, Bovine, Pig; Sensitivity: Endogenous. anti-MRLC2 antibody, rabbit (Cell Signaling; #3672): The antibody guarantee covers the use of the antibody for WB application. Species reactivity: Human, Mouse, Rat; Sensitivity: Endogenous. anti-myosin IIA antibody, rabbit (Sigma-Aldrich; #M8064): The antibody guarantee covers the use of the antibody for IF, WB, and microarray applications. Species reactivity: Human, Canine, Rat. anti-myosin IIB antibody, rabbit (Sigma-Aldrich; #M7939): The antibody guarantee covers the use of the antibody for WB application. Species reactivity: Human, Canine, Rat. anti-GAPDH antibody, rabbit (Invitrogen; #PA1-987): The antibody guarantee covers the use of the antibody for WB application. Species reactivity: Dog, Human, Mouse, Non-human primate, Rat.
------------	---

Eukaryotic cell lines

Policy information about [cell lines and Sex and Gender in Research](#)

Cell line source(s)	Female human HL-60 cell line (ATCC #CCL-240; RRID:CVCL_0002) was obtained from Orion Weiner lab, UCSF. Dictyostelium AX2 (dictyBase #DBS0235521): Lab stock (originally gift from R.R. Kay, MRC LMB, Cambridge, UK). Dictyostelium C2GAPB null cell line: lab stock (PMID: 30194235). Dictyostelium Gb null cell line: lab stock (PMID: 8099335)
Authentication	HL-60 cell line was originally authenticated by the suppliers using morphology and STR profiling. Dictyostelium cell lines were authenticated by morphology and species-specific primers.

Mycoplasma contamination

No mycoplasma contamination was detected.

Commonly misidentified lines
(See [ICLAC](#) register)

No cell lines used in this study are listed in ICLAC register. No commonly misidentified cell lines were used in this study.

Palaeontology and Archaeology

Specimen provenance

Provide provenance information for specimens and describe permits that were obtained for the work (including the name of the issuing authority, the date of issue, and any identifying information). Permits should encompass collection and, where applicable, export.

Specimen deposition

Indicate where the specimens have been deposited to permit free access by other researchers.

Dating methods

If new dates are provided, describe how they were obtained (e.g. collection, storage, sample pretreatment and measurement), where they were obtained (i.e. lab name), the calibration program and the protocol for quality assurance OR state that no new dates are provided.

Tick this box to confirm that the raw and calibrated dates are available in the paper or in Supplementary Information.

Ethics oversight

Identify the organization(s) that approved or provided guidance on the study protocol, OR state that no ethical approval or guidance was required and explain why not.

Note that full information on the approval of the study protocol must also be provided in the manuscript.

Animals and other research organisms

Policy information about [studies involving animals; ARRIVE guidelines](#) recommended for reporting animal research, and [Sex and Gender in Research](#)

Laboratory animals

For laboratory animals, report species, strain and age OR state that the study did not involve laboratory animals.

Wild animals

Provide details on animals observed in or captured in the field; report species and age where possible. Describe how animals were caught and transported and what happened to captive animals after the study (if killed, explain why and describe method; if released, say where and when) OR state that the study did not involve wild animals.

Reporting on sex

Indicate if findings apply to only one sex; describe whether sex was considered in study design, methods used for assigning sex. Provide data disaggregated for sex where this information has been collected in the source data as appropriate; provide overall numbers in this Reporting Summary. Please state if this information has not been collected. Report sex-based analyses where performed, justify reasons for lack of sex-based analysis.

Field-collected samples

For laboratory work with field-collected samples, describe all relevant parameters such as housing, maintenance, temperature, photoperiod and end-of-experiment protocol OR state that the study did not involve samples collected from the field.

Ethics oversight

Identify the organization(s) that approved or provided guidance on the study protocol, OR state that no ethical approval or guidance was required and explain why not.

Note that full information on the approval of the study protocol must also be provided in the manuscript.

Clinical data

Policy information about [clinical studies](#)

All manuscripts should comply with the ICMJE [guidelines for publication of clinical research](#) and a completed [CONSORT checklist](#) must be included with all submissions.

Clinical trial registration

Provide the trial registration number from ClinicalTrials.gov or an equivalent agency.

Study protocol

Note where the full trial protocol can be accessed OR if not available, explain why.

Data collection

Describe the settings and locales of data collection, noting the time periods of recruitment and data collection.

Outcomes

Describe how you pre-defined primary and secondary outcome measures and how you assessed these measures.

Dual use research of concern

Policy information about [dual use research of concern](#)

Hazards

Could the accidental, deliberate or reckless misuse of agents or technologies generated in the work, or the application of information presented in the manuscript, pose a threat to:

- | | |
|----|--|
| No | <input checked="" type="checkbox"/> Yes |
| | <input type="checkbox"/> Public health |
| | <input checked="" type="checkbox"/> National security |
| | <input checked="" type="checkbox"/> Crops and/or livestock |
| | <input checked="" type="checkbox"/> Ecosystems |
| | <input type="checkbox"/> Any other significant area |

Experiments of concern

Does the work involve any of these experiments of concern:

- | | |
|----|--|
| No | <input checked="" type="checkbox"/> Yes |
| | <input type="checkbox"/> Demonstrate how to render a vaccine ineffective |
| | <input type="checkbox"/> Confer resistance to therapeutically useful antibiotics or antiviral agents |
| | <input type="checkbox"/> Enhance the virulence of a pathogen or render a nonpathogen virulent |
| | <input type="checkbox"/> Increase transmissibility of a pathogen |
| | <input type="checkbox"/> Alter the host range of a pathogen |
| | <input type="checkbox"/> Enable evasion of diagnostic/detection modalities |
| | <input type="checkbox"/> Enable the weaponization of a biological agent or toxin |
| | <input type="checkbox"/> Any other potentially harmful combination of experiments and agents |

Plants

Seed stocks

Report on the source of all seed stocks or other plant material used. If applicable, state the seed stock centre and catalogue number. If plant specimens were collected from the field, describe the collection location, date and sampling procedures.

Novel plant genotypes

Describe the methods by which all novel plant genotypes were produced. This includes those generated by transgenic approaches, gene editing, chemical/radiation-based mutagenesis and hybridization. For transgenic lines, describe the transformation method, the number of independent lines analyzed and the generation upon which experiments were performed. For gene-edited lines, describe the editor used, the endogenous sequence targeted for editing, the targeting guide RNA sequence (if applicable) and how the editor was applied.

Authentication

Describe any authentication procedures for each seed stock used or novel genotype generated. Describe any experiments used to assess the effect of a mutation and, where applicable, how potential secondary effects (e.g. second site T-DNA insertions, mosaicism, off-target gene editing) were examined.

ChIP-seq

Data deposition

- Confirm that both raw and final processed data have been deposited in a public database such as [GEO](#).
- Confirm that you have deposited or provided access to graph files (e.g. BED files) for the called peaks.

Data access links

May remain private before publication.

For "Initial submission" or "Revised version" documents, provide reviewer access links. For your "Final submission" document, provide a link to the deposited data.

Files in database submission

Provide a list of all files available in the database submission.

Genome browser session (e.g. [UCSC](#))

Provide a link to an anonymized genome browser session for "Initial submission" and "Revised version" documents only, to enable peer review. Write "no longer applicable" for "Final submission" documents.

Methodology

Replicates

Describe the experimental replicates, specifying number, type and replicate agreement.

Sequencing depth

Describe the sequencing depth for each experiment, providing the total number of reads, uniquely mapped reads, length of reads and whether they were paired- or single-end.

Antibodies

Describe the antibodies used for the ChIP-seq experiments; as applicable, provide supplier name, catalog number, clone name, and lot number.

Peak calling parameters	Specify the command line program and parameters used for read mapping and peak calling, including the ChIP, control and index files used.
Data quality	Describe the methods used to ensure data quality in full detail, including how many peaks are at FDR 5% and above 5-fold enrichment.
Software	Describe the software used to collect and analyze the ChIP-seq data. For custom code that has been deposited into a community repository, provide accession details.

Flow Cytometry

Plots

Confirm that:

- The axis labels state the marker and fluorochrome used (e.g. CD4-FITC).
- The axis scales are clearly visible. Include numbers along axes only for bottom left plot of group (a 'group' is an analysis of identical markers).
- All plots are contour plots with outliers or pseudocolor plots.
- A numerical value for number of cells or percentage (with statistics) is provided.

Methodology

Sample preparation	Describe the sample preparation, detailing the biological source of the cells and any tissue processing steps used.
Instrument	Identify the instrument used for data collection, specifying make and model number.
Software	Describe the software used to collect and analyze the flow cytometry data. For custom code that has been deposited into a community repository, provide accession details.
Cell population abundance	Describe the abundance of the relevant cell populations within post-sort fractions, providing details on the purity of the samples and how it was determined.
Gating strategy	Describe the gating strategy used for all relevant experiments, specifying the preliminary FSC/SSC gates of the starting cell population, indicating where boundaries between "positive" and "negative" staining cell populations are defined.

- Tick this box to confirm that a figure exemplifying the gating strategy is provided in the Supplementary Information.

Magnetic resonance imaging

Experimental design

Design type	Indicate task or resting state; event-related or block design.
Design specifications	Specify the number of blocks, trials or experimental units per session and/or subject, and specify the length of each trial or block (if trials are blocked) and interval between trials.
Behavioral performance measures	State number and/or type of variables recorded (e.g. correct button press, response time) and what statistics were used to establish that the subjects were performing the task as expected (e.g. mean, range, and/or standard deviation across subjects).

Acquisition

Imaging type(s)	Specify: functional, structural, diffusion, perfusion.
Field strength	Specify in Tesla
Sequence & imaging parameters	Specify the pulse sequence type (gradient echo, spin echo, etc.), imaging type (EPI, spiral, etc.), field of view, matrix size, slice thickness, orientation and TE/TR/flip angle.
Area of acquisition	State whether a whole brain scan was used OR define the area of acquisition, describing how the region was determined.
Diffusion MRI	<input type="checkbox"/> Used <input type="checkbox"/> Not used

Preprocessing

Preprocessing software	Provide detail on software version and revision number and on specific parameters (model/functions, brain extraction, segmentation, smoothing kernel size, etc.).
------------------------	---

Normalization

If data were normalized/standardized, describe the approach(es): specify linear or non-linear and define image types used for transformation OR indicate that data were not normalized and explain rationale for lack of normalization.

Normalization template

Describe the template used for normalization/transformation, specifying subject space or group standardized space (e.g. original Talairach, MNI305, ICBM152) OR indicate that the data were not normalized.

Noise and artifact removal

Describe your procedure(s) for artifact and structured noise removal, specifying motion parameters, tissue signals and physiological signals (heart rate, respiration).

Volume censoring

Define your software and/or method and criteria for volume censoring, and state the extent of such censoring.

Statistical modeling & inference**Model type and settings**

Specify type (mass univariate, multivariate, RSA, predictive, etc.) and describe essential details of the model at the first and second levels (e.g. fixed, random or mixed effects; drift or auto-correlation).

Effect(s) tested

Define precise effect in terms of the task or stimulus conditions instead of psychological concepts and indicate whether ANOVA or factorial designs were used.

Specify type of analysis: Whole brain ROI-based Both

Statistic type for inference

Specify voxel-wise or cluster-wise and report all relevant parameters for cluster-wise methods.

(See [Eklund et al. 2016](#))

Correction

Describe the type of correction and how it is obtained for multiple comparisons (e.g. FWE, FDR, permutation or Monte Carlo).

Models & analysis

n/a Involved in the study

- Functional and/or effective connectivity
- Graph analysis
- Multivariate modeling or predictive analysis

Functional and/or effective connectivity

Report the measures of dependence used and the model details (e.g. Pearson correlation, partial correlation, mutual information).

Graph analysis

Report the dependent variable and connectivity measure, specifying weighted graph or binarized graph, subject- or group-level, and the global and/or node summaries used (e.g. clustering coefficient, efficiency, etc.).

Multivariate modeling and predictive analysis

Specify independent variables, features extraction and dimension reduction, model, training and evaluation metrics.